011023-2-T

THE UNIVERSITY OF MICHIGAN

COLLEGE OF ENGINEERING

High Altitude Engineering Laboratory

Departments of

Aerospace Engineering

Atmospheric and Oceanic Science

Technical Report

FEASIBILITY OF SATELLITE MEASUREMENT OF STRATOSPHERIC MINOR CONSTITUENTS BY SOLAR OCCULTATION

by

S. R. Drayson
F. L. Bartman
W. R. Kuhn
R. Tallamraju

ORA Project 011023

under contract with:

NATIONAL OCEANIC AND ATMOSPHERIC ADMINISTRATION

GRANT NG-10-72

administered through

OFFICE OF RESEARCH ADMINISTRATION ANN ARBOR

October 1973

ABSTRACT

The determination of stratospheric concentration of minor constituents by satellite solar occultation is examined. The method is shown feasible for ozone up to 50 km, water vapor up to 50 km, nitrous oxide up to 30 km, methane up to 50 km and carbon monoxide up to 20 km. Transmittance calculations for these and other gasses are presented for optimal spectral regions. Calculations of extinction by aerosols in the lower stratosphere show a dominant effect in the window regions near 10μm. Several inversion techniques are developed and examples of profiles retrieved by different methods are compared. Computer programs are described to calculate the transmittances by the use of a band model and by the line-by-line integration technique.

TABLE OF CONTENTS

TABLE OF CONTENTS (concluded)

Chapter 1. Introduction

The purpose of the work performed under this grant is to examine the feasibility of determining stratospheric concentrations of minor constituents and/or pollutants from satellite measurements of infrared absorption during solar occultation. Before such a task can be undertaken it is important to have some estimates of typical distributions of the constituents either from actual measurements or from theoretical models involving chemistry, photochemistry, diffusion etc. It is also necessary to have the capability of calculating the infrared spectral absorption along a tangent path through the atmosphere once the distribution of the atmospheric constituents has been specified, i.e., we require to know the spectral line parameters for each constituent absorbing in a given spectral region.

Our earlier report (Drayson, et al., 1972) contained a survey of the stratospheric distribution and the spectral properties of the minor constituents. For several molecules the optical masses along a tangent path were calculated for several tangent altitudes and for some molecules the absorptions along the tangent paths were roughly estimated from available laboratory data or approximate calculations. The report also considered stratospheric aerosols whose distributions are of considerable interest and which also may interfer with the absorption by molecular constituents.

In this report we describe the progress made in the continuation of the investigation. In Chapter 2 we examine more closely the absorption by stratospheric molecules with the main emphasis on the more abundant of the minor constituents, for two reasons :

i) The absorption by the more abundant minor constituents is large even averaged over spectral intervals several wavenumbers wide, so that a comparitively simple instrument of medium spectral resolution could be employed for satellite measurement.

ii) The spectral absorption properties of these molecules are known comparitively well. In particular several of them appear on the magnetic tape of line parameters compiled by AFCRC (McClatchey et al., 1973).

Transmittance calculations have been made either by the use of a band model or by a line-by-line integration computer program (described in the Appendix). In general we have not attempted to determine the accuracy of the spectral line parameters, although an exception was made in the case of ozone.

The extinction of solar radiation by stratospheric aerosols is examined in Chapter 3. The aerosols are important for two reasons:

i) They may interfer with a sounding of a molecular constituent so that an accurate estimate of the extinction by the aerosol alone is required to determine the vertical profile of the molecular component.

ii) The distribution of dust and aerosols in the stratosphere is known to be a factor that influences the climate at the surface and a continuous monitoring would aid our understanding of this problem as well as processes within the stratosphere itself.

In Chapter 4 we consider the inversion problem, i.e. how to determine the vertical profile of the constituents from the occultation measurements. In the absense of noise the problem is compartively simple but in a realistic situation some smoothing constraints must be applied to prevent domination of the solution by the noise present. Several different techniques are examined and compared.

REFERENCES

Drayson, S. R., F. L. Bartman, W. R. Kuhn and R. Tallamraja (1972), Satellite Measurement of Stratospheric Pollutants and Minor Constituents by Solar Occultation: A Preliminary Report, University of Michigan Technical Report 011023-1-T.

McClatchey, R. A., W. S. Benedict, S. A. Clough, D. E. Burch, R. F. Calfee, K. Fox, L. S. Rothman and J. S. Garing (1973), AFCRL Atmospheric Absorption Line Parameters Compilation, AFCRL Environmental Research Paper No. 434.

Chapter 2. Stratospheric Absorption by Molecular Constituents.

2.1 Introduction

The previous report dealt primarily with 1) the distributions of stratospheric minor constituents, 2) the locations of and available data on the infrared bands, and 3) a crude estimate of the maximum absorption one might expect from these various bands. These latter results were only very approximate, since they were obtained from absorption profiles given in McCaa and Shaw (1967) for the ozone bands, and in Burch et al. (1962) for other molecules, and the mass paths and pressures which were used generally did not correspond to stratospheric conditions. In addition, the measurements were all made at room temperature, and the absorption, especially in the wings of the bands, may depend strongly on temperature.

The emphasis of the present investigation has been to construct transmission curves vs. height for stratospheric tangent paths corresponding to extreme or typical distributions of the minor constituents. These transmissions correspond to small wavenumber intervals (generally $1 cm^{-1}$) and were chosen to represent as nearly as possible the maximum absorption in each of the bands. A band model or direct line by line integration has been used to represent the absorption and the validity of the model and/or the band parameters have been compared with experimental results. Finally, the feasibility of using the various bands for tangent-path remote soundings is discussed.

2.2 Band Model

The band model is essentially a random model, i.e., the spectral lines are assumed to be randomly distributed. In addition, the actual number of lines is used which is a feature of the quasi-random model developed by Wyatt et al. (1962). The lines are grouped into intensity intervals, and all lines in the intervals are given a strength equal to the average of the strengths of lines within that interval. The magnitude of the intensity interval is variable. For those spectral regions for which the lines have very similar intensities, the variation in intensity is chosen small, while for the intervals whose line intensities vary over many orders of magnitude, the lines are grouped into intensity decades.

The transmission T_i is given as,

$$T_i = \prod_{k=1}^{j} \left\{ \frac{1}{\Delta\omega_i} \int_{\Delta\omega_i} \exp\left(-S_k P_i(u)\right) d\omega_i \right\}^{n_k} \tag{2. 1}$$

where $\Delta\omega_i$ is the width of the spectral interval over which the transmission is determined; S_k and n_k are the mean line strength and number of lines in the intensity interval, P_i is the profile function, and u is the mass path of the absorbing gas.

The profile function which must be used for stratospheric tangent path studies is the Voigt profile, since both collision and Doppler broadening contribute to the line profile in this height range. This profile is given by,

$$P = \frac{a}{\pi} \int_{-\infty}^{\infty} \frac{e^{-y^2}\, dy}{a^2 + [f(x) - y]^2} \tag{2. 2}$$

where $a = \alpha_L \sqrt{\ln 2} / \alpha_D$, with α_L and α_D being the collision and Doppler half-widths respectively. The collision half width is given for standard temperature and pressure (t_o, P_o) and is found for any other temperature and pressure by the relation $\alpha_L = \alpha_o P \sqrt{t_o} / P_o \sqrt{t}$. The Doppler half width is calculated from $\alpha_D = (2kt \ln 2 / mc^2)^{1/2} \omega$, where k is Boltzmann's constant, m is the molecular mass, and c the speed of light. ω is actually line center but we assume a value equal to the center of the spectral interval; i. e., all lines in the interval are given the same Doppler half-width. This is also true for the collision half-width. The parameter $f(x) = \Delta\omega_i \sqrt{\ln 2} \cdot x / 2\alpha_D$, where x is essentially a measure of distance from line center given by $x = 2(\omega - \omega_o) / \Delta\omega_i$.

If equations (2. 1) and (2. 2) are combined, the transmission for a single line (represented by the quantity in brackets in (2. 1), is,

$$T_k = \int_0^1 \exp\left[-\frac{S_k u}{\alpha_D} \left(\frac{\ln 2}{\pi}\right)^{\frac{1}{2}} P(a, f(x))\right] dx \qquad (2.3)$$

Unfortunately equation (2. 3) has no analytical solution, and must be evaluated numerically. Accordingly, a three dimensional table was prepared for which the parameters and their ranges are,

$$-6 \leq \log (S_k u / \Delta\omega) \leq 6$$
$$-7 \leq \log (a) \leq 3$$
$$2 \leq \log(\Delta\omega / \alpha_D) \leq 6$$

The first two are evaluated at intervals of 0. 1, while the interval for the latter is 1. The actual transmission for a given set of parameters is found by bilinear interpolation on the table. In order to reduce the computing time, yet maintain the necessary accuracy for this feasibility study, we have excluded the contribution to the absorption from spectral lines outside the interval of interest; this is equivalent to requiring that the total line absorptivity fall within the specified spectral interval. Thus log $\Delta \omega/\alpha_D$ was taken as 6 and the spectral interval adjusted accordingly.

Uncertainties in the calculated transmission functions can occur from inaccurate line parameters from which the model is constructed, or from the actual model itself, i. e., the lines may not be randomly distributed. One would not expect the latter to be a major problem for the non-linear molecules since their vibration-rotation spectra are quite complex. As an example, Fig. 2. 1 compares a band model calculation with an "exact line by line" calculation averaged over one-tenth wavenumber intervals. While there is some "clustering" of the lines (at, e. g. 1124. 3 cm^{-1}) the band model represents an average transmission quite well. The averaging interval for the band model is also not critical as the average of the 0. 5 cm^{-1} intervals gives nearly the same transmission as the average of the 1 cm^{-1} intervals.

The line parameters used for both the band model and line by line integration are from McClatchey et al. (1973). A magnetic tape containing these data was graciously provided. This tape containing the most recently published tabulations provides line strengths, positions half widths, and ground state energies for selected bands of ozone, water vapor, carbon monoxide and dioxide, nitrous oxide, methane and oxygen. Approximately 110, 000 lines are included for wavelengths longer than 1 micrometer.

2. 3 Ozone

Ozone bands and the corresponding spectral intervals chosen for the stratospheric tangent path calculations are given in Table 2. 1.

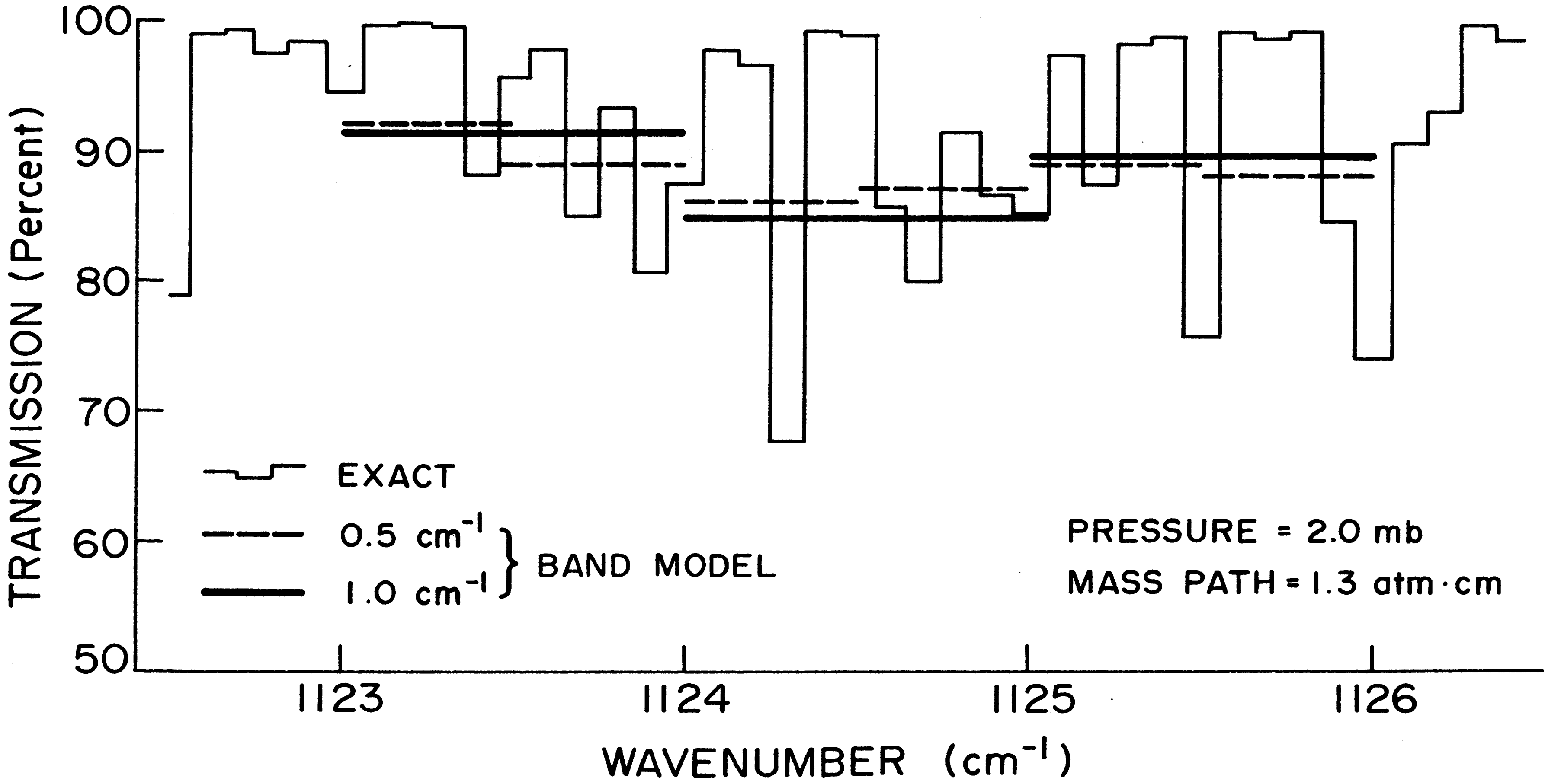

Fig. 2.1 Comparison of exact calculation and band model.

These intervals were chosen so that they give maximum or near maximum absorption for each band. McCaa and Shaw's (1967) absorption profiles were used to locate approximately these regions, and the final identification utilized the line positions and strengths as given by McClatchey et. al. (1973). It should be noted that the present analysis does not include three combination bands (1728, 1792 and 3181 cm^{-1}) discussed in the previous report. Their line parameters are not given by McClatchey et al., and we are not aware of any line listings for these bands. The 3181 cm^{-1} ($2\nu_1 + \nu_3$) band is not important for this study since our earlier work indicated that even with the maximum realistic ozone distribution, maximum absorption within the band as estimated from the McCaa and Shaw data is only 9% at 24 km. However, the 1728 cm^{-1} ($\nu_1 + \nu_3$) band gives a comparable absorption but with the minimum ozone amount. The 1792 cm^{-1} ($\nu_1 + \nu_2$) band is intermediate to these two. Fortunately, it will be shown that the bands given in Table 2. 1 provide the necessary absorption throughout the stratosphere, and it is not necessary to consider these additional bands.

Band	ν_1	ν_2	ν_3	$\nu_1 + \nu_3$	$\nu_1 + \nu_2 + \nu_3$	$3\nu_3$
Wavenumber (cm^{-1})	1124.5	717	1025	2131	2795	3046

Table 2. 1 Centers of the 3 cm^{-1} spectral intervals of tangent path calculations ozone bands selected for the stratospheric

The model atmosphere from which the tangent path absorptivities were determined is fully explained in the previous report. The USSA (1962) was assumed and ozone distributions corresponding to the largest and smallest amounts one might expect to observe were constructed. These extreme ozone mass paths for these heights as well as the tangent path pressures and temperatures are given in Table 2. 2. The latter were evaluated from a Curtis Godson approximation, i. e., they were weighted by the ozone mass path.

Tangent Height (km)	Pressure (mb)	Temperature (^oK)	Mass Path (atm-cm)
12	88. 5 - 110.	218	45. 0 - 7. 1
20	37. 9 - 37. 7	220	24. 7 - 5. 6
30	8. 3 - 8. 4	232	6. 8 - 1. 2
40	2. 0 - 1. 6	255	1. 6 - 0. 28
50	. 56 - . 56	266	0. 43 - 0. 074

Table 2.2 Curtis-Godson pressures and temperatures for selected tangent heights for extreme ozone amounts. The temperatures are the same for both extreme ozone mass paths.

1123 - 1126 cm^{-1} (ν_1 band)

The 1123 - 1126 cm^{-1} spectral interval contains 63 lines of the ν_1 band in the McClatchey et al. data. Line strengths range over four orders of magnitude at room temperature. A collision half width of 0. 110 cm^{-1} is given.

A comparision between the band model and experimental profiles of McCaa and Shaw (1967) is shown in Table 2. 3. Note that the transmissions, when averaged over a 3 cm^{-1} interval which is

Pressure (mb)	20	20	67	400
Mass Path (atm-cm)	1. 3	2. 9	4. 2	12. 7
1123 - 1124	. 92	. 87	. 75	. 38
1124 - 1125	. 85	. 78	. 53	. 23
1125 - 1126	. 90	. 86	. 76	. 31
Average	. 89 (.88)	. 84 (.83)	. 68 (.70)	. 31 (.29)
Experimental (McCaa and Shaw)	. 92	. 88	. 72	. 34

Table 2. 3 A comparison of theoretical (band model) and experimental (McCaa and Shaw, 1967) transmissivities for the 1123-1126 cm^{-1} spectral interval. The transmissions shown in parentheses refer to an averaging interval of 0. 5 cm^{-1} rather than 1 cm^{-1}

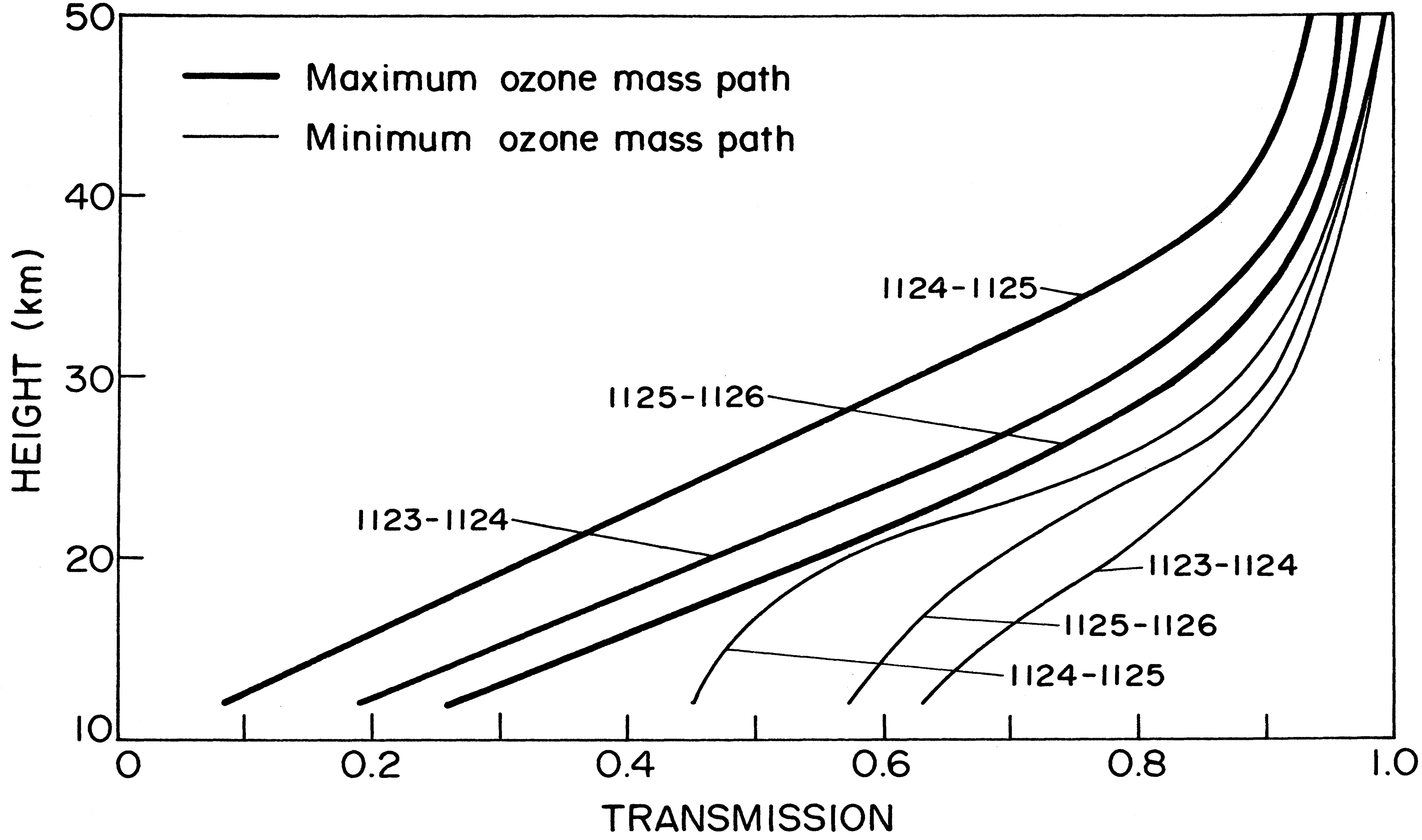

Fig. 2. 2 Stratospheric tangent path transmissivities for the spectral region 1123-1126 cm^{-1} for extreme ozone mass paths.

close to the spectral resolution of McCaa and Shaw (1967), agree to within four percent of the experimental results. This accuracy is certainly adequate to estimate the feasibility of using this band for remote soundings.

The importance of knowing the spectral resolution for these rather small intervals when comparing with experimental data is important, e.g. the absorption is larger in the 1124-1125 cm^{-1} interval than the adjacent intervals by as much as 19% in the one case.

The band model calculation does not depend strongly on the width of the spectral subintervals over which the individual transmissions are calculated. For example, if a 0.5 cm^{-1} rather than a 1 cm^{-1} interval is used, the average transmission is within 0.02 of the 1 cm^{-1} subinterval (shown in parentheses in Table 2.3).

The stratospheric tangent path transmissivities for the three 1 cm^{-1} spectral intervals for extreme ozone amounts (Table 2.1) are shown in Fig. 2.2. If the spectral resolution is 3 cm^{-1} or less, and if enough energy is available, then this ν_1 band in the spectral region near 1124.5 cm^{-1} should be adequate for tangent path remote soundings, at least to the midstratosphere. Of course, a larger spectral resolution would increase the transmission and lower the effective height.

<u>715.5 - 718.5 cm^{-1} (ν_2 band)</u>

One would generally not consider the ν_2 band for remote sensing of ozone because of its strong overlap with the ν_2 band of carbon dioxide, centered about 667 cm^{-1}. The integrated band strength is only about 18 $atm^{-1}cm^{-2}$ (McCaa and Shaw, 1967) while the ν_2 band of carbon dioxide is about 214 $atm^{-1}cm^{-2}$ (Drayson, 1973). Nevertheless, a comparison of the band model transmissions with the spectra of McCaa and Shaw (1967) was made for completeness. The spectral region of maximum absorption was taken as 715.5 to 718.5 cm^{-1}. That this band is highly structured can be observed from both the experimental profiles of McCaa and Shaw and the data of McClatchey et al. In Table 2.4 is given the number of lines for each 1 cm^{-1} interval as well as the mean line strengths for each intensity subinterval; these distributions were used in the band model calculations.

715.5 - 716.5 cm^{-1}	716.5 - 717.5 cm^{-1}	717.5 - 718.5 cm^{-1}
.0327 (5)	.0254 (12)	.0163 (7)
.0089 (9)	.0085 (14)	.0035 (6)
.0020 (1)	.0018 (4)	.0010 (1)

Table 2.4 Mean line strengths (atm^{-1} -cm^{-2}) and numbers of lines (parentheses) used in the band model study for the 715.5 to 718.5 cm^{-1} spectral region of the ν_2 band of ozone.

A comparison of the band model transmissivities with the McCaa and Shaw absorption profiles is given in Table 2.5. The obvious clustering of the lines is apparent from the rather large variation in transmissions among the three spectral intervals. The average of these results gives a transmission about ten percent smaller than the experimental spectra indicate. However, because of the clustering, a small discrepancy in the location of band center or a spectral interval somewhat larger than 3 cm^{-1} would increase the band model transmissions. We have not analyzed further this difference because, as explained previously, one would not choose this band for remote soundings.

Pressure (mb)	20	66.6	66.6	533	533
Mass Path (atm-cm)	.84	4.20	2.0	9.4	3.0
715.5 - 716.5 cm^{-1}	.832	.599	.709	.164	.508
716.5 - 717.5 cm^{-1}	.708	.379	.525	.039	.294
717.5 - 718.5 cm^{-1}	.896	.703	.771	.329	.661
Average	.81	.56	.67	.18	.49
Experimental (McCaa and Shaw)	.90	.67	.77	.27	.59

Table 2.5 Comparison of band model transmissions with experimental spectra of McCaa and Shaw for the 715.5 to 718.5 cm^{-1} spectral interval of the ν_2 ozone band.

Tangent path transmissivities for only ν_2 band ozone lines in the interval of 715.5 to 718.5 cm^{-1} are shown in Fig. 2.3. If one were to include the very strong absorption by carbon dioxide, the transmission values would be much reduced, and it is likely that only in the upper atmosphere, if at all, would the transmission be large enough for remote sounding studies.

1023.5 - 1026.5 cm^{-1} (ν_3 band)

More studies have been devoted to the ν_3 and ν_1 bands than any of the other ozone vibration bands. The spectra are complex and analysis is difficult because of the interaction of these bands. The line parameters of McClatchey et al. are the latest which appear in the open literature. These parameters are primarily from the work of Clough and Kneizys (1965, 1966) although some hot bands and isotopic bands have been added. Aida (1973) has also calculated line parameters but unfortunately the ground state energies are not available so that the line strengths cannot be calculated for arbitrary temperatures. The total number of lines which appears in his tabulation is about 10,000.

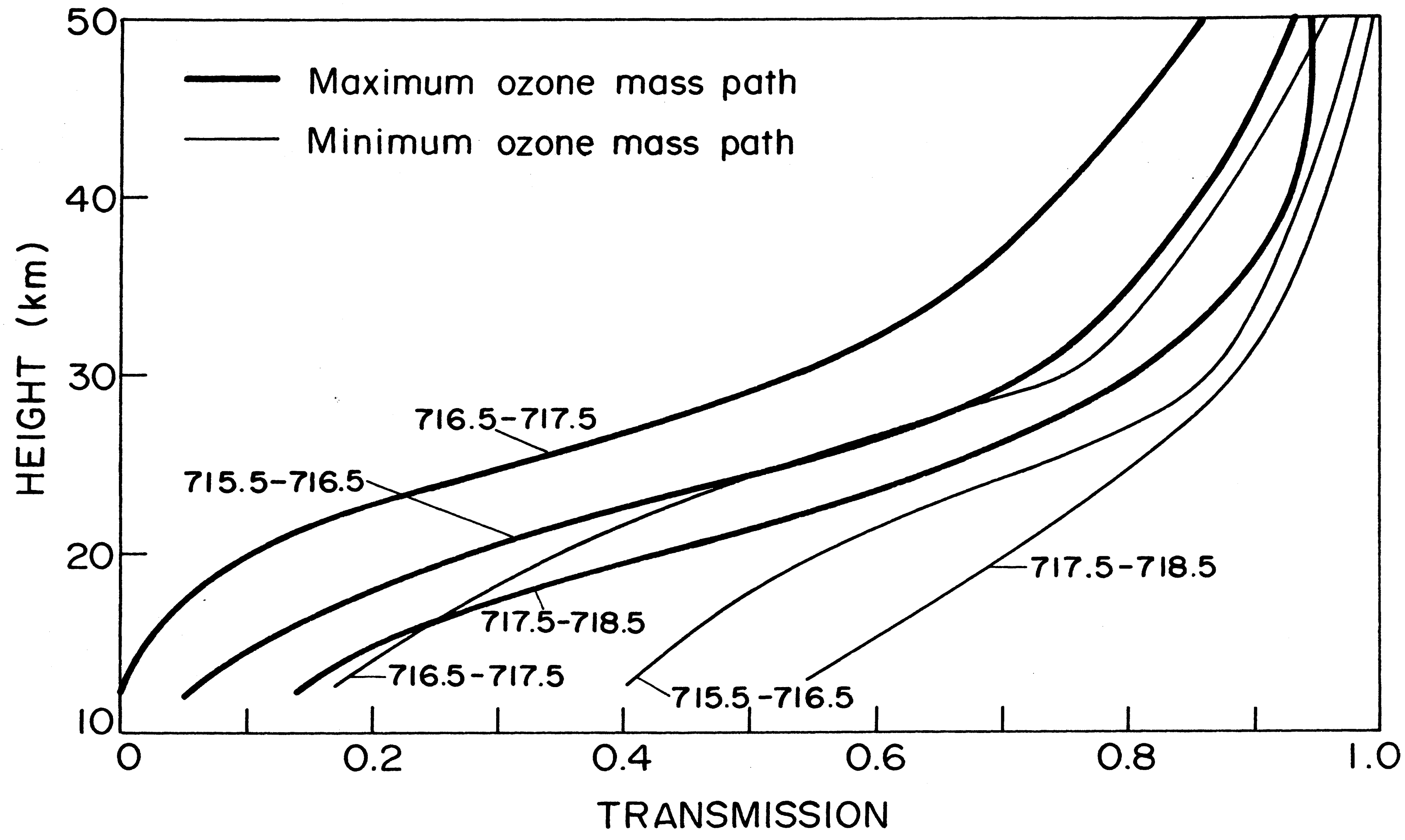

Fig. 2.3 Stratospheric tangent path transmissivities for the ν_2 band ozone lines in the spectral region of 715.5 - 718.5 cm^{-1}.

Although much effort has been devoted to an analysis of the ν_1 and ν_3 bands, discrepancies still exist among the calculated line parameters. The half width as given by McClatchey et al. is 0.11 cm^{-1} (from Lichtenstein et. al., 1971), while Aida calculated a half width for each line adjusted to a mean line width of 0.078 cm^{-1} (from Walshaw, 1955). Also the band centers for the overtone band $2\nu_3 - \nu_3$ and the ν_3 band of the isotope $^{16}O^{16}O^{18}O$ are different for the two calculations. For the overtone band McClatchey et al. give a band center of 1027.096 cm^{-1}, while Aida (1973) gives 1012.1 cm^{-1}. Similarly McClatchey et al. give 1028.096 for the center of the isotopic band while Aida gives 1024.1 cm^{-1}.

Although the intensities of these bands are small (4.26 $atm^{-1}cm^{-2}$ for the overtone and 1.54 $atm^{-1}cm^{-2}$ for the isotope), they can strongly influence the absorption in some parts of the spectrum. For example, in a 1 cm^{-1} interval, centered about 970 cm^{-1}, the total line strength as given by McClatchey et al. is about 13×10^{-3} $atm^{-1}cm^{-2}$, while Aida's results give a strength of 40×10^{-3} $atm^{-1}cm^{-2}$. Much of this discrepancy can be resolved if the $2\nu_3 - \nu_3$ band is given the same center in both calculations. For example if the band center in the McClatchey et al. data is shifted down 14.9 cm^{-1} to agree with that of Aida, then the total line strength from the McClatchey et al. data is about $41 \times 10^{-3} cm^{-2} atm^{-1}$, agreeing well with that of Aida. A comparison of transmissions with experimental data of McCaa and Shaw indicates better agreement when the $2\nu_3 - \nu_3$ band is centered at 1012.1 cm^{-1}; for example at 20 mb and a mass path of 4.62 atm-cm, the transmission in the interval 969.5 to 970.5 is 0.94 for the unshifted data, while a shift of the $2\nu_3 - \nu_3$ band gives a transmission of 0.83. The latter agrees much better with the value of 0.80 as given by McCaa and Shaw (1967).

Band model transmissions for the 1023.5 to 1026.5 cm^{-1} spectral interval are compared with experimental data from McCaa and Shaw in Table 2.6. The difference approaches ten percent in some cases. For this model the half width was chosen as 0.08 cm^{-1} and the distribution of mean line strengths (averaged over an intensity interval of 0.4) is shown in Table 2.7.

Pressure (mb)	20	20	20	66.6	66.6
Mass Path (atm-cm)	12.6	2.6	.45	.41	.87
1023.5 - 1024.5	.012	.228	.652	.493	.344
1024.5 - 1025.5	.006	.177	.603	.415	.277
1025.5 - 1026.5	.013	.243	.670	.515	.296
Average	.010	.216	.641	.474	.305
Experimental (McCaa and Shaw)	.02	.19	.55	.48	.22

Table 2.6 Comparison of band model and experimental transmissivities in the 1023.5 to 1026.5 cm^{-1} intervals for the ν_3 ozone band.

1023.5 - 1024.5	1024.5 - 1025.5	1025.5 - 1026.5
.739 (6)	.797 (7)	.783 (5)
.192 (3)	.229 (4)	.260 (3)
.0090 (16)	.00986 (15)	.0129 (14)
.00088 (111)	.00101 (121)	.0011 (110)
.000045 (5)	.000055 (9)	.000049 (24)

Table 2.7 Distribution of mean line strengths and numbers of lines (in parentheses) as used in the band model calculation for the 1023.5-1026.5 cm^{-1} spectral region of the ν_3 ozone band.

If the $2\nu_3 - \nu_3$ band is shifted to 1012.1 cm^{-1} the transmissions and mean line strengths are as given in Tables 2.8 and 2.9 respectively. While the agreement is somewhat better, it is not definitive. The weak overtone lines change only slightly the overall strength in this spectral region (Compare Tables 2.7 and 2.9).

Pressure (mb)	20	20	20	66.6	66.6
Mass Path (atm-cm)	12.6	2.6	.45	.41	.87
1023.5 - 1024.5 cm^{-1}	.012	.221	.629	.478	.266
1024.5 - 1025.5 cm^{-1}	.006	.166	.578	.399	.206
1025.5 - 1026.5 cm^{-1}	.013	.234	.648	.502	.301
Average	.010	.207	.618	.459	.257

Table 2.8 Band model transmissions for the 1023.5 to 1026.5 cm^{-1} spectral interval in the 3 ozone band. Center of the 2 3 - 3 band has been shifted to 1012.1 cm^{-1}

1023.5 - 1024.5 cm^{-1}	1024.5 - 1025.5 cm^{-1}	105.5 - 1026.5 cm^{-1}
.739 (6)	.797 (7)	.783 (5)
.192 (3)	.229 (4)	.260 (3)
.0107 (21)	.0105 (23)	.0131 (19)
.000803 (96)	.000937 (99)	.000999 (100)
.000034 (11)	.000047 (14)	.000044 (25)

Table 2.9 Distributions of mean line strengths ($cm^{-2}atm^{-1}$) and numbers of lines (in parentheses) as used in the band model calculations given in Table 2.8

These calculations presented in Tables 2.6 and 2.8 were made with a half width of 0.08 cm^{-1} which corresponds to the mean half width given by Aida (1973). If the half width is 0.11, the value given by McClatchey et al., then the transmissions are as shown in Table 2.10. The distribution of line strengths corresponds to Table 2.9. It is not obvious which half width is more appropriate. For the mass paths of 2.6, 0.45, and 0.87 atm-cm, the half width of 0.11 cm^{-1} gives better agreement while for the other mass paths, the best agreement is found for a width of 0.08 cm^{-1}. Actually the only significant difference between the theoretical and experimental transmissivities is for the mass path of 0.41 atm-cm, where our band model value is about 0.07 smaller than the value from McCaa and Shaw.

Pressure (mb)	20	20	20	66.6	66.6
Mass Path (atm-cm)	12.6	2.6	.45	.41	.87
1023.5 - 1024.5 cm^{-1}	.007	.199	.600	.429	.235
1024.5 - 1025.5 cm^{-1}	.003	.14	.525	.35	.168
1025.5 0 1026.5 cm^{-1}	.007	.209	.601	.454	.258
Average	.005	.182	.575	.411	.220

Table 2.10. Band model transmissions for the 1123.5 to 1126.5 cm^{-1} interval in the ν_3 ozone band corresponding to line strength parameters as given in Table 2.9 with half width of 0.11 cm^{-1}

A calculation was also made for the ν_3 isotope $^{16}O^{16}O^{18}O$ shifted down 4 cm^{-1}, to 1024.1 cm^{-1}, in agreement with Aida. The transmissions in the 1023.5 to 1024.5 cm^{-1} interval changed by less than one percent.

Stratospheric tangent path transmissivities for two 1 cm^{-1} spectral intervals, at 1024.5 - 1025.5 cm^{-1} corresponding to a region of maximum absorption, and 969.5 - 970.5 cm^{-1}, located in the wing, are shown in Fig. 2.4. The region of maximum absorption in the ν_3 band can be used for remote sounding from the midstratosphere at least to the stratopause. However in the low stratosphere, the transmission is small, and a spectral region in the wing of the band could be used. It appears that a wavenumber somewhat greater than 970 cm^{-1} should be appropriate.

The agreement in transmission between experimental and our band model results is better for the ν_3 and ν_1 bands than for the others investigated; one would expect this to be the case since more work, both theoretical and experimental, has been done on these bands.

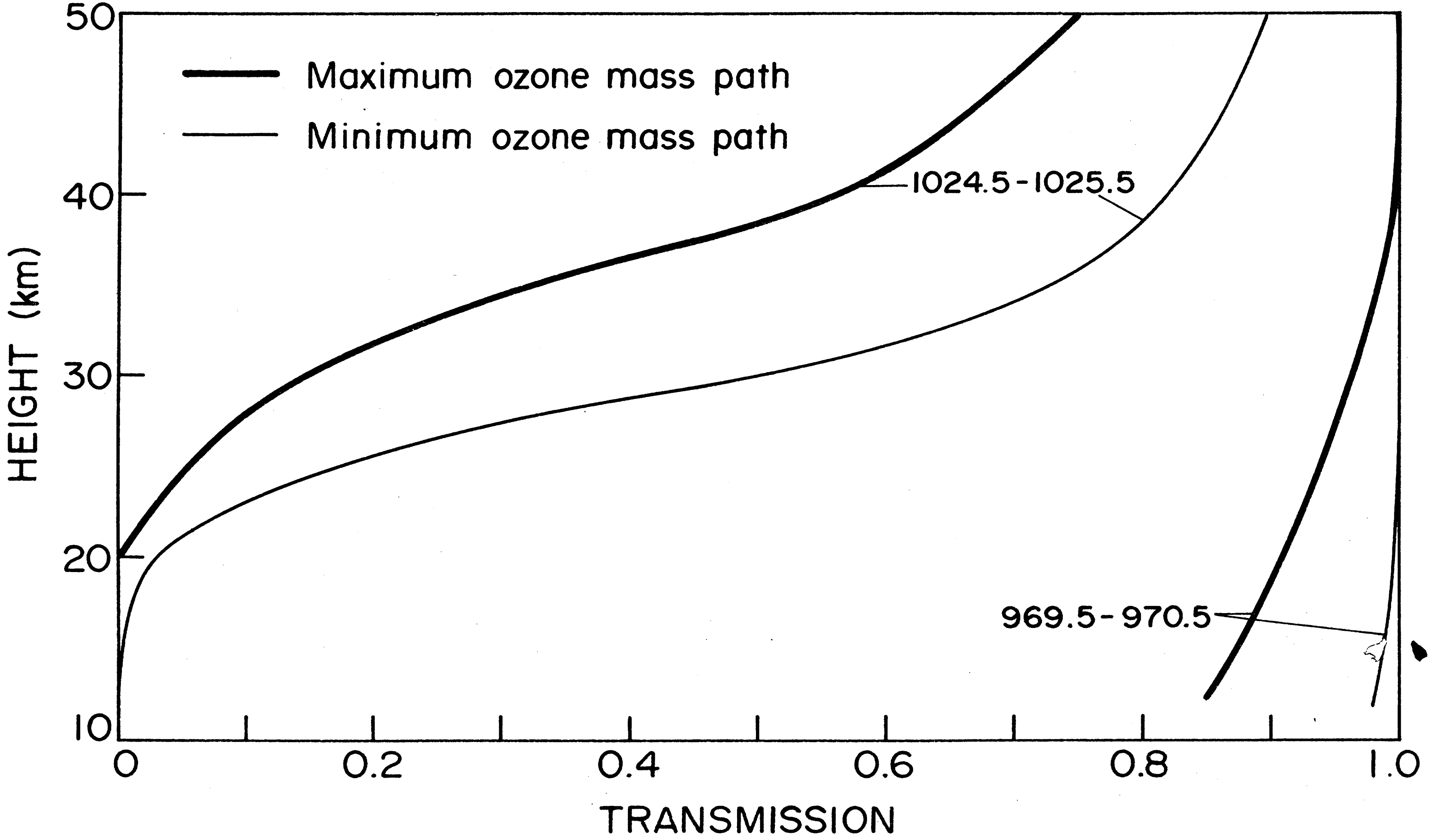

Fig. 2.4 Stratospheric tangent path transmissions for the spectral regions 1024.5-1025.5 cm^{-1} and 969.5 - 970.5 cm^{-1}.

Fortunately the ν_3 band appears to be the most desirable for remote sensing work. The band is strong enough so that one could choose a number of spectral intervals within the band so that soundings could be made throughout the stratosphere.

There are a number of disadvantages to using this band which should be mentioned. The line density is so large that direct line by line calculations are probably not feasible, and some empirical or band model approach might have to be employed. Secondly, there are still discrepancies among the theoretical line parameter tabulations which need to be resolved, e. g., the half widths and centers of isotope and overtone bands. The weaker lines may not be important near band center, but in the wings these lines become extremely important because of their strong temperature dependence. To illustrate, we show in Table 2. 11, the transmission in two spectral intervals, the one at 1025 cm^{-1} being a region of the band corresponding to maximum absorption and containing many strong lines, and the 970 cm^{-1} region on the wing of the band. For example, at 300K the strongest lines in the 1025 cm^{-1} region are about one-hundred times stronger than in the 970 cm^{-1} region and at 200 K this difference increases to about one-thousand. The strongest lines are less temperature dependent and this is clearly shown in Table 2. 11 where the transmission for the 1025 cm^{-1} region varies by less than one percent, while the variation for the wing region is about forty-eight percent. Thus the line parameters must be accurately known because the stratospheric temperature range is similar to that given in Table 2. 11. It is unfortunate that there are no low temperature ozone measurements against which we can compare our theory.

An additional disadvantage in using this spectral region is that the aerosol absorption especially in the low stratosphere is quite large. This problem is discussed in Chapter 3.

Temperature	300	275	250	225	200
969.5 - 970.5	.466	.605	.637	.876	.952
1024.5 - 1025.5	.147	.145	.147	.152	.153

Table 2.11. Effect of temperature on transmission in the spectral intervals of 969.5-970.5 (20mb and 26 atm·cm) and 1024.5-1025.5 cm^{-1} (20mb and 2.6 atm·cm)

2129.5 - 2132.5 cm^{-1} ($\nu_1 + \nu_3$)

A comparison of the band model calculations for the $\nu_1 + \nu_3$ band with the absorption profiles of McCaa and Shaw is shown in Table 2.12. The band model transmissivities represent averages over 1 cm^{-1} spectral intervals, centered about 2130, 2131 and 2132 cm^{-1}. Note that in all but the last case, the model transmissivities are smaller than the experimental results, in one case by as much as twenty-eight percent.

Mass Path (atm·cm)	13.8	4.5	0.87	4.8	0.23
Pressure (mb)	20	20	20	66.6	66.6
2129.5 - 2130.5 cm^{-1}	.185	.303	.564	.180	.862
2130.5 - 2131.5 cm^{-1}	.172	.243	.593	.214	.873
2131.5 - 2132.5 cm^{-1}	.251	.279	.778	.269	.938
Average	.20(.23)	.27(.29)	.64(.64)	.22(.25)	.89(.89)
Experimental (McCaa & Shaw)	.33	.55	.82	.30	.85

Table 2.12. Comparison of band model transmissivities with the experimental study of McCaa and Shaw (1967) for the spectral interval 2129.5 to 2132.5 cm^{-1} for the $\nu_1 + \nu_3$ ozone band. The transmissions in parentheses refer to a single spectral interval extending from 2129.5 cm^{-1} to 2132.5 cm^{-1}.

This discrepancy is probably not due to experimental resolution since the transmissions of all three spectral intervals are less than the experimental values. The discrepancy is also not due to a difference in band center, since the line parameters were chosen so as to give minimum transmission in the band and the experimental results do not yield such small values at any wavenumber within the band. In addition, the experimental results include the effect of the CO fundamental at 2143 cm^{-1}; McCaa and Shaw state that the absorptance of this band was never greater then twenty percent. This effect, although small, would make the experimental ozone transmissivities even higher, giving a larger disagreement with the band model.

The band model also does not appear responsible for the discrepancy. Two possible sources of error were the averaging interval and the assumed intensity subintervals. The former was checked by applying the band model to a single interval extending from 2129.5 to 2132.5 cm^{-1}, and the transmissions are shown in parentheses in Table 2.12; the agreement is within three percent. Also rather than grouping the lines into intensity decades, which yielded two intensity subintervals, they were grouped for intervals of 0.2, 0.4, 0.6 and 0.8, as well.[1] The various intensity intervals are shown in Table 2.13 for the 2129.5 to 2130.5 cm^{-1} interval, and the effect on the transmission is shown in Table 2.14. The uncertainty in the transmission is less than five percent. Similar results were found for the other two spectral intervals.

---

[1] For an intensity interval of 0.4, for example, and if S_m is the strongest line in the spectral interval, then the intensity intervals would be S_m to 0.4 S_m, 0.4 S_m to $(0.4)^2 S_m$, $(0.4)^2 S_m$ to $(0.4)^3 S_m$, etc.

0.1	0.2	0.4	0.6	0.8
.002 (29) .0028 (6)	.026 (24) .0045 (11)	.030 (17) .010 (14) .0022 (4)	.035 (10) .020 (13) .0055 (10) .0019 (2)	.044 (3) .030 (10) .018 (9) .008 (6) .003 (7)

Table 2.13. Distributions of line intensities for various line strength intervals for the 35 spectral lines in the 2129.5 to 2130.5 cm^{-1} spectral interval of the $\nu_1 + \nu_3$ ozone band.

Mass Path (atm·cm)	13.8	4.5	0.87	4.8	0.23
Pressure (mb)	20	20	20	66.6	66.6
0.1	.185	.303	.564	.18	.862
0.2	.185	.321	.604	.161	.868
0.4	.191	.325	.581	.207	.856
0.6	.200	.327	.558	.171	.866
0.8	.197	.310	.570	.204	.869

Table 2.14. Band model transmissivities for the 2129.5 to 2130.5cm^{-1} ozone band distributions of line intensities as given in Table 2.13. Compare with Table 2.12.

There is still much uncertainty in the line parameters for this band and we suspect this is the reason for the discrepancy between the band model and experimental results. McClatchey et al. (1973) state that the line positions up to J=20 and K_a=4 are accurate to 0.3cm^{-1} with "the error in line position significantly greater for higher quantum numbers." Although the total band intensity as used by McClatchey et al. agrees with the experimentally determined value of 32 $atm^{-1}cm^{-2}$ of McCaa and Shaw, nevertheless, an incorrect distribution of intensities of these lines could cause the lower transmission. In any case, it is o obvious that our present knowledge of the $\nu_1 + \nu_3$ band is not adequate for application to remote sensing.

Stratospheric tangent path transmissivities for the spectral interval 2129.5 to 2132.5 cm^{-1} are presented in Fig. 2.5. If the line parameters could be improved, then this band could be used for remote sensing at least in the lower stratosphere.

<u>3044.5 - 3047.5 cm^{-1} $(3\nu_3)$</u>

A similar comparison of the 3044.5 - 3047.5 cm^{-1} spectral interval with the McCaa and Shaw results is shown in Table 2.15.

Pressure (mb)	20	66	400	400	400
Masspath (atm·cm)	14.6	1.4	19.1	6.1	14.3
3044.5 - 3045.5	58	92	24	67	33
3045.5 - 3047.5	51	90	22	64	32
3046.5 - 3047.5	53	90	16	62	28
Average	.54	.90	.21	.64	.31
Experimental (McCaa and Shaw)	76	93	49	76	56

Table 2.1 . Comparison of band model transmissivities with experimental results of McCaa and Shaw (1967) for the 3044.5 to 3047.5 cm^{-1} spectral interval for the $3\nu_3$ ozone band.

As in the prior case the band model transmissivities are much smaller and the discrepancy is probably also due to the uncertainties in the line parameters. Few details on the calculation of the line parameters for this band are given, but McClatchey et al. do state that the line positions are accurate only to ±5 cm^{-1}, which is certainly not adequate for application to remote sensing.

Stratospheric tangent path transmissivities for the region of maximum absorption in this band is shown in Fig. 2.6. If one takes into account that the computed transmissivities are probably smaller than is

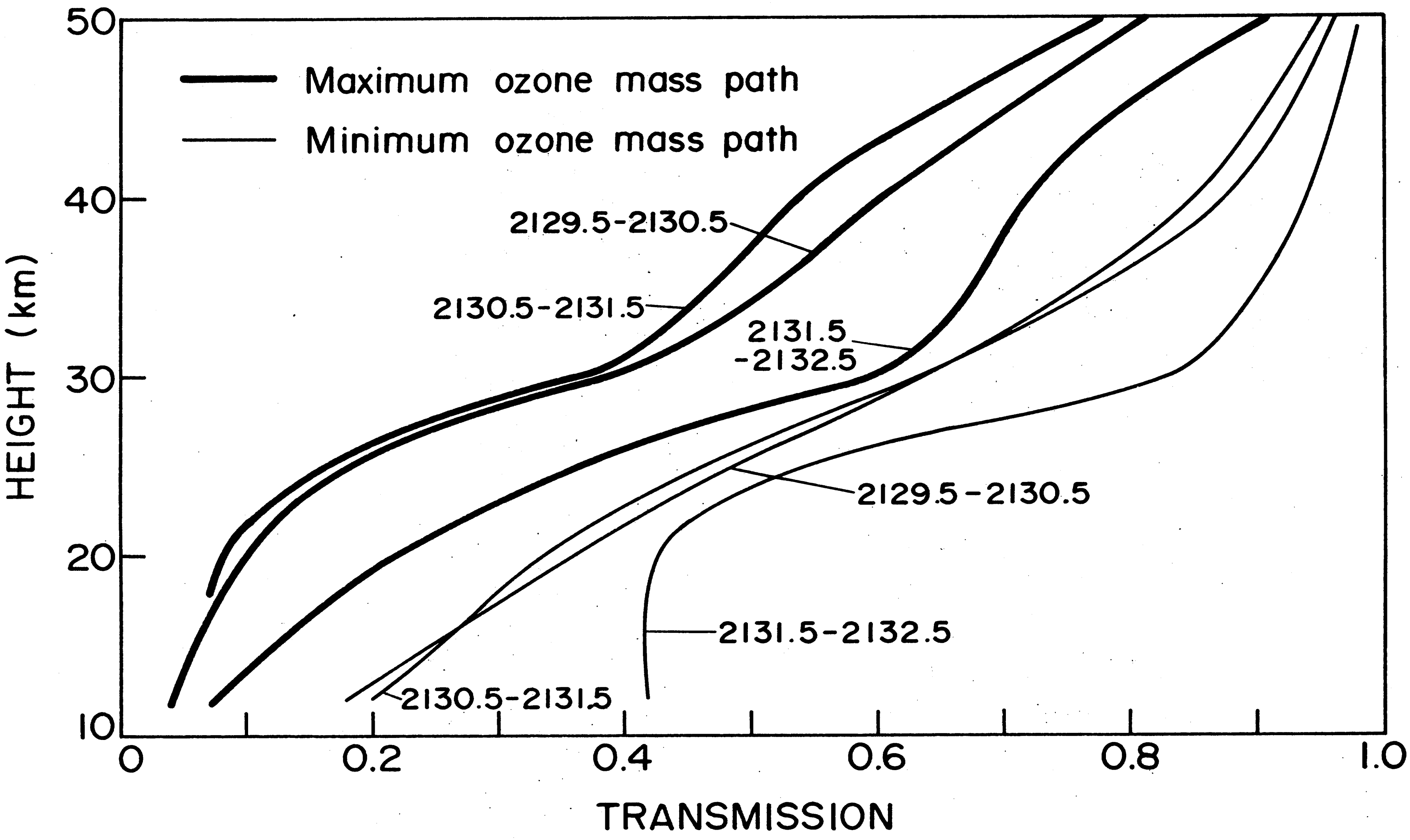

Fig. 2.5 Stratospheric tangent path transmissions for the spectral interval 3044.5 - 3047.5 cm^{-1}.

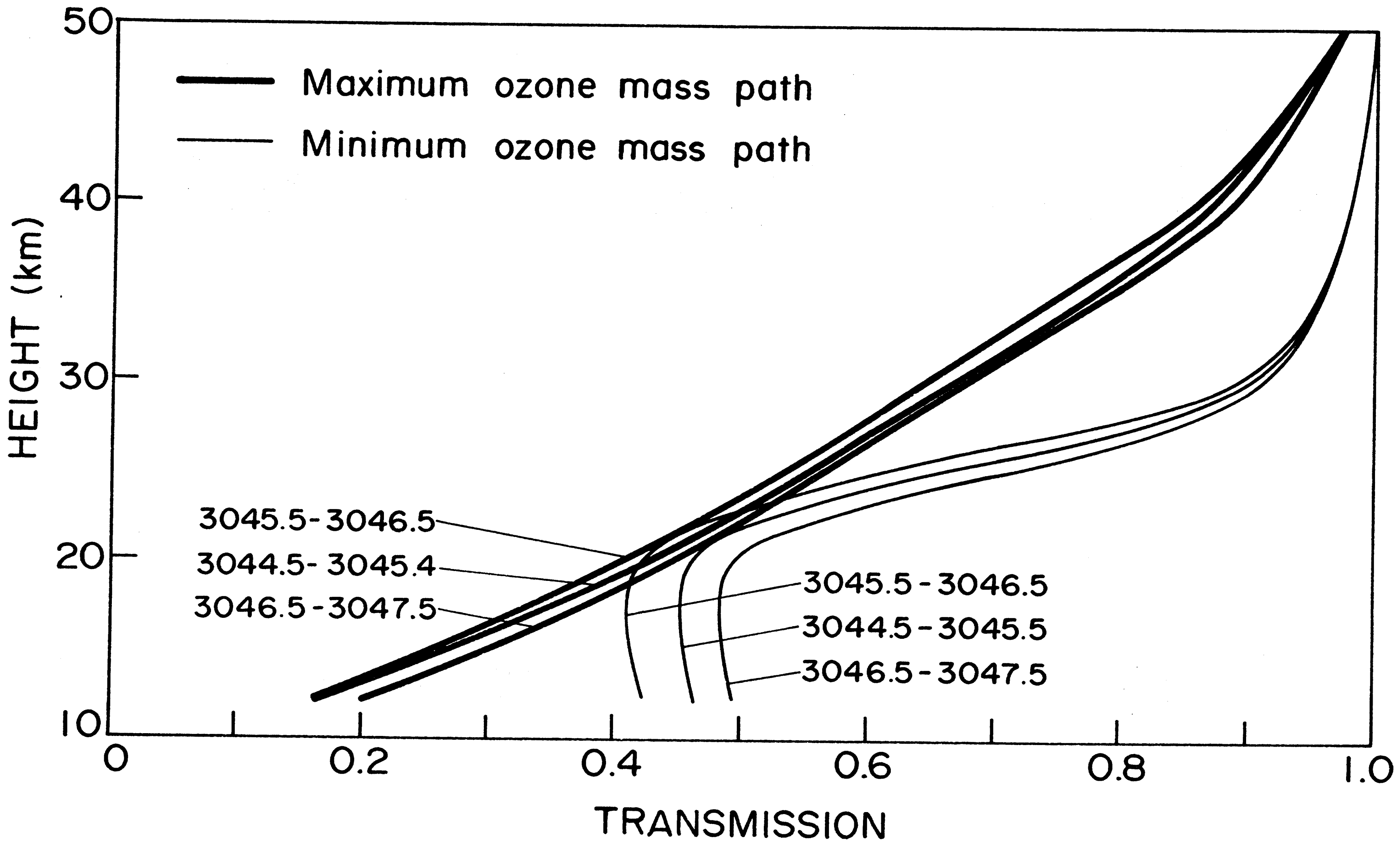

Fig. 2.6 Stratospheric tangent path transmissions for the spectral interval 3044.5-3047.5 cm^{-1}.

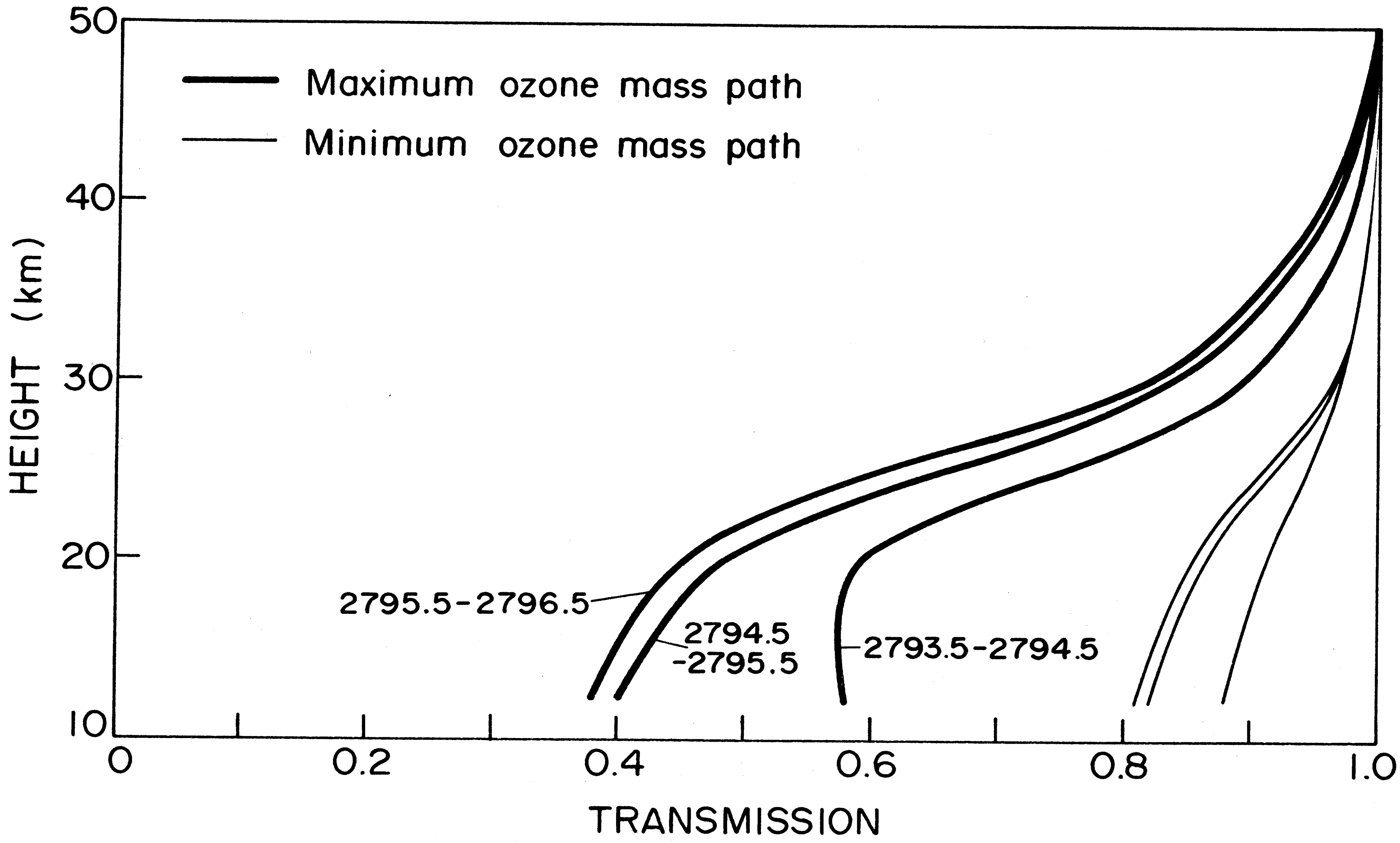

Fig. 2.7 Stratospheric tangent path transmissions for spectral interval 2793.5 -2796.5 cm^{-1}.

the actual case (see Table 2.15), then only in the low stratosphere could this band be useful for remote sensing of ozone.

<u>2793.5 - 2796.5 cm^{-1} ($\nu_1 + \nu_2 + \nu_3$)</u>

Band model transmissivities for this combination band are also much smaller than the experimental values, and are compared in Table 2.16. The line parameters were calculated by McClatchey et al. from a rigid rotor analysis and include lines for J less than 25 and K_a less than 6. The discrepancy may again be due to the distribution of intensities among the lines.

Pressure (mb)	20	66.6	66.6	400	400
Mass Path (atm·cm)	14.6	1.2	4.5	14.3	19.1
2793.5 - 2794.5 cm^{-1}	.82	1.00	.95	.83	.79
2794.5 - 2795.5 cm^{-1}	.73	1.00	.92	.74	.68
2795.5 - 2796.5 cm^{-1}	.70	1.00	.91	.71	.65
Average	.74	1.0	.93	.76	.71
Experimental (McCaa & Shaw)	.90	.99	.97	.88	.83

Table 2.16. Comparison of band model and experimental transmissivities for the 2793.5 to 2796.5 cm^{-1} spectral interval in the $\nu_1 + \nu_2 + \nu_3$ ozone band.

Stratospheric tangent path transmissivities are given in Fig. 2.7. As indicated in Table 2.16, these transmissions are probably too small; thus even in the region of maximum absorption of this band, the absorption would be small, making remote soundings difficult.

2.4 Water Vapor

Calculations similar to those for ozone have been carried out for regions of maximum or near maximum absorption in three water vapor bands. The spectral regions are given in Table 2.17.

Band	ν_2	ν_1, ν_3, etc.	$\nu_2 + \nu_3$, $3\nu_2$, $\nu_1 + \nu_2$, etc.
Wavenumber (cm^{-1})	1660-1675	3743-3753	5335-5355

Table 2.17. Spectral intervals of selected water vapor bands used in stratospheric tangent path transmission calculations.

The spectral intervals of 3743-3753 cm^{-1} and 5335 - 5355 cm^{-1} contain lines of numerous bands and a few of these are listed above. According to McClatchey, et al., the line positions are generally accurate to 0.01 cm^{-1}. Half widths for the individual lines are given, although for this analysis, we assumed a mean half width of 0.08 cm^{-1}. The spectral interval of 1660-1675 cm^{-1} contains 59 lines and was subdivided into three 5 cm^{-1} intervals. The spectral region around 3700 cm^{-1} is highly structured and the interval was divided into two 5 cm^{-1} subintervals; the total number of lines is 82. The 5335 to 5355 cm^{-1} interval was divided into two 10 cm^{-1} subintervals containing 110 lines. These spectral intervals were chosen so as to be compatible with the experimental resolution of Burch et al. (1962), whose data were used for comparison with the band model calculations.

The model atmosphere used for deducing the tangent path transmissivities is given in Table 2.18.The extreme mass paths were taken from the previous report.

Tangent Height (km)	Pressure (mb)	Temperature °K	Mass Path (atm· cm)
12	134 - 113	217 - 218	72.0 - 33.1
20	38.2 - 31.8	220 - 221	40.9 - 9.45
30	8.31 - 8.5	232 - 231	14.5 - 2.01
40	2.0 - 2.06	255	2.85 - .46
50	.56 - .575	266 - 267	.64 - .12

Table 2.18. Curtis-Godson pressures and temperatures for selected tangent heights for extreme water vapor mass paths.

1660 - 1675 cm^{-1} (ν_2)

A comparison of the band model transmissions with the experimental data of Burch et al. (1962) for the 1660 - 1675 cm^{-1} spectral interval is shown in Table 2.19. The agreement is excellent with the average of the band model results agreeing to within three percent of the experimental values. The absorption profiles are complex as can be seen from Table 2.19; in the one case the absorption varies by twenty-six percent in adjacent spectral intervals. Thus the spectral interval must be carefully chosen if this band is to be used for remote sensing.

Mass Path (atm· cm)	2.12	21.9	44.7	43.8	95.8
Pressure (mb)	18.7	140	50.6	140	1070
1660 - 1665	.944	.591	.623	.445	.000
1665 - 1670	.926	.444	.456	.275	.000
1670 - 1675	.946	.665	.698	.536	.007
Experimental (Burch et al.)	.94	.57	.62	.42	.0

Table 2. 19. A comparison of band model transmissivities with data of Burch et al. (1962) for the water vapor spectral interval of 1660 to 1675 cm^{-1} (ν_2).

The stratospheric tangent path transmissions for two spectral regions in the ν_2 band are given in Fig. 2.8. The 1538 - 1544 cm^{-1} region is representative of maximum absorption in the band. The transmission is near one-hundred percent in the upper stratosphere and remote soundings are questionable. A smaller spectral interval would be desirable if the available energy is adequate. Numerous other spectral regions in this band would be adequate for remote soundings at least up to the midstratosphere, e.g., the 1660 - 1675 region, which is also shown in Fig. 2.8.

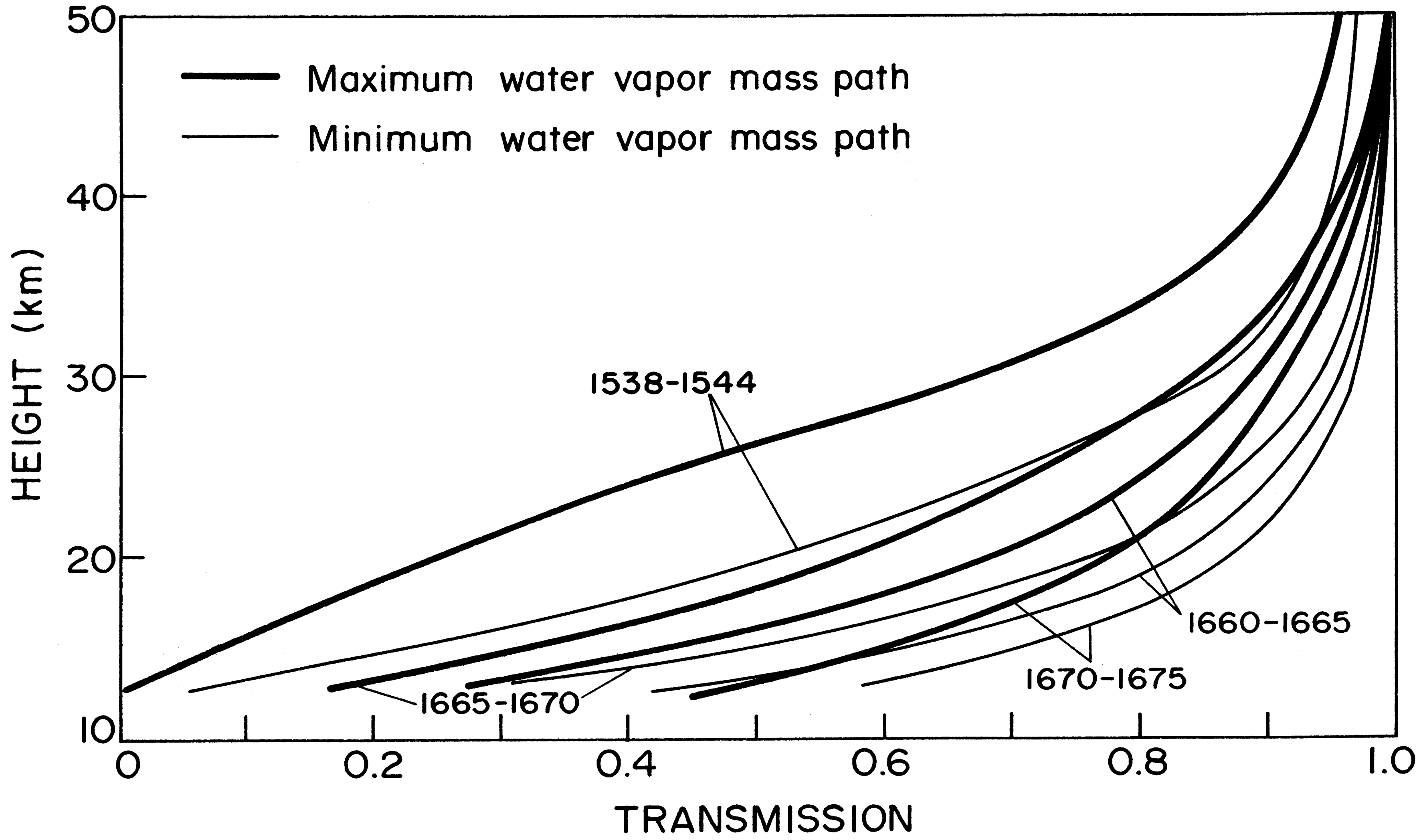

Fig. 2.8 Stratospheric tangent path transmissivities for water vapor for the spectral intervals of 1660-1675 cm^{-1} and 1538 -1544 cm^{-1}.

$3743 - 3753 \, cm^{-1}$ spectral region

As mentioned previously, this spectral region contains lines of many bands, and the absorption spectra are extremely complex (see, e. g , Burch et al., 1962). Also Burch et al. give the resolution of their absorption profiles as approximately 10 cm^{-1}; thus there is probably an uncertainty of at least a few wavenumbers. Both these factors make comparison of the band model transmissions with their data rather difficult. However, we have attempted a comparison which is shown in Table 2. 20. The band model transmissions are significantly

Pressure (mb)	1150	1043	151.	92.	36. 7
Mass Path (atm-cm)	135	4. 42	146.	4. 42	4. 42
$3743 - 3748 \, cm^{-1}$	0	. 09	0	. 51	. 64
$3748 - 3753 \, cm^{-1}$	0	. 10	0	. 51	. 60
Experimental (Burch et al.)	0	. 26	. 03	. 57	. 78

Table 2. 20 Comparison of band model and experimental transmissitivities for water vapor lines in the 3743 to 3753 cm^{-1} spectral interval.

lower but this was anticipated since the spectral interval was chosen to maximize the absorption. The spectral interval could be increased about 2 cm^{-1} without significantly increasing the absorption, and this increase would be well within the resolution range. Thus the comparison neither justifies nor negates the band model and/or line parameters.

Tangent path transmissivities are shown in Fig. 2. 9. If the contribution to the transmission from other molecular species is not large, then this band could be used for remote sensing of water vapor, at least in the lower stratosphere.

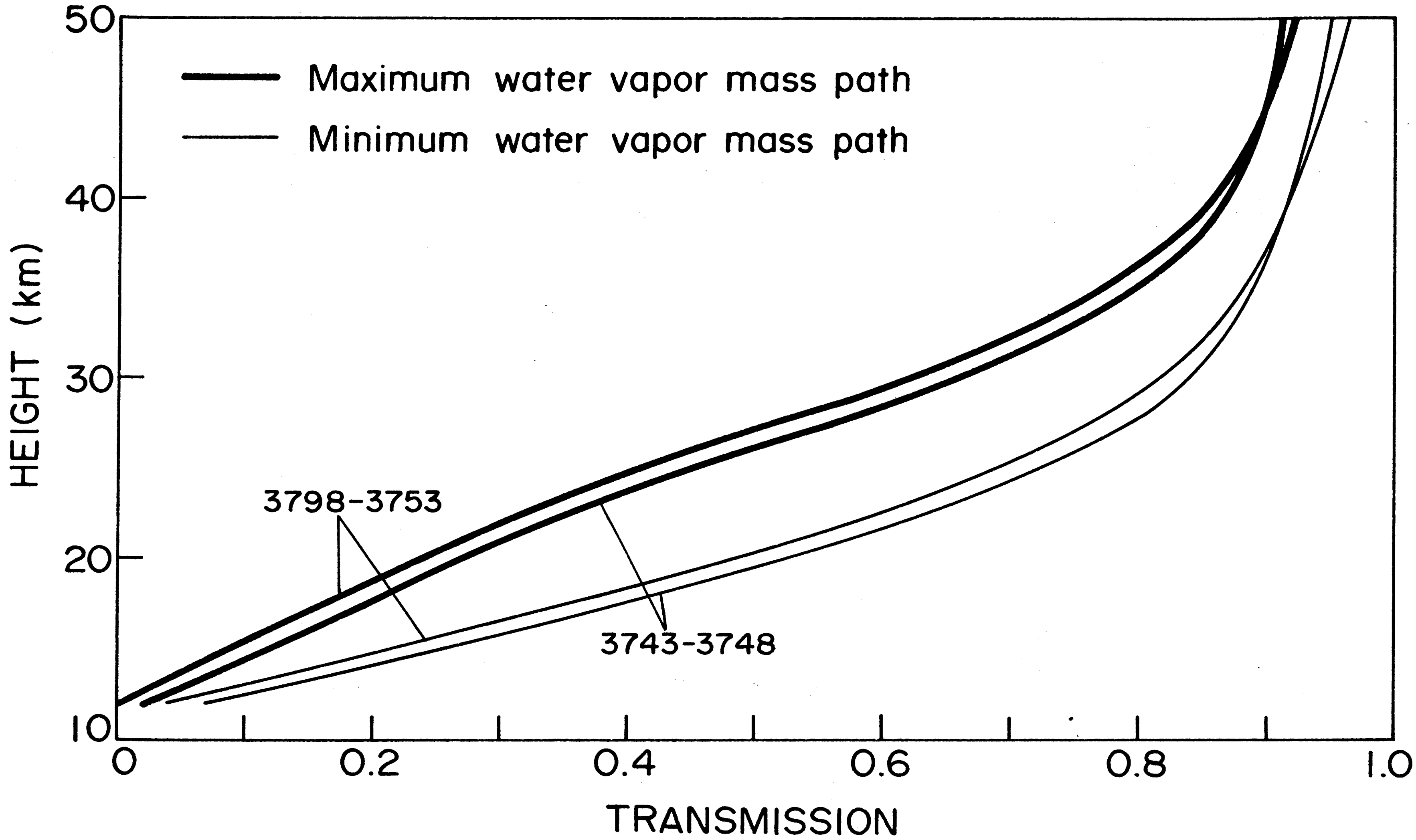

Fig. 2. 9 Stratospheric tangent path transmissivities for the 3743-3753 cm^{-1} spectral region.

5335 - 5355 cm^{-1} spectral region

Results of the analysis for this spectral region are quite similar to those for the 3743 - 3753 cm^{-1} region. The band model transmissions are smaller than Burch et al's results, but again, the model was chosen to give maximum absorption, which appears as a narrow peak in the Burch et al. absorption profile. Also the resolution is given as "approximately 20 cm^{-1}, and if it is only slightly larger, the transmission will decrease significantly. The tangent path transmissivities are given in Fig. 2. 10, and indicate that this band is not suitable for remote sensing of water vapor. Only in the low stratosphere is there significant absorption and in this height range the 1600 cm^{-1} spectral region could be used which contains fewer lines from other molecular species.

2.5 Methane

Although an extensive analysis on the feasibility of detecting methane by the solar occultation technique has not as yet been completed, our preliminary study seems promising. The strongest bands are the ν_3 (3019 cm^{-1}) and ν_4 (1306 cm^{-1}) fundamentals with strengths of 370 and 204 $atm^{-1}cm^{-2}$ respectively. A difficulty is that the line parameters need improvement, especially in extending the calculations to higher rotational quantium numbers and improving the intensities. Thus a detailed comparison with experimental transmissivities has not been made.

The stratospheric tangent path transmission for a single spectral interval is given in Fig. 2. 11 which represents a region of maximum absorption in the ν_4 band. This band model calculation

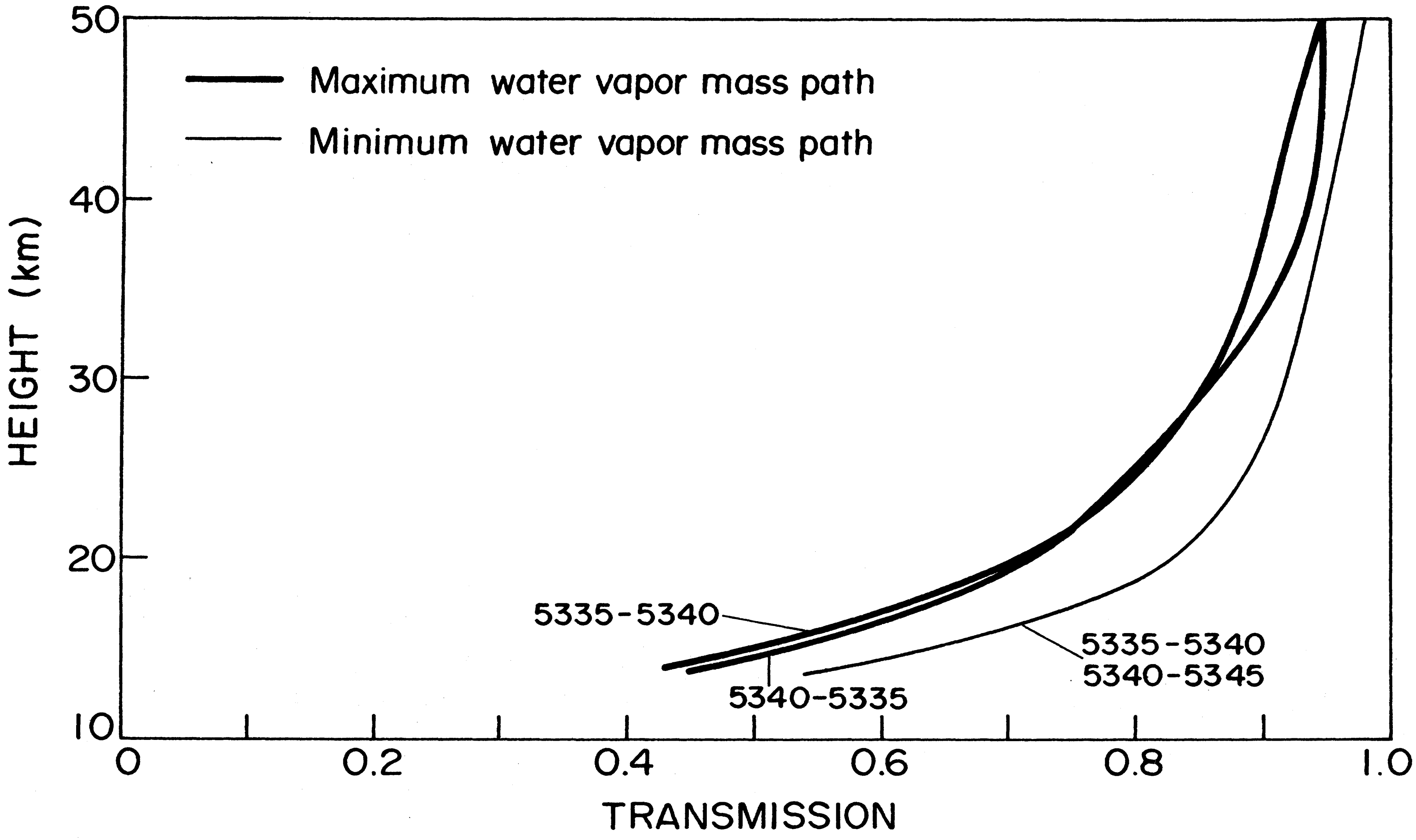

Fig. 2.10 Stratospheric tangent path transmissivities for water vapor in the 5335-5345 cm^{-1} region.

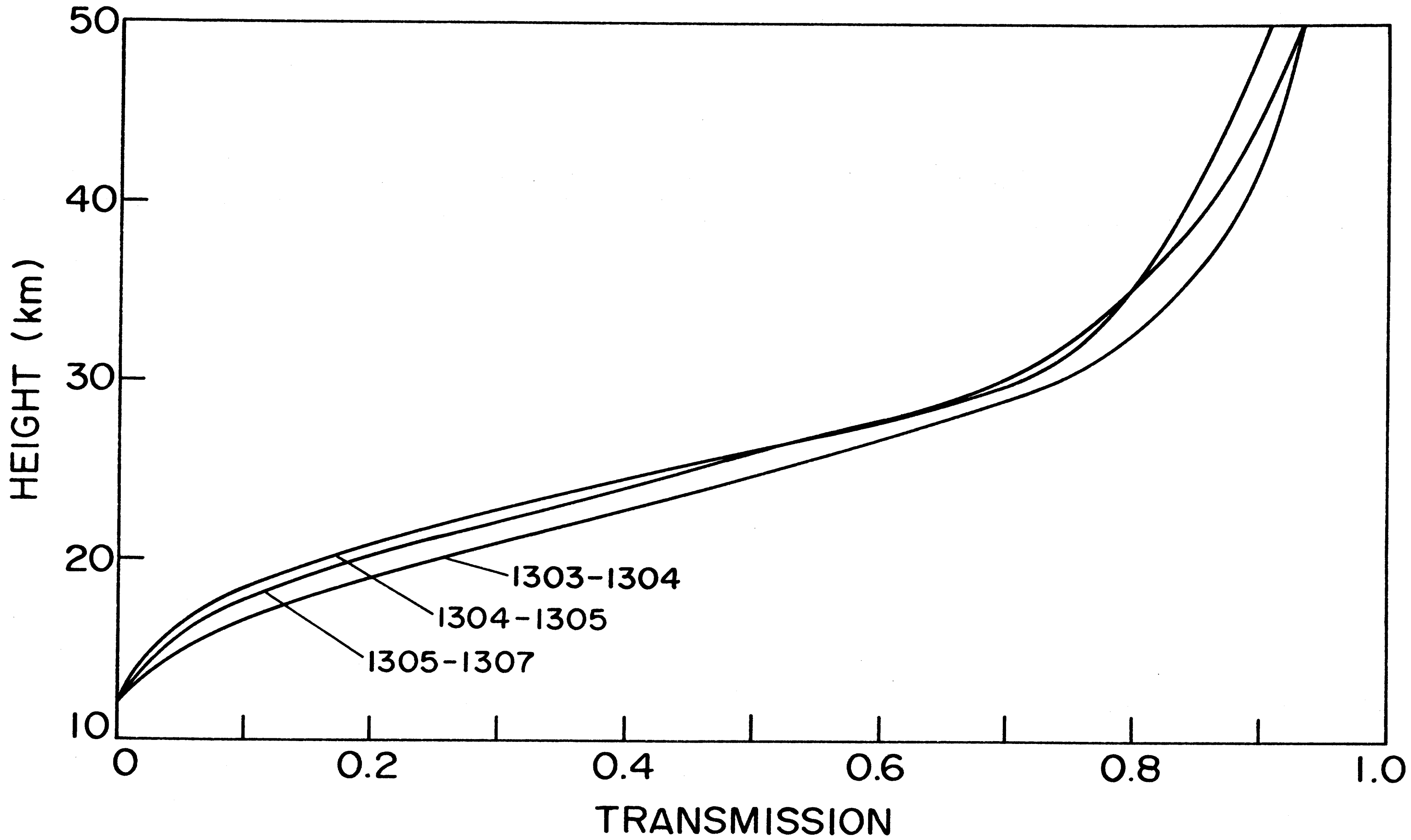

Fig. 2.11 Stratospheric tangent path transmissivities for the 1304-1307 cm^{-1} region of methane.

indicates that remote sensing may be feasible throughout much of the stratosphere. One must keep in mind, however, that the tabulation of McClatchey et al. excludes numerous weak lines which may significantly alter the atmospheric absorption.

None of the stronger bands of methane is in a spectral region free from interference by other molecules. Nitrous oxide absorbs in the ν_4 band and ozone overlaps the ν_3 band so that these gasses would have to be sounded simultaneously. The best region would appear to be in the ν_4 Q-branch between 1304 and 1307 cm^{-1} (see Fig. 2. 11). The width of this channel is critical and there is overlap with N_2O. At 1350 cm^{-1} the absorption by CH_4 is less by about a factor of two, but the problem of overlap is less severe. Alternatively the Q-branch of the ν_3 band (3016 - 3019 cm^{-1}) can be used while the region near 2960 cm^{-1} has less absorption but also less interference by ozone.

2. 6 Carbon Monoxide

Assuming various constituent profiles, calculations of atmospheric transmittances have been made. Table 2. 21 shows the effect of slight changes in concentration of CO on the atmospheric transmittance. The calculations shown are for 2 model CO profiles, at a resolution of 5 cm^{-1} at the spectral region 2173 cm^{-1} near the peak of the R branch of the fundamental 4. 6μm band. The second model constituent profile is 10% higher than the profile in the first model.

The line parameters used in the calculations are from Kunde (1968). Column 4 in Table 2. 21 shows the transmission with the increased CO concentration. At low altitudes (where the spectral line is essentially Lorentz broadened) the absorption has increased by about 5% and this is consistent with the result obtained using a strong line approximation, in which the absorption is proportional to the square root of the optical mass. At higher altitudes the increase in absorption is less than 5% because Doppler broadening becomes important, and as the line centers are completely absorbed, there is lesser wing contribution. This result can be expected to hold for other molecules in spectral regions where the lines are non-overlapping along the absorption paths.

The region near 2173 cm^{-1} also contains absorption lines of carbon dioxide and nitrous oxide. No attempt has been made to calculate the absorption by these gasses but some interference can be expected because of the low stratospheric mixing ratios of CO. The 2-0 band of CO is much weaker and would be difficult to use. Hence the region near 2173 cm^{-1} appears to be the best choice for a CO measurement.

Tangent Height km	CO concentration Model 1 Vol. Mix.Ratio ppm	Atmospheric Transmission with Model 1	Atmospheric Transmission with Model 2 (10%inc. of CO)	Perc.Increase of Absorption
70	1.0	-	-	-
60	0.08	-	-	-
50	0.05	.99825	.99821	2.29
40	0.02	.99784	.99779	2.31
30	0.02	.99618	.99604	3.66
20	0.02	.98384	.98305	4.89
10	0.1	.85910	.85196	5.07

Table 2.21 Atmospheric Absorption by CO

2.7 Nitrous Oxide N_2O

The line parameter tape (McClatchey et. al. 1973) contains spectral line parameters for N_2O. The molecule is linear . The theory of its spectrum is well understood. In addition, many experimenters have investigated the absorption properties of the stronger absorption bands, so that the parameters on the tape should be fully adequate for the calculations described here.

The strongest of all the N_2O bands is the ν_3 centered near 2223.8 cm^{-1}, and is a factor of seven more intense than the next strongest band, the ν_1 centered at 1284.9 cm^{-1}. The maximum stratospheric absorption by the ν_3 band occurs at the peak of the P and R-branches is near 2210 and 2236 cm^{-1} respectively. Calculations in these two spectral regions were made using the line-by-line program described in the Appendix. Carbon dioxide also absorbs in this region and similar calculations were made of the transmittance of this gas. Carbon monoxide lines of the 1-0 band also occur near 2210 cm^{-1} but these are weak and were not considered here. Water vapor absorption is small under stratospheric conditions.

Figure 2.12 shows the transmittances for N_2 O and CO_2 for 4 cm^{-1} intervals centered at 2210.5 and 2236.5 cm^{-1}. The N_2O concentrations are from Table 4.1.3 of our earlier report (Drayson et. al., 1972) and the U. S. Standard Atmosphere (1962) has been used. The CO_2 concentration is assumed constant at 320 ppm V.

The N_2O transmittances are almost identical for the two intervals but the CO_2 transmittance is remarkably higher at 2210.5 cm^{-1} making this the clear choice of a spectral region to sound N_2O. It should be pointed out that there may be some uncertainty in the line

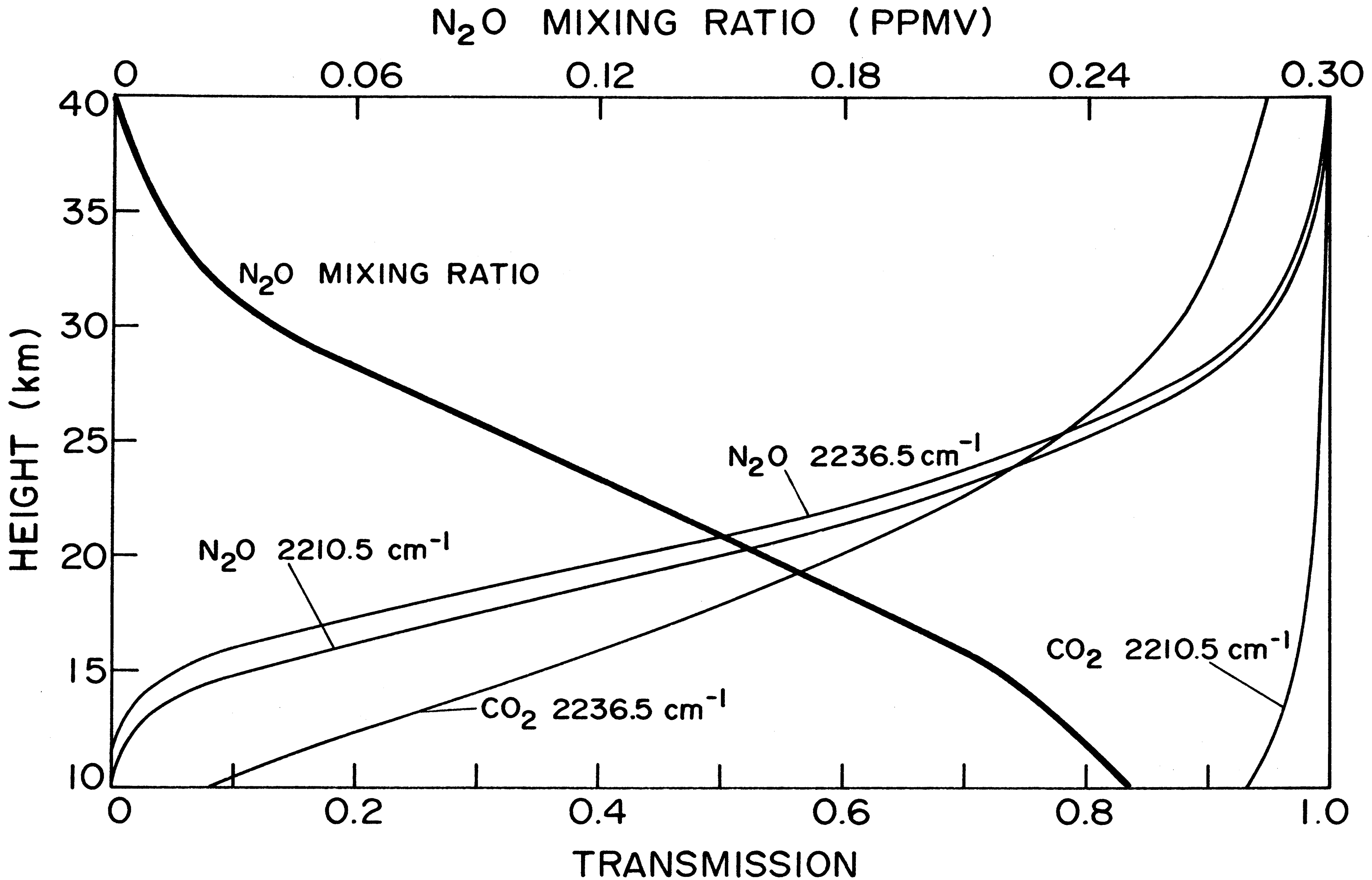

Fig. 2. 12 Stratospheric Tangent path transmittance of N_2O and CO_2.

parameters of CO_2 since hot bands dominate the absorption in these regions and the intensities of the bands have a higher degree of uncertainty than the fundamentals. At 2236.5 cm^{-1} the carbon dioxide band with the most intense lines appears to have been included twice on the tape so the transmittance may in fact be higher than indicated.

Another possible spectral region for sounding N_2O is near 1270 cm^{-1} (R-branch of the ν, band) which gives considerably less absorption and has some interference by CH_4 absorption. The ν_2 band is much weaker than either the ν_1 or ν_3 bands but has the advantage of closely spaced lines in the Q-branch near 590 cm^{-1}. However absorption by CO_2 is again strong and a rough estimate showed the CO_2 absorption to be at least as large as the N_2O throughout the stratosphere.

The peak of the P-branch of the ν_3 band of N_2O near 2210 cm^{-1} appears to be the best spectral region for sounding N_2O. The instrument resolution and exact wavenumber are not critical factors and the interference by other molecules is minimal.

REFERENCES

Aida, Masaru, 1973: The spectral absorptivity by the 9.6 micron ozone band. Paper presented at the Radiation Commission in Sendai, Japan, Data tape containing Aida's band parameters was provided by Dr. James Russell, Langley Research Center.

Burch, D. E., D. A. Gryvnak, E. B. Singleton, W. L. France and D. Williams, 1962: Infrared absorption by carbon dioxide, water vapro and minor atmospheric constituents. AFCRL-62-698 Air Force Cambridge Res. Labs.

Clough, S. A., and F. X. Kneizys, 1965: Ozone absorption in the 9.0 micron region. AFCRL-65-862 or Physical Sciences Research Paper no. 170, 79pp.

Clough, S. A. and F. X. Kneizys, 1966: Coriolis interaction in the ν_1 and ν_3 fundamentals of ozone. J. Chem. Phys. 44, 1855-1861.

Drayson, S. R., F. L. Bartman, W. R. Kuhn and R. Tallamraju, 1972: Satellite measurements of stratospheric pollutants and minor constituents by solar occultation: A preliminary report. High Altitude Eng. Lab. Tech. Report No. 011023-1-T. University of Michigan. 143 pp.

Drayson, S. R., 1973: A listing of wavenumbers and intensities of carbon dioxide absorption lines between 12 and 20 μm. Technical Report 036350-4-T, University of Michigan.

Kunde, V. G., 1967: Tables of Theoretical Line Positions and Intensities for the $V = 1$, $V = 2$ and $V = 3$ Vibration-Rotation Bands of $C^{12}O^{16}$ and $C^{13}O^{16}$. NASA TMX-63183.

McCaa, D. J. and J. H. Shaw, 1967: The Infrared Absorption Bands of Ozone. AFCRL-67-0237, 93pp.

Walshaw, C. D., 1955: Line widths in the 9.6 μ band of ozone. Proc. Phys. Soc. A, 68, 530-534.

Walshaw, C. D. 1957: Integrated absorption by the 9.6 μ band of ozone. Quart. J. Roy. Meteor. Soc. 83, 315-321.

Wyatt, P. J., V. R. Stull, and G. N. Plass, 1962: Quasi-random model of band absorption, J. Opt. Soc. Amer., 52, 1209-1217.

Chapter 3. Extinction of Infrared Solar Radiation by Aerosols on a Tangent Path Through the Stratosphere

3.1 Introduction

In order to determine the effect of aerosols on a beam of infrared radiation, it is necessary to know the complex index of refraction of the aerosol and its particle size distribution. Since the stratospheric aerosol probably contains several or all of the following constituents; H_2SO_4, $(NH_4)_2SO_4$, H_2O_2, HNO_3, $NOHSO_4$ and HNO_3 - H_2SO_4 - H_2O (Remsberg, 1971) a precise calculation would involve knowing the relative amounts, particle size distribution and complex index of refraction of each of these constituents.

As an initial calculation, the infrared extinction due to two greatly simplified models of stratospheric aerosol, containing only aqueous solutions of sulfuric acid (Remsberg, 1973), was determined.

3.2 The Aerosol Model

The stratospheric aerosol model discussed by Remsberg (1973) was used in this calculation. It is a bi-model distribution described by the equations (see also fig. 3.1):

$$\frac{dN}{d(\log r)} = 10^4 \qquad 0.03 \leq r \leq 0.05\ \mu m \qquad (3.1)$$

$$\frac{dN}{d(\log r)} = 10^{+3.72} r^{+4.19} \qquad 0.1 \leq r \leq 0.3\ \mu m \qquad (3.2)$$

$$\frac{dN}{d(\log r)} = 10^{-0.474} r^{-3.82} \qquad 0.3 \leq r \leq 1\ \mu m \qquad (3.3)$$

The particle number density in each size range, obtained by integrating the above equations, and the mass density in each size range, obtained from:

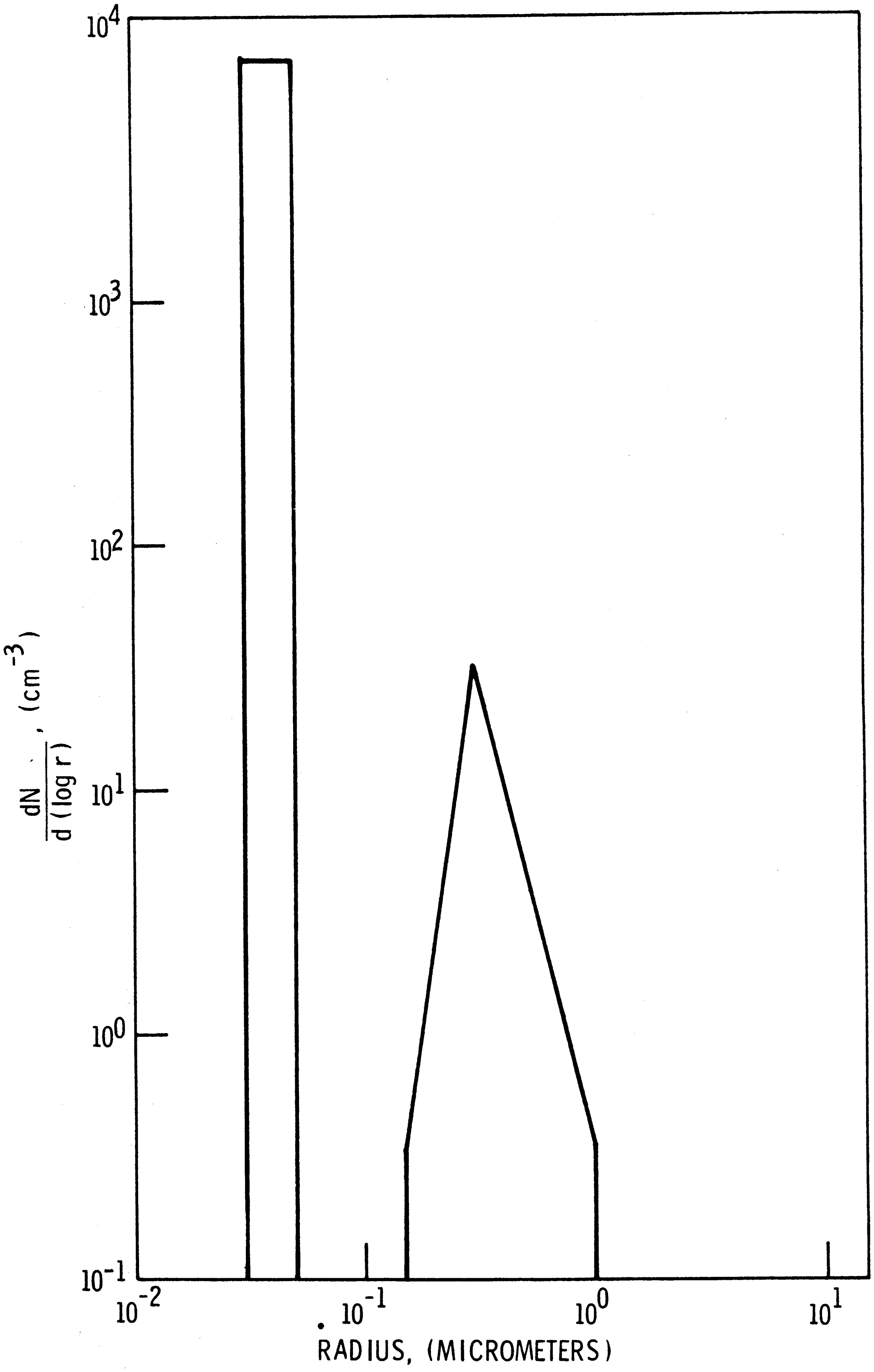

Fig. 3.1 Bi-model aerosol size distribution used for tangent path extinction calculations (after Remsberg, 1973).

$$M = \frac{4}{3}\rho \int_{r_1}^{r_2} \pi r^3 \frac{dN(r)}{dr} dr \qquad (3.4)$$

with the density of sulfuric acid, $\rho = 1.8$ g/cm^3, are:

r, μm.	.03 - .05	.1 - .3	.3 - 1
N, cm.$^{-3}$	2219.4	7.99	3.76
M, gr.cm.$^{-3}$	$1.077 \cdot 10^{-12}$	$0.414 \cdot 10^{-12}$	$2.258 \cdot 10^{-12}$

The model contains a fairly large number of Aitken nuclei, however not as many as indicated by DeBary and Rossler (1970). The mass density M is intermediate between values given by DeBary and Rossler and by Lazrus (1971). The model, then, may represent an average condition in the stratosphere. Larger numbers of particles would exist after volcanic explosions.

The relative altitude distribution f_k used for this calculation is shown in figure 3.2 and is similar to that measured by Chagnon and Jung (1961). In the altitude range 17-22 km., the number of particles is the exact number(N_{max}) given by the equations 3.1 to 3.3. At all other altitudes the total number is scaled by the ratio given in figure 3.1 (i.e. $N = f_k N_{max}$) however the relative size distribution is not changed. Note that the aerosol density has been assumed to be constant in one kilometer layers.

The length of a slant path through a 1 km spherical shell layer in the atmosphere is given by (neglecting refraction) (Drayson, et. al. 1972).

$$\Delta X_k = 2 \left(\sqrt{R_{k+1}^2 - R_o^2} - \sqrt{R_k^2 - R_o^2} \right) \qquad (3.5)$$

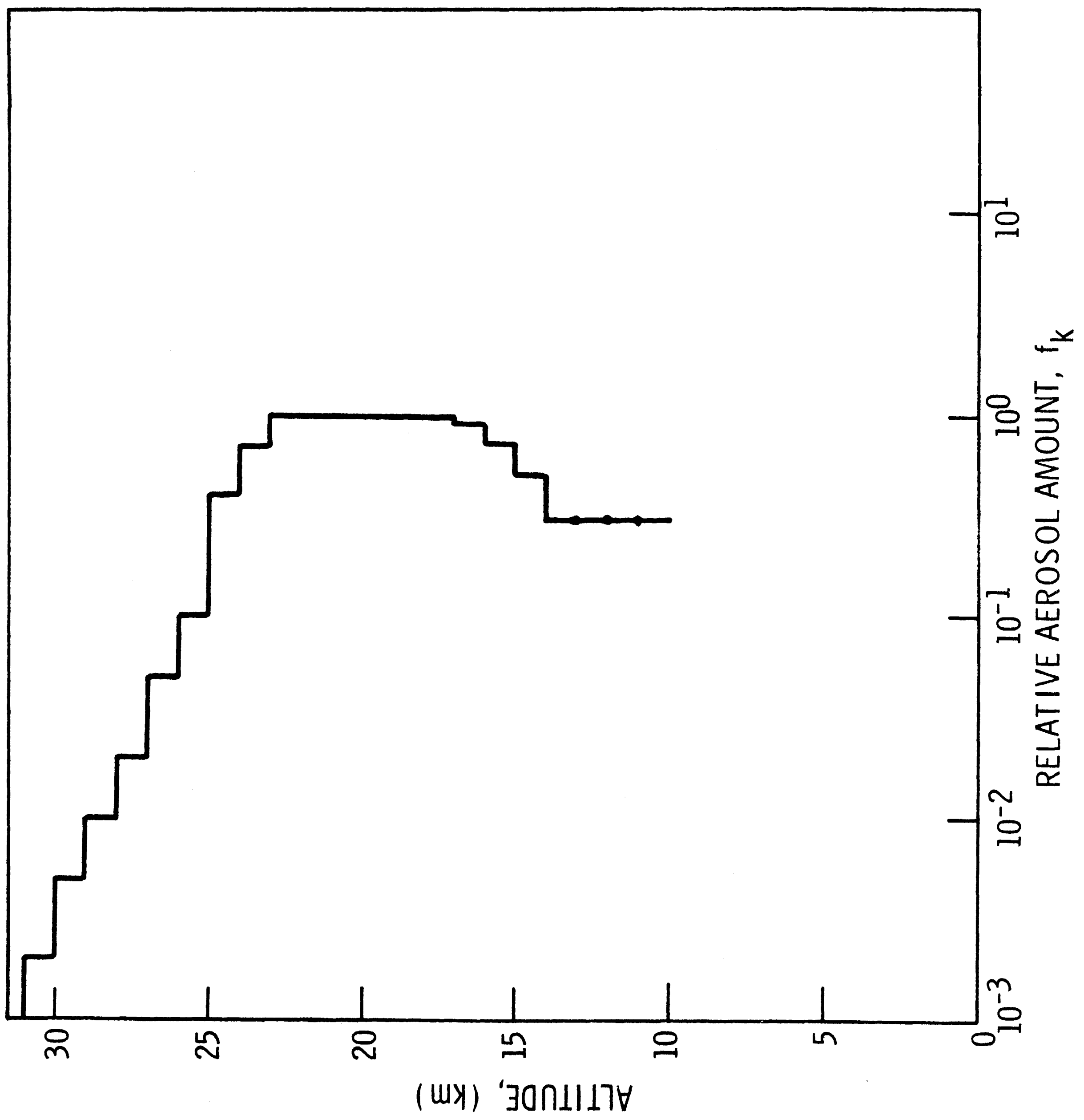

Fig. 3.2 Relative altitude distribution of aerosols, f_k, used for tangent path extinction calculations.

between the altitudes specified by radial distances R_{k+1} and R_k. The total amount of aerosol traversed along the tangent path is:

$$D = \sum_k f_k \; \Delta X_k \tag{3.6}$$

where D has units equal to km. of aerosol of number density given by equations 3.1 to 3.3. That is, equivalent km. of aerosol at the concentration N_{max}. A curve of the values of D versus tangent altitude is given in figure 3.3. It can be noticed that the shape of D vs. tangent altitude is vaguely similar to the curve of f_k vs. altitude.

3.3 Optical Characteristics of Aqueous H_2SO_4

Values of the real and imaginary parts of the complex index of refraction of 75% and 90% aqueous solutions of H_2SO_4 (Remsberg, 1971) are given in table 3.1 and figures 3.4 and 3.5 for the wavenumber range 750 to 1570 cm^{-1}.

Extinction coefficients for the aerosol of size distribution specified above, calculated from the relation:

$$B_{ext}(\lambda) = \int_{r_1}^{r_2} \pi \, r^2 Q_{ext}(r, \lambda, \hat{n}) \frac{dN(r)}{dr} \, dr \tag{3.7}$$

where $Q_{ext}(r, \lambda, \hat{n})$ is the efficiency factor calculated from Mie theory of scattering, are given by Remsberg(1973) for 75% and 90% H_2SO_4 for the wavenumber range 750 to 1150 cm^{-1} (see figures 3.6 and 3.7).

Approximate extinction coefficients for the range 1150 to 1570 cm^{-1} were determined using relations given by Remsberg (1973), i.e.:

TABLE 3.1

Optical Constants ($\hat{n} = n - ik$) of Aqueous H_2SO_4

75% H_2SO_4

FREQ	k	n
1571.0	.14352	1.29568
1508.3	.13326	1.34542
1433.1	.14802	1.26802
1383.1	.18988	1.19644
1338.0	.27709	1.12007
1297.2	.42056	1.11362
1255.1	.52732	1.13369
1231.7	.62023	1.16010
1209.7	.69276	1.21735
1184.8	.74664	1.31945
1165.2	.79953	1.40849
1150.2	.79673	1.49183
1131.1	.74543	1.59253
1114.0	.68356	1.63027
1104.2	.64292	1.62611
1094.6	.62505	1.59725
1085.2	.61812	1.57582
1079.1	.63433	1.55688
1072.2	.66775	1.56030
1059.6	.76254	1.60811
1053.8	.79410	1.63656
1041.8	.78138	1.76056
1032.8	.74167	1.82434
1019.8	.63816	1.88088
1011.4	.57044	1.88976
1004.8	.53086	1.87327
988.9	.45388	1.83372
971.6	.41524	1.77328
951.0	.38927	1.73457
934.9	.39814	1.67112
927.2	.42728	1.64740
920.3	.48341	1.62958
907.6	.57254	1.67483
901.7	.59737	1.73149
896.0	.58872	1.78764
887.5	.55768	1.84973
871.9	.44108	1.86926
856.7	.32979	1.83481
844.5	.28252	1.80852
840.3	.31144	1.80826
828.3	.26172	1.77577
818.2	.25650	1.75167
804.4	.23696	1.72780
786.2	.23446	1.69800
765.4	.23902	1.66782
748.2	.25159	1.64731

90% H_2SO_4

FREQ	k	n	FREQ	k	n
1570.3	.06519	1.32194	1033.4	.37559	1.51173
1530.5	.06004	1.29689	1023.7	.35152	1.47172
1493.6	.05938	1.25767	1014.4	.36357	1.40098
1456.8	.07099	1.18325	1007.7	.39439	1.35505
1434.5	.08932	1.11536	1002.8	.44602	1.30615
1415.5	.16894	1.01961	997.2	.53795	1.27432
1408.6	.22500	.99501	992.4	.63043	1.27656
1395.1	.35646	1.01282	987.8	.72579	1.31102
1384.1	.43227	1.06756	981.6	.82897	1.39028
1377.7	.46363	1.10853	977.1	.90717	1.46549
1371.3	.48821	1.15374	972.7	.90743	1.56620
1358.9	.47339	1.24597	966.1	.93171	1.69371
1352.8	.46908	1.27375	961.1	.87506	1.79688
1342.8	.43757	1.30709	956.8	.83078	1.85250
1333.0	.38449	1.32172	949.9	.72717	1.92317
1321.6	.35226	1.30987	944.5	.61114	1.94337
1310.4	.33114	1.29498	938.5	.52953	1.90728
1285.5	.34575	1.25624	933.2	.47916	1.86843
1266.9	.38496	1.24231	929.4	.44649	1.83665
1247.5	.42762	1.23318	932.7	.43794	1.79859
1224.5	.49547	1.21762	918.7	.47298	1.77194
1214.2	.54171	1.22111	914.4	.50752	1.77024
1202.8	.60234	1.24946	911.4	.53047	1.78253
1195.8	.63789	1.27660	904.8	.55422	1.83406
1190.3	.67201	1.31293	901.9	.54875	1.85984
1180.8	.69002	1.38008	899.0	.52618	1.89470
1172.9	.70626	1.43635	891.6	.45885	1.93520
1163.9	.68149	1.49979	887.7	.41549	1.94322
1156.3	.67557	1.54355	883.8	.36516	1.94595
1148.9	.63875	1.58053	880.0	.33020	1.92861
1140.4	.62270	1.60280	874.7	.28120	1.90672
1136.8	.60050	1.61745	865.3	.23288	1.86844
1133.3	.56369	1.63732	859.7	.20708	1.84727
1120.6	.49683	1.66145	853.8	.20083	1.81158
1111.6	.45509	1.67053	843.6	.18622	1.76891
1102.9	.41969	1.66178	830.1	.16132	1.73590
1094.3	.38950	1.64046	819.1	.16432	1.70130
1082.9	.36166	1.61575	802.7	.15708	1.66877
1072.9	.35821	1.57053	787.7	.16121	1.63697
1065.1	.39423	1.52436	770.0	.15996	1.61359
1056.4	.40302	1.51570	754.5	.16197	1.59681
1048.9	.42562	1.51649	747.3	.17297	1.58389
1040.6	.40177	1.52266			

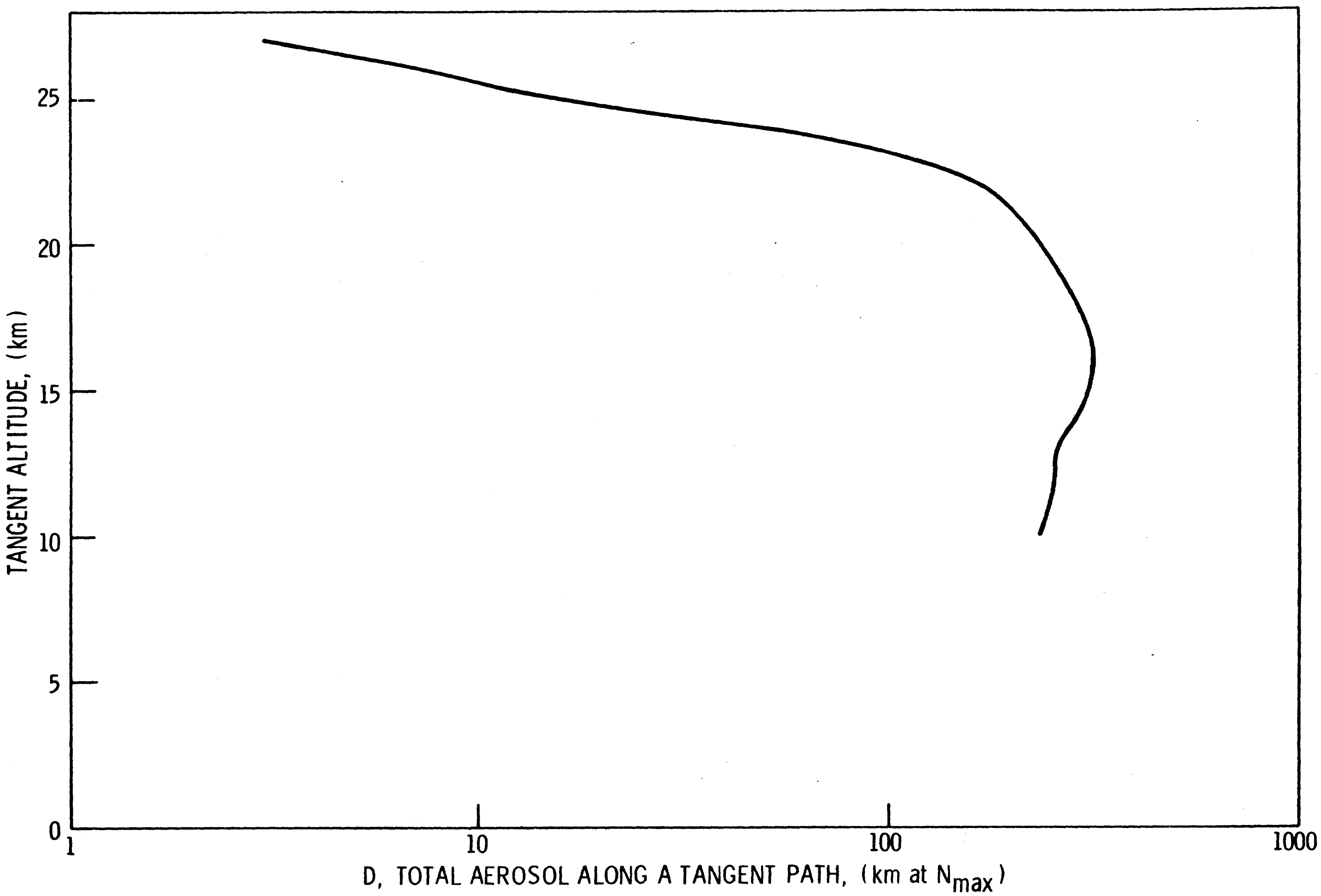

Fig. 3.3 Total aerosol, D, traversed along a tangent path.

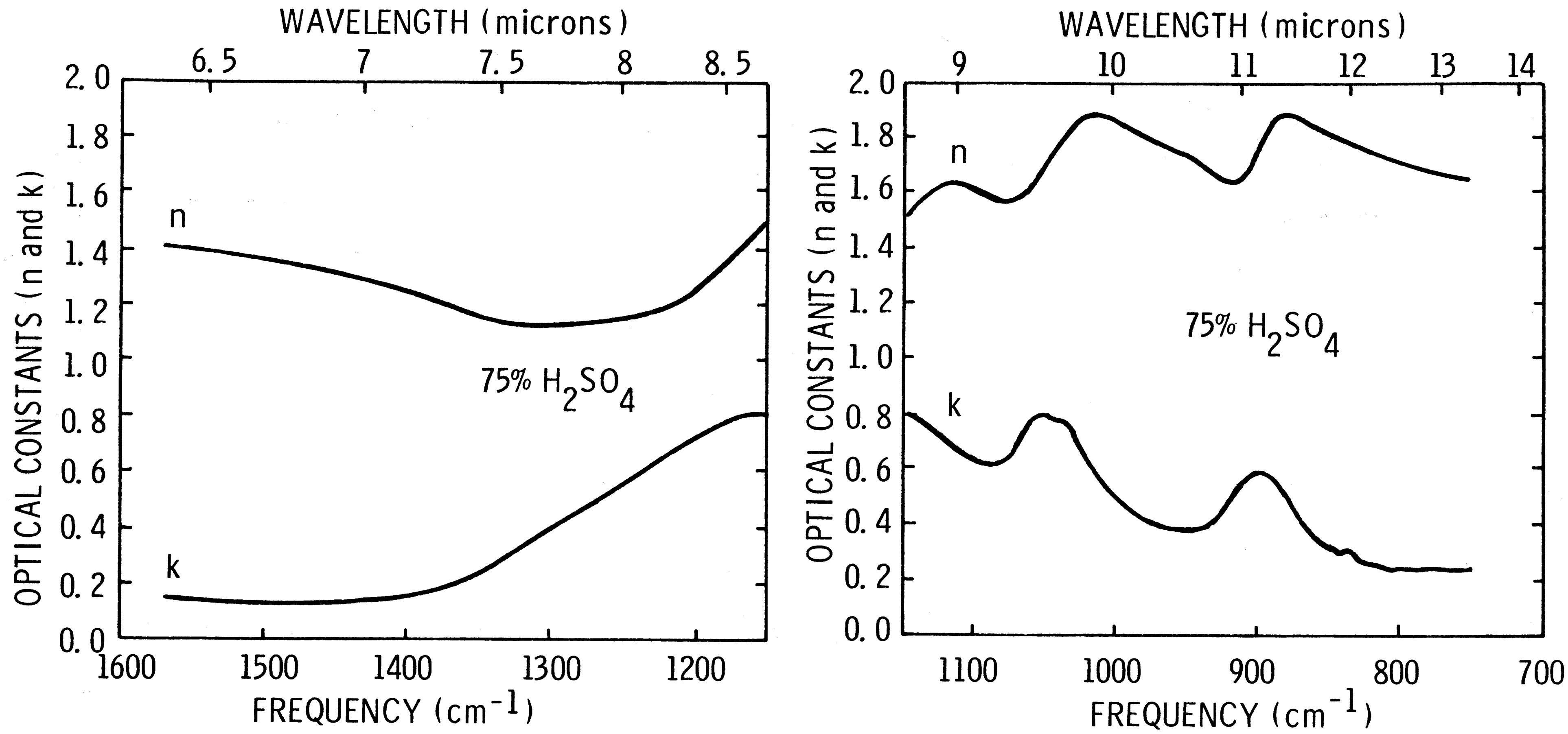

Fig. 3.4 Optical constants for 75% H_2SO_4.

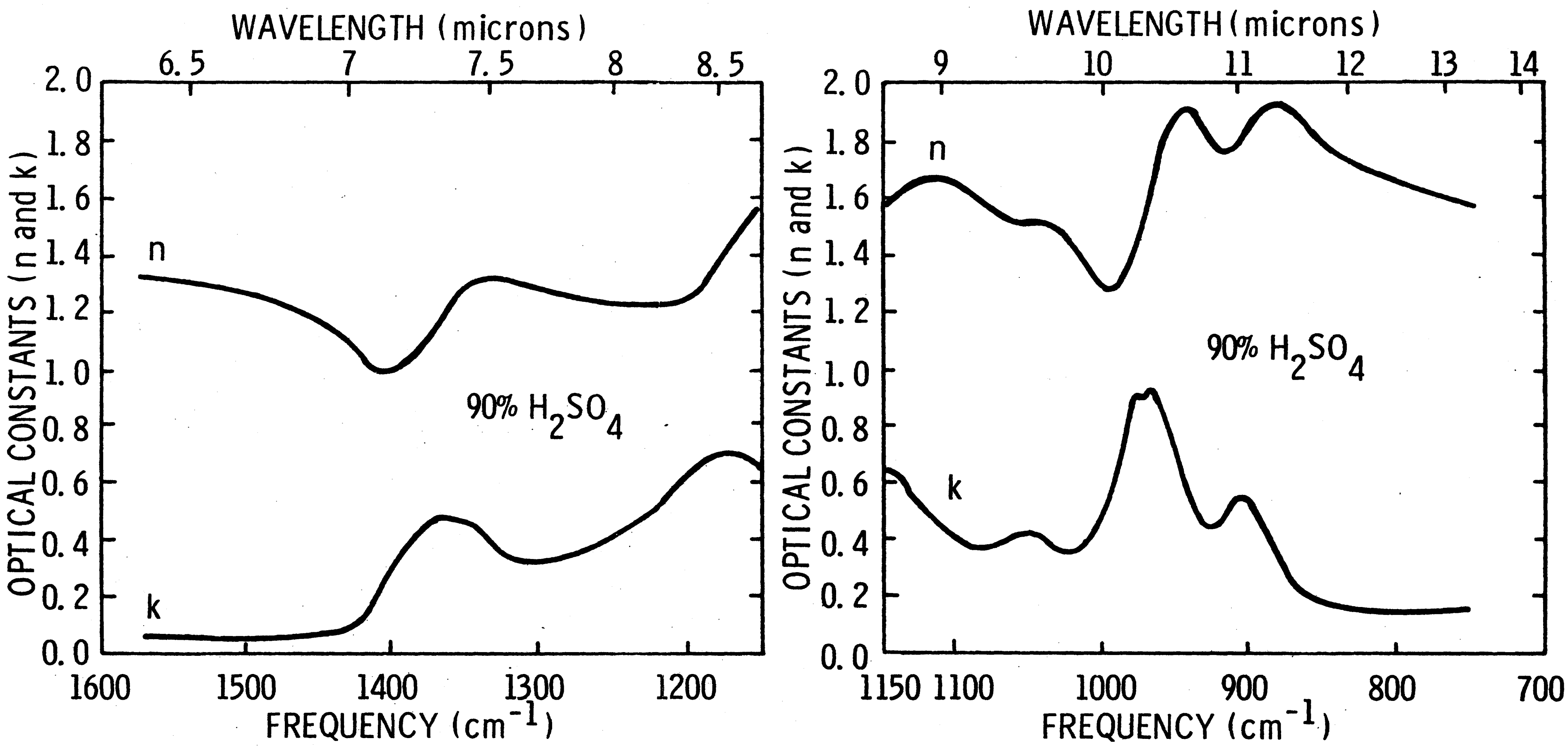

Fig. 3.5 Optical constants for 90% H_2SO_4.

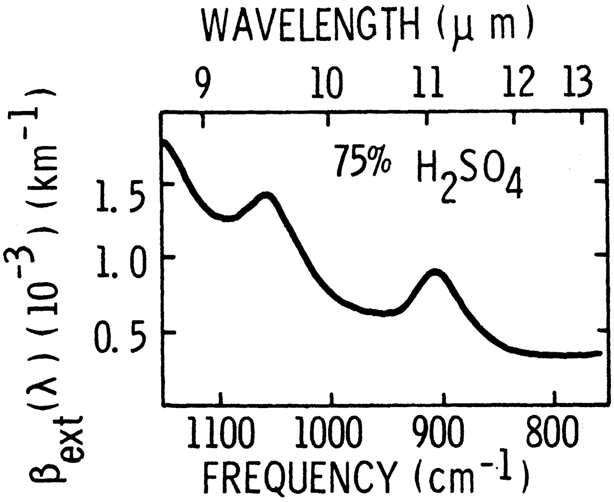

Fig. 3.6 Spectral extinction coefficient for 75% H_2SO_4 (Remsberg 1971).

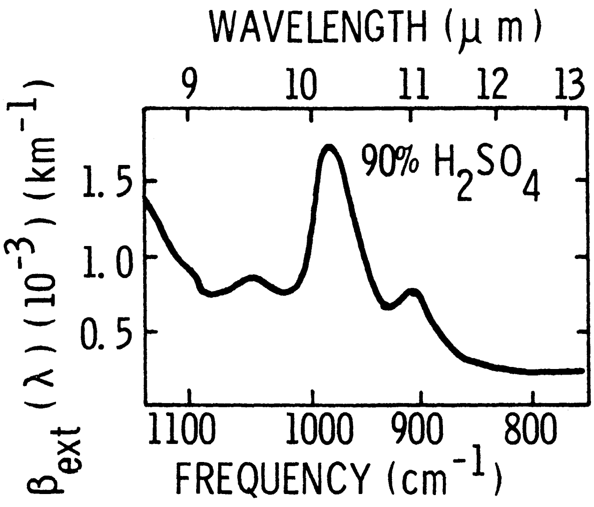

Fig. 3.7 Spectral extinction coefficient for 90% H_2SO_4 (Remsberg 1971).

$$Q_{ext} = Q_{abs} + Q_{sca} \approx Q_{abs} \tag{3.8}$$

since:

$$Q_{sca} < Q_{abs} \tag{3.9}$$

in the wavenumber range of interest. Also:

$$Q_{abs} \approx 24nk \left(\frac{2\pi r}{\lambda} \right) \left[(n^2-k^2+2)^2 + 4n^2k^2 \right]^{-1} \tag{3.10}$$

$$B_{ext}(\lambda) \approx \frac{48\pi nk}{\lambda} \left[(n^2-k^2+2)^2 + 4n^2k^2 \right]^{-1} \int_{r_1}^{r_2} \pi r^3 \frac{dN(r)}{dr} \, dr \tag{3.11}$$

then:

$$\frac{B_{ext}(\lambda_1)}{B_{ext}(\lambda_2)} = \frac{\left\{ \frac{nk}{\lambda} \left[(n^2-k^2+2)^2 + 4n^2k^2 \right]^{-1} \right\}_{\lambda_1}}{\left\{ \frac{nk}{\lambda} \left[(n^2-k^2+2)^2 + 4n^2k^2 \right]^{-1} \right\}_{\lambda_2}} \tag{3.12}$$

Approximate extinction coefficients for 75% and 90% H_2SO_4 were calculated from equation 3.12, using Remsbergs B_{ext} at 1150 cm^{-1} as a reference value. The approximate extinction coefficients calculated in this fashion are shown in figures 3.8 and 3.9, Remsbergs values and the approximate values are compared in the wavelength range 1000-1150 cm^{-1}. Note the excellent agreement in the range of overlap between the two sets of values.

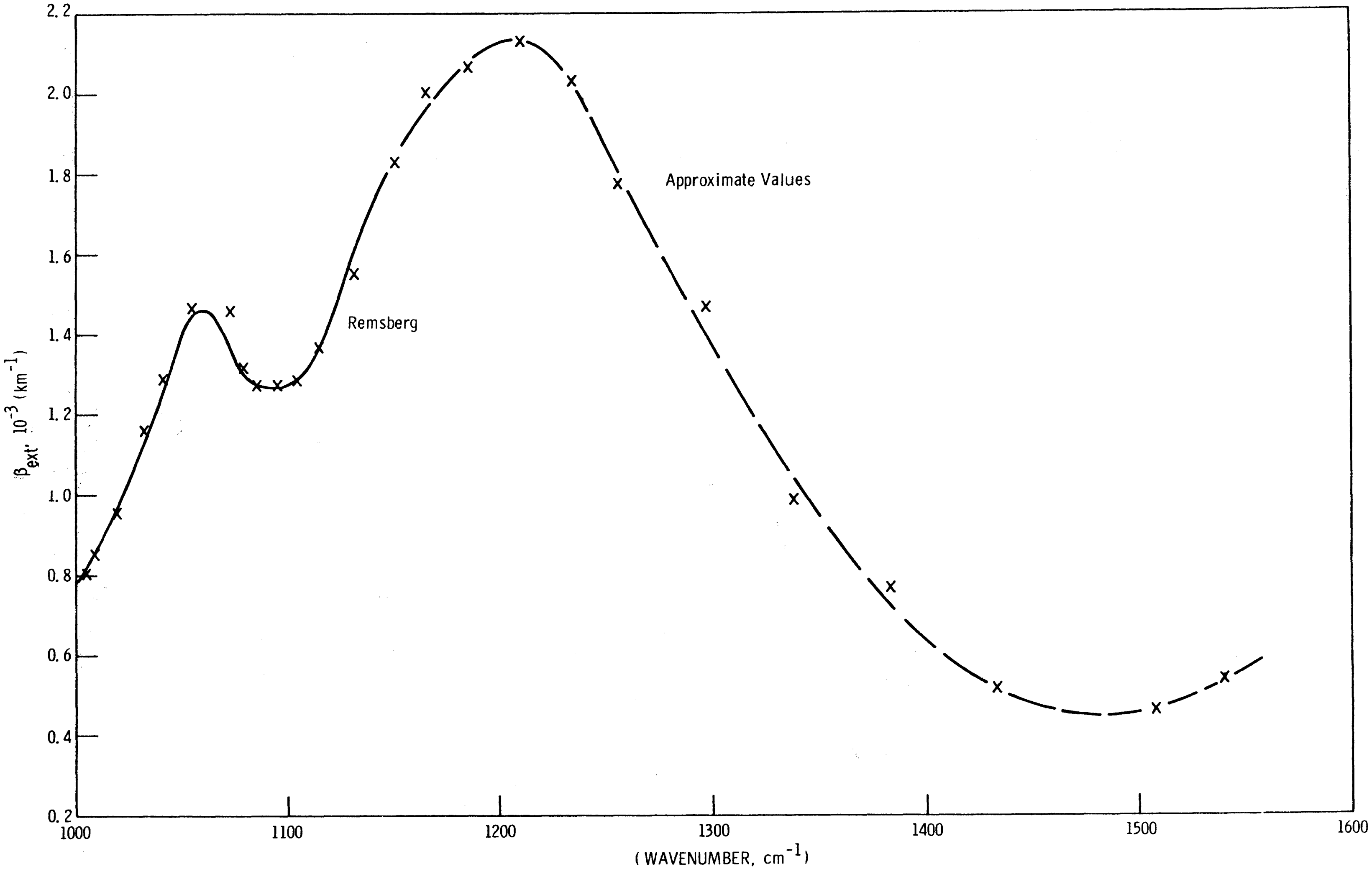

Fig. 3.8 Approximate extinction coefficients for 75% H_2SO_4.

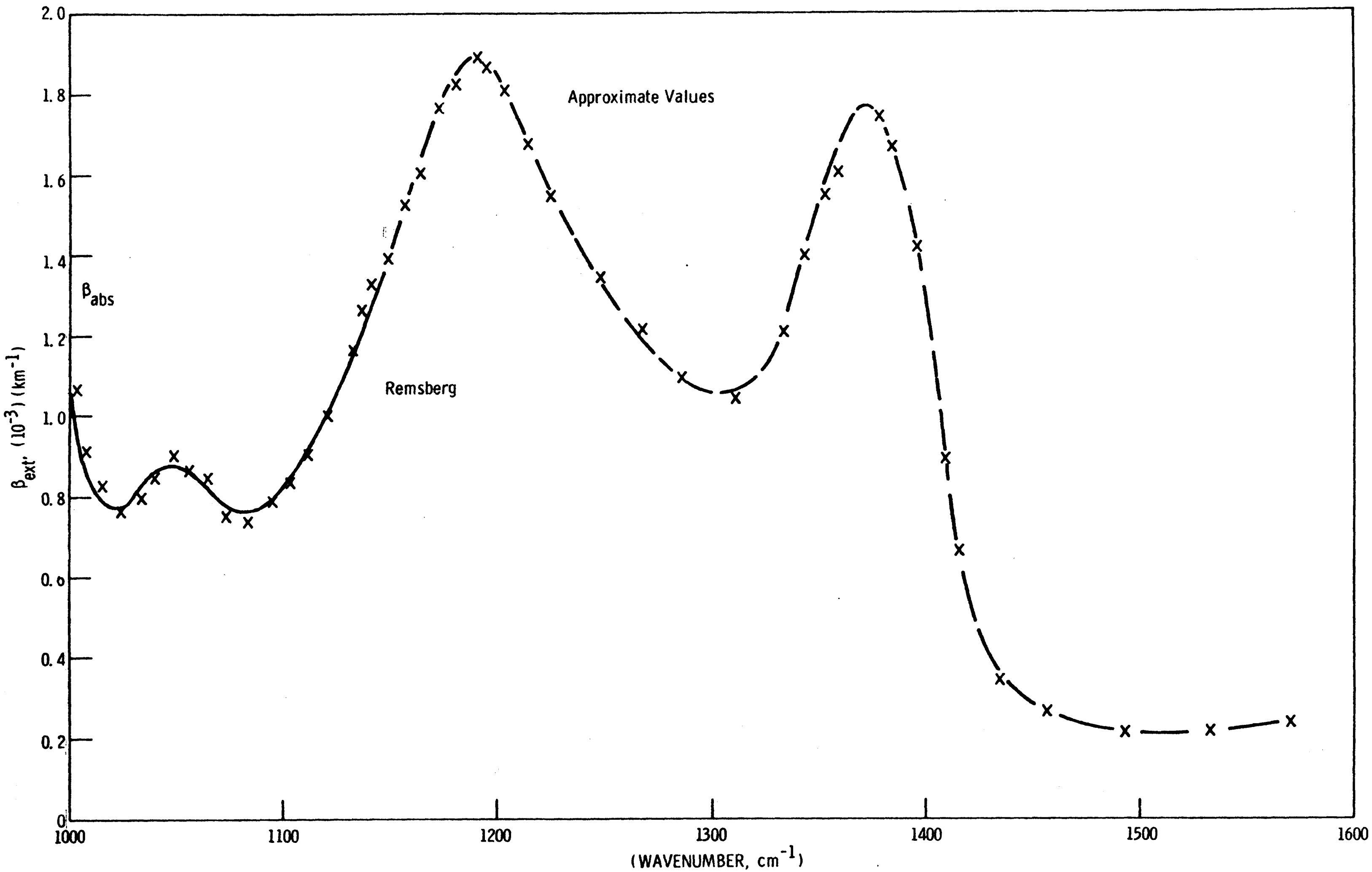

Fig. 3.9 Approximate extinction coefficients for 90% H_2SO_4.

3.4 Infrared Transmissivities along Tangent Paths

The infrared transmissivity of a tangent path through the aerosol layer was calculated by the equation:

$$T(\lambda) = \exp\left[- B_{ext}(\lambda) \cdot \sum_k f_k \; \Delta X_k \right] \tag{3.13}$$

for several paths tangent in the range of altitudes 16-26.6 km. The results are shown in figures 3.10 and 3.11 for 75% and 90% H_2SO_4, respectively.

3.5 The Extinction of Infrared Solar Radiation

The extinction, due to the aerosol models described above, of solar infrared radiation along paths through the earth's atmosphere was calculated from the equations

$$I(\lambda) = T(\lambda) \cdot B(\lambda, T_s) \tag{3.14}$$

where $I(\lambda)$ is the spectral intensity (spectral radiance) of the solar radiation after traversing a tangent path through the earth's atmosphere, $T(\lambda)$ is the transmissivity defined above and $B(\lambda, T_s)$ is the radiance of the photosphere of the sun, assumed to be a blackbody at temperature $T_s = 5036^{\circ}K$ (Saiedy and Goody, 1959). Figures 3.12 and 3.13 show the results for tangent paths at altitudes of 16 to 26.6 km for 75% H_2SO_4 and 90% H_2SO_4.

Discussion of Results:

The results shown above indicate the significant difference between the absorption of 75% and 90% aqueous solutions of H_2SO_4, each with the same particle size distribution and with the same relative

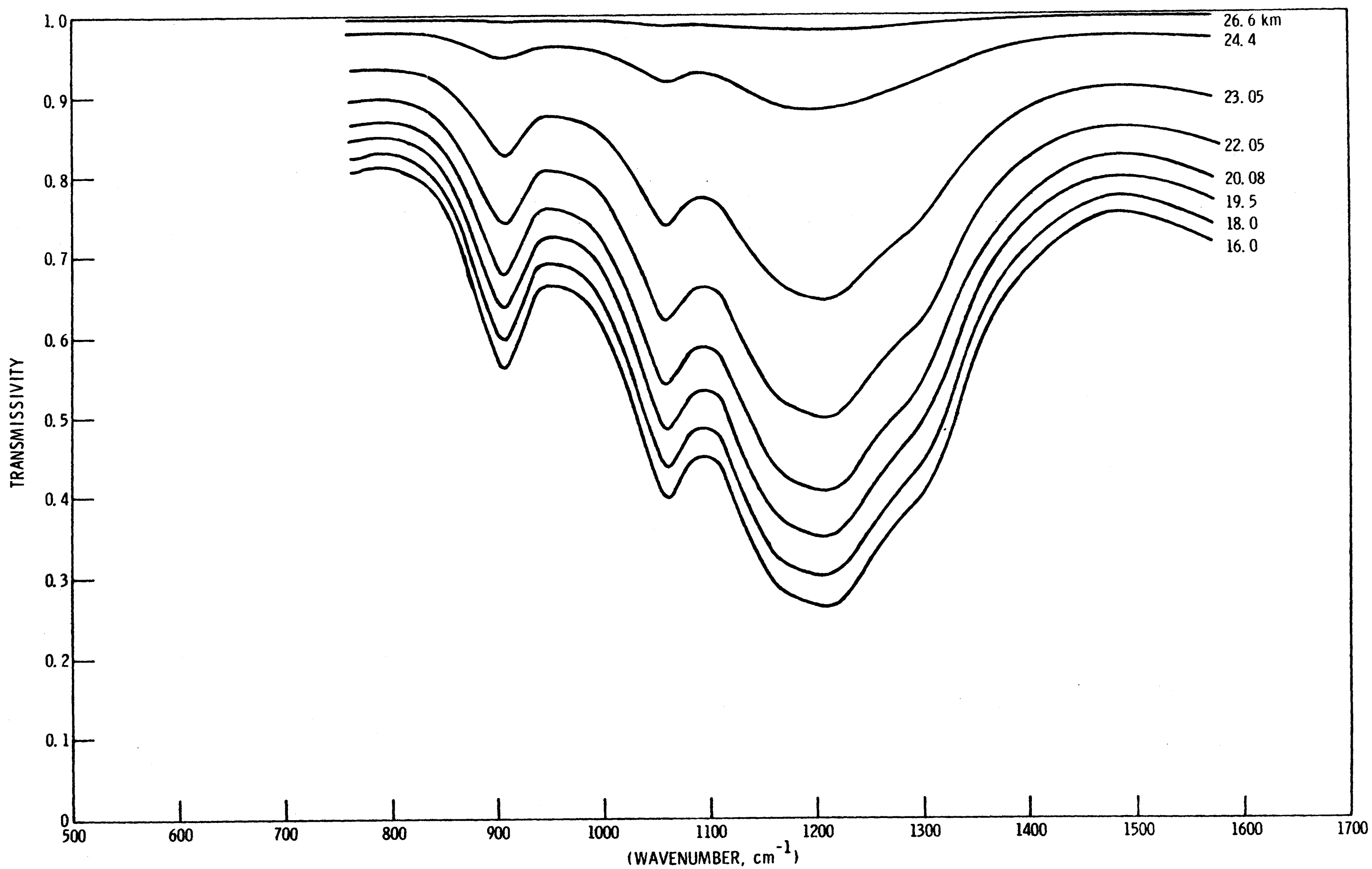

Fig. 3.10 Tangent path transmissivities for 75% H_2SO_4.

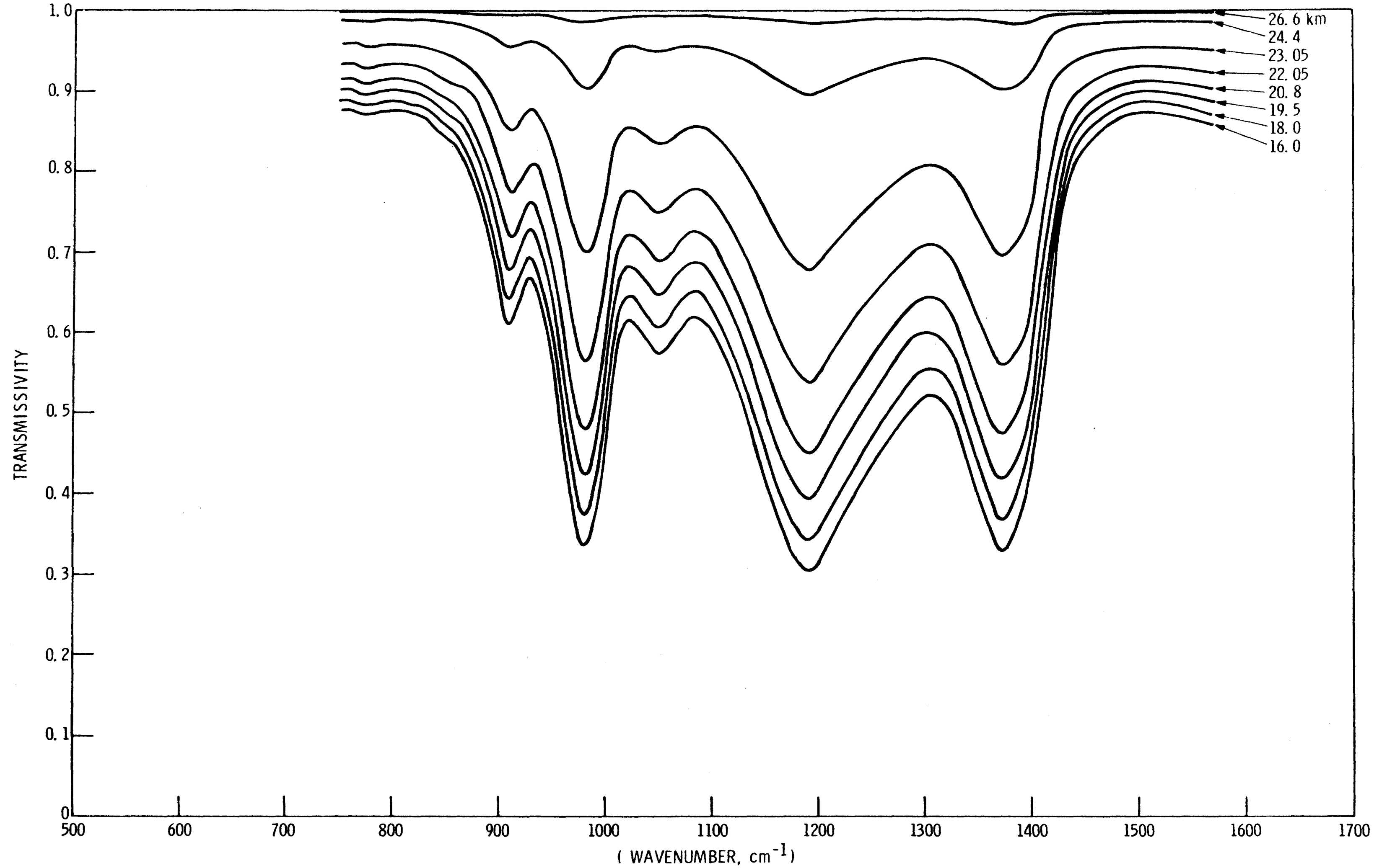

Fig. 3.11 Tangent path transmissivities for 90% H_2SO_4.

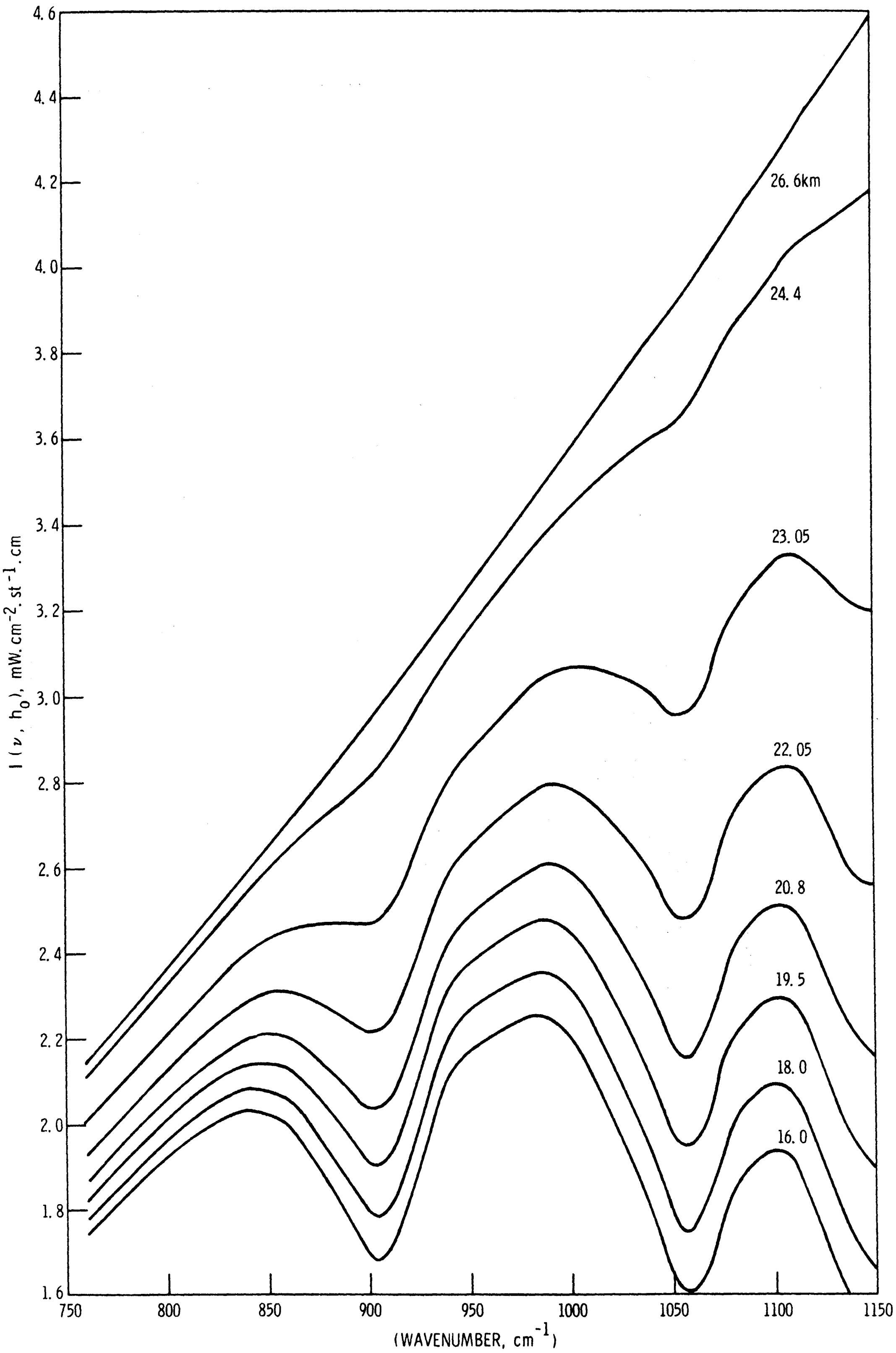

Fig. 3.12 Extinction of solar infrared radiation, by aerosols, on tangent paths through the earth's atmosphere (75% H_2SO_4).

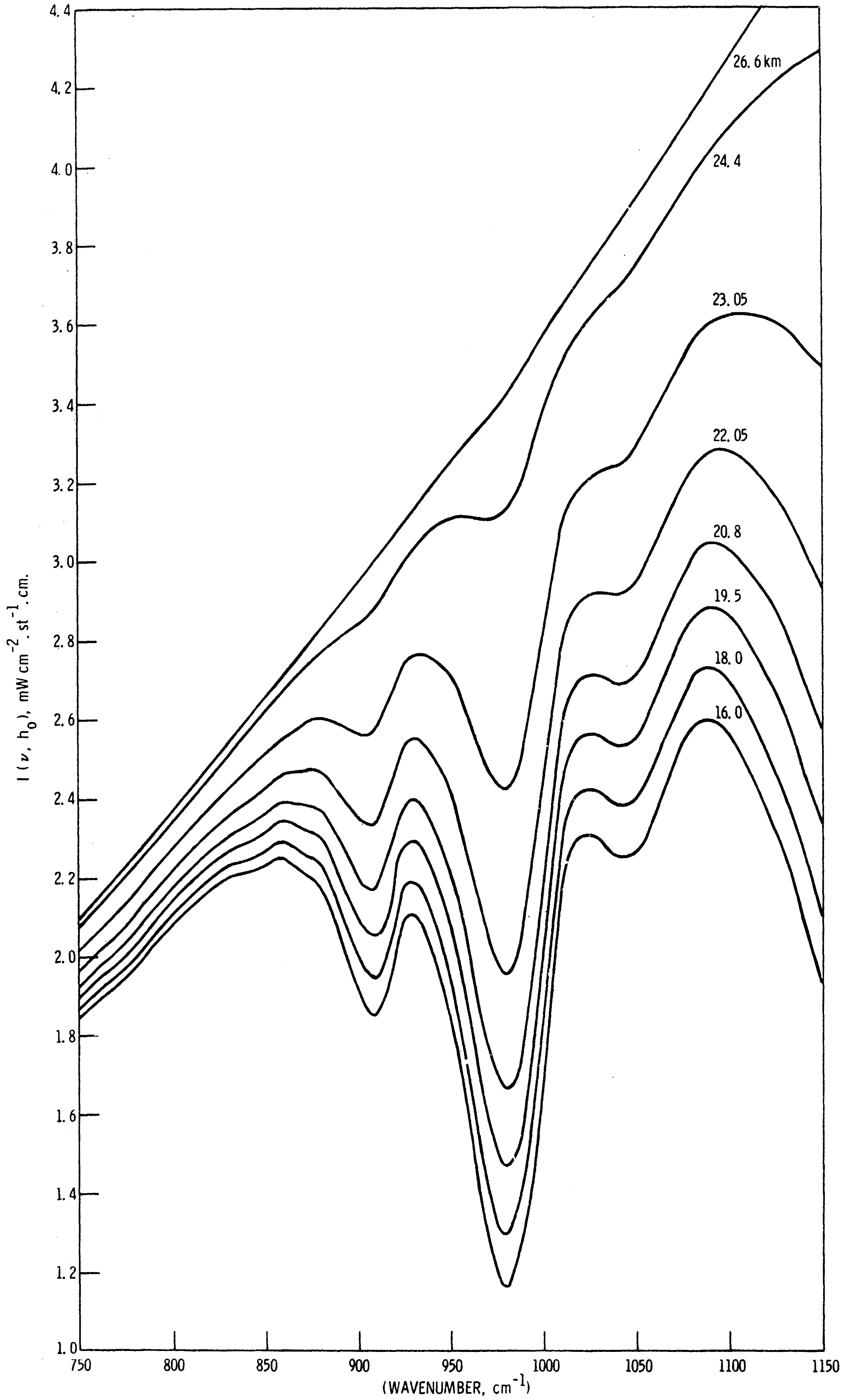

Fig. 3.13 Extinction of solar infrared radiation, by aerosols, on tangent paths through the earth's atmosphere (90% H_2SO_4).

number distribution as a function of altitude. The differences in complex index of refraction are reflected in turn in extinction coefficients, transmissivities for tangent paths through the atmosphere and in solar radiation intensities after traversing tangent paths.

The 75% H_2SO_4 aerosol shows strong absorption bands centered at 900 cm^{-1}, 1060 cm^{-1} and 1200 cm^{-1}. There is strong absorption near these wavenumbers for 90% H_2SO_4 as well (the bands are shifted slightly, they appear to be centered at 908 cm^{-1}, 1050 cm^{-1} and 1150 cm^{-1}). In addition, 90% H_2SO_4 , shows great absorption at 980 cm^{-1} and 1375 cm^{01}.

Measurements of solar radiation in the window region of the spectrum through tangent paths in the atmosphere should provide an excellent measurement of the extinction of stratospheric aerosols, although the absorption at 1050 cm^{-1} will be almost completely masked by absorption due to the ν_3 band of O_3 at 1042 cm^{-1}. The absorption of either 75% H_2SO_4 or 90% H_2SO_4 at the 900 cm^{-1} wavenumber region should be clearly noticeable in window region measurements.

The 980 cm^{-1} and 1375 cm^{-1} absorption may also be recognizable in tangent path spectra although the former may be interfered with by the 1042 cm^{-1} O_3 , 961 cm^{-1} CO_2 and the 884 cm^{-1} HNO_3 absorption regions, and the latter may conflict with 1594 H_2O, 1306 CH_4, 1285 N_2O and 1333 HNO_3.

3.6 Additional Calculations and Improvement of the Model

Additional calculations should be made for 75% and 90% H_2SO_4 with other aerosol size distributions. A mixture, in equal amounts, of 75% and 90% H_2SO_4 should also be considered.

The exact nature of this mixture is an interesting problem in itself. Would such a mixture contain 50% of each 75% and 90% aqueous H_2SO_4 for each particle size? Or would the smaller sizes tend to be mostly or all 90% H_2SO_4, with larger sizes being 75% H_2SO_4? Calculations can be made for both possibilities, however the physical process describing the formation of the aerosol particles should shed some light on this question.

The aerosol model should be improved by adding the effects of the other most likely constituents $(NH_4)_2SO_4$, H_2O_2, HNO_3, $NOHSO_4$, and HNO_3 - H_2SO_4 - H_2O.

The altitude range of the model should be increased to include effects at 50 km, where a secondary aerosol layer may cause noticeable absorption on tangent paths through the atmosphere (Elliott, 1970).

REFERENCES

Chagnon, C. W. and C. E. Junge, (1961), The Vertical Distribution of Sub-Micron Particles in the Stratosphere, J. Meteorol., 18, 746-752.

de Bary, E. and F. Rossler, (1966), Size Disbributions of Atmospheric Aerosols Derived from Scattered Radiation Measurements Aloft, J. Geophys. Res., 71, 1011.

Drayson, S. R., F. L. Bartman, W. R. Kuhn and R. Tallamraju, (1972), Satellite Measurements of Stratospheric Pollutants and Minor Constituents by Solar Occultation: A Preliminary Report, Univ. of Michigan Report No. 011023-1-T, Final Report on N. O. A. A. Grant NG-10-72, High Altitude Engineering Laboratory, Departments of Aerospace Engineering and Atmospheric and Oceanic Science.

Elliott, D. D., (1970), Effect of a High Altitude (50 Km) Aerosol Layer on Topside Ozone Sounding, Space Research XI, Proc. of 13th Plenary Meeting of Cospar, Leningrad, 1970, Akademic-Verlag, Berlin 1971.

Lazrus, A. L., B. Gandrud, and R. D. Cadle, (1971), Chemical Composition of Air Filtration Samples of the Stratospheric Sulfate Layer, J. Geophys. Res., 76, 8083-8088.

Remsberg, E., (1971), Radiative Properties of Several Probable Constituents of Atmospheric Aerosols, Ph. D. Thesis, University of Wisconsin, Madison.

Remsberg, E., (1973), Stratospheric Aerosol Properties and Their Effects on Infrared Radiation, J. Geophys. Res., 78, No. 9, 1401-1408.

Saiedy, F. and R. M. Goody, (1959), The Solar Emission Intensity at 11 Microns, Monthly Notices, Roy. Astron. Soc., 119, 213.

Chapter 4. INVERSION PROCEDURES

4.1 Introduction

This chapter deals with the inversion procedures, by which the atmospheric concentration of the absorbing species can be obtained from the solar occultation measurements of the radiant intensity I. The problems of inversion for atmospheric temperature from radiance measurements have been studied by many authors. (Kaplan 1959, King 1964, Wark and Fleming 1966, Smith 1972, Chahine 1968, Gille 1968, Burn and Uplinger 1970, Rodgers 1970, Wark 1970, McKee and Cox 1973). Inference of water vapor and ozone from radiance measurements have been reported by Yamamoto and Tanaka (1966), Venkateswaran et al. (1961), Conrath (1969), House and Ohring (1969), Prabhakara et al. (1970), Smith (1970).

For the solar occultation experiment the maximum intensity (I_∞) is obtained when the measurement is made at maximum tangent heights and there is essentially no atmospheric absorption. The problem reduces to one of obtaining the concentration of species from the atmospheric transmittances ($T = I/I_\infty$), since emission from the atmosphere is very small and can be safely neglected in comparison to the total intensity. Rayleigh scattering at the spectral regions we are interested in is also small. Mie scattering by aerosols becomes important below tangent heights of approximately 30 km. and has to be included in the calculations. (See Chapter 3)

We have seen from the previous chapters how the calculation of the atmospheric transmittance is very complicated. Not only is the distribution of absorbing constituents required for such a calculation but also the atmospheric pressure and temperature distribution is required. Calculations of transmittances for the 15μm band of CO_2 have been published by Drayson (1966) and Kunde (1967). These calculations require a detailed knowledge of the line positions, strengths, widths of the spectral lines in the region studied and also involve a large amount of computer time for the calculations. Therefore in cases where no such detailed knowledge of the spectral band is available or when use of large amounts of computer times is prohibitive, simplified calculations of atmospheric transmittance using Band Models have been used. (Goody 1964).

Because of this factor we have decided to try out the inversion procedures assuming that the transmittances can be calculated by the strong line approximation where the absorption is proportional to the square root of the optical mass.

$$T = 1 - 2 \cdot \sqrt{S . \bar{u} \ \alpha} / \delta \tag{4.1}$$

where S, α and δ are the strength, half-width and spacing between lines and $\bar{u}$ the optical mass, is the sum over all layers along line of sight

$$\bar{u} = \sum u \tag{4.2}$$

The half-width is proportional to pressure

$$\alpha = \alpha_o \cdot \bar{p} \tag{4.3}$$

where $\bar{p}$ is the equivalent or mean pressure for the entire path

$$\bar{p} = \sum p . u / \sum u \tag{4.4}$$

and similarly $\bar{t}$ is the equivalent temperature

$$\bar{t} = \sum t \cdot u / \sum u \tag{4.5}$$

However it is easy to incorporate the detailed calculation of transmittances instead of the above strong line approximation at a latter stage.

4.2 Geometry and Technique

Consider one absorbing constituent in the spectral region of interest and the atmosphere, spherically stratified and symmetric is divided into n thin concentric spherical shells. Horizontal gradients in temperature and pressure have been considered in the calculations by Davis (1969). Measurements of radiant intensity are made at n tangent heights where the line of sight from satellite to the sun passes through an increasing amount of atmosphere and number of shells as occultation proceeds. The tangent height is defined as the minimum altitude of the line of sight from the earth's surface. The pressure temperature and mixing ratio of constituent is assumed constant within each shell. For all inversion methods an assumption of the absorber concentration above the top most shell is necessary for accurate inversion at the upper tangent heights.

We have measured transmittances

$$T_{m_i}, \quad i = 1, n \tag{4.6}$$

and we are to determine the mixing ratio in each of these shells.

$$C_i, \quad i = 1, n \tag{4.7}$$

One can formulate mathematically

$$T_{m_i} = F_i \, (C_j, \; j \quad i) \quad i = 1, n \tag{4.8}$$

where the function F_i depends on tangent height and hence the temperature and pressure variations in the atmosphere. There is not contribution from the atmosphere below the tangent ray and thus for the shell at the top of the atmosphere

$$T_{m_1} = F_1(C_1) \tag{4.9}$$

Figure 4.1 shows the geometry of the occultation experiment.

4.3 Methods of Inversion

"Onion Peeling"

The onion peeling method developed by Russell (1970), McKee et al. (1969), Russell and Drayson (1972) starts the inversion at the topmost layer, and after the concentration in the first shell is obtained the procedure is carried out for the next lower shell and so on until the lowest shell.

We assume a concentration C_1 for the topmost shell and calculate T_{c_1}. If the assumed concentration is close to the actual, that we can make a linear approximation between measured transmittance T_{m_1} and calculated transmittance T_{c_1}

$$T_{m_1} = T_{c_1} + \left[\frac{\partial T_{c_1}}{\partial C_1}\right] \cdot \Delta C_1 \tag{4.10}$$

The partial derivative is calculated and the perturbation parameter is determined from

$$\Delta C_1 = \Delta T_1 \Big/ \left[\frac{\partial T_{c_1}}{\partial C_1}\right] \tag{4.11}$$

where $\Delta T_1 = T_{m_1} - T_{c_1}$

This value of ΔC_1 is added to the original assumed concentration C_1 and the process if repeated until a desired convergence criteria is met. The procedure is next carried out for shell 2. It is convenient to assume the initial guess for C_2 equal to the above C_1 obtained after inversion. The process is repeated and continues downwards one shell at a time to the lowest shell.

The measurements T_{m_i} inevitably contain errors, like radiant intensity bias errors, scale errors and random noise errors. Besides these there are errors in the determination of tangent heights, atmospheric pressures, temperatures and knowledge of absorption line parameters, etc. The effect of random noise errors can be reduced by either smoothing the input transmittances or smoothing the retrieved profile.

Eigenvectors and Smoothing Matrix Methods

The method of eigenvectors has been developed by Mateer (1964) and used by Russell and Drayson (1973). We can write n equations.

$$\Delta T_i = \sum_{k=1}^{n} \frac{\partial T_{c_i}}{\partial C_k} \cdot \Delta C_k \tag{4.12}$$

or in matrix form

$$\Delta T = B \cdot \Delta C \tag{4.13}$$

The least squares solution is given by

$$\Delta C = (B' \cdot B)^{-1} \cdot (B' \cdot \Delta T) \tag{4.14}$$

where B' is transpose of matrix B. The above equation is unstable and leads to erroneous results when noise is present. The matrix B'. B is symmetric and has real non-negative eigenvalues The eigenvalues $\lambda_1, \lambda_2 \ldots \lambda_n$ have corresponding orthonormal eigenvectors $v_1, v_2 \ldots v_n$. The column matrix $B' \cdot \Delta T$ is now expressed as

$$B' \cdot \Delta T = \sum_{i=1}^{n} b_i \cdot v_i \tag{4.15}$$

where b_i are constants for each eigenvector. The constants b_i are determined by solving the n above equations. We have

$$\Delta C = (B' \cdot B)^{-1} \cdot B' \cdot \Delta T \tag{4.16}$$

$$= (B' \cdot B)^{-1} \cdot \sum_{i=1}^{n} b_i v_i \quad = \sum_{i=1}^{n} \frac{b_i}{\lambda_i} \cdot v_i$$

Now the errors in measurements incorporated in T_{m_i} and the errors in calculations incorporated in T_{c_i}, the partial derivatives $\frac{\partial T_{c_i}}{\partial C_k}$, B, B' are all contained in the constants b_i. Therefore we can write

$$\Delta C = \sum_{i=1}^{n} \frac{b_i'}{\lambda_i} \cdot v_i + \sum_{i=1}^{n} \frac{e_i}{\lambda_i} \cdot v_i \tag{4.17}$$

where b_i' are values of constants with no error, and e_i are the error terms. If λ_i are ordered in decreasing magnitude, for larger i, λ_i may be very small, and error terms will then be large. Inclusion of eigen-vectors v_i corresponding to the smaller λ_i gives the details of the solution which may or may not be due to noise, and cause instability or erroneous results when noise is present. We therefore truncate and use only a limited number of terms, so as to control the noise. The selection of where to truncate depends on a priori knowledge of the amount of noise present. To trucate too much would mean inferior results due to elimination of valid information.

Another technique of smoothing (Wark and Fleming 1966) is to introduce a smoothing matrix H and a smoothing parameter γ. The selection of appropriate values for H and γ has been discussed in papers by Phillips (1962) and Twomey (1963). The solution is given by

$$\Delta C = (B' \cdot B + \gamma H)^{-1} \cdot B' \cdot \Delta T \tag{4.18}$$

Increasing smoothing by increasing γ , makes the solution more dependent on matrix γH. If H is the identity matrix, the method is related to the eigenvector expansion since the eigenvectors of $B'B + \gamma H$ are the same as those of $B'B$ and the eigenvalues are $\lambda_i + \gamma$. The eigenvector expansion is not truncated but is replaced by the expression

$$\Delta C = \sum_{i=1}^{n} \frac{b_i}{\lambda_i + \gamma} \cdot v_i \tag{4.19}$$

However the eigenvalues never become smaller than γ and the problem of amplification of the noise may be controlled by choosing a sufficiently large value of γ .

If the matrix $B'B$ is non-singular, solution with $\gamma = 0$ corresponds exactly to the eigenvector method with all terms included.

Kalman-Bucy Filter

Gray et al. (1973) have discussed a technique of smoothing using the Kalman Bucy filter. This technique (as also the above two methods) is efficient when the initial guess of constituent density C_i is close to the actual value and the linear relation between T_{mi} and T_{c_i} is valid. The method assumes an initial guess of concentration C_i and updates this state vector after each measurement by calculating the "filter gain" (Newell and Gray 1972) vector K_i

$$K_i = P_{i-1} \cdot B'_i \left[B_i \cdot P_{i-1} \cdot B'_i + R \right]^{-1} \tag{4.20}$$

where B'_i is the transpose of vector $B_i = \left[\frac{\partial T_{c_i}}{\partial C_1}, \frac{\partial T_{c_i}}{\partial C_2} \ldots \frac{\partial T_{c_i}}{\partial C_i}, 0 \ldots \right]$

R is the noise covariance and P_{i-1} is the covariance matrix which is originally assumed and updated after each measurement by

$$P_i = P_{i-1} - K_i \cdot B_i \cdot P_{i-1} \tag{4.21}$$

The state vector is updated

$$C_i = C_i + K_i \cdot \Delta T_i \qquad (4.22)$$

The three matrix methods, i. e. the truncated eigenvector expansion, the smoothing matrix and the Kalman Bucy filter, have a common characteristic. The initial guess of the concentration profile is modified only if the measurements indicate a real deviation from the initial profile. Thus if the absorption is very small at the upper levels the measurements contain mostly noise and little information and the inversions show little modification of the initial guess at these levels. Similarly if the absorption is almost complete at the lower levels the measurements also contain little information on the concentrations and the initial guess again retained.

<u>Abel Equation</u>

The Abel integral equation

$$X_i = 2 \int_{r_i}^{\infty} \frac{x(r) \cdot r \cdot dr}{\sqrt{r^2 - r_i^2}} \qquad (4.23)$$

has been inverted (Roble and Hays 1972) and the inversion for constituent profiles has been tried. The values of $X_i = (\overline{u}_i \cdot \overline{p}_i)$ are determined from the measured transmittances T_{m_i}

$$X_i = \overline{u}_i \cdot \overline{p}_i = \left\{ (1 - T_{m_i}) \cdot \delta / 2 \right\}^2 / (S \cdot \alpha_o) \qquad (4.24)$$

The solution for $x(r)$ is given by

$$x(r) = -\frac{1}{\pi} \int_{r}^{\infty} \frac{dX_i / dr_i}{\sqrt{r_i^2 - r^2}} \cdot dr_i \qquad (4.25)$$

where $x(r)$ is the product of C and p.

The values for X_i are discrete, since measurements are made at selected tangent heights only. Between individual data points, X_i is assumed to have an exponential variation given by

$$X_i (r) = A_i \exp \left[- B_i (r-r_i) \right] \tag{4.26}$$

where the coefficients A_i and B_i are chosen to fit the data with desired amount of smoothing incorporated . Thus for smoothing M/2 data points on either side of the i-th data point, A_i and B_i are calculated so as to fit the data from (i-M/2) to (i + M/2) in a least squares sense with a minimum variance.

$$\sigma_i^2 = \sum_{k=(i-M/2)}^{(i+M/2)} \left[X_k - A_i \exp \left\{ - B_i (r_k - r_i) \right\} \right]^2 \tag{4.27}$$

Now the derivative dX/dr near the i-th data point is given by

$$\frac{dX}{dr} = - A_i \cdot B_i \exp \left\{ - B_i (r-r_i) \right\} \tag{4.28}$$

Substituting the above expression and replacing the integral by a finite sum, the solution for $x(r_\ell)$ can be written as

$$x (r_\ell) = \frac{1}{\pi} \sum_{i=\ell}^{1} A_i \cdot B_i \int_{r_i^-}^{r_i^+} \frac{\exp \left[- B_i (r-r_i) \right]}{\sqrt{r^2 - r_\ell^2}} \cdot dr \tag{4.29}$$

where $r_\ell^- = r_\ell$, $r_i^- = (r_i + r_{i+1})/2$ and $r_i^+ = (r_{i-1} + r_i) / 2$

Roble and Norton (1972) have discussed the evaluation of the integral in the above equation. From the values of x, the constituent profile C is obtained.

It is important to note that the use of the Abel Integral equation as developed in this section is dependent on the strong line approximation contained in equation (4. 24). In the other inversion methods the approximation was used as a convenience in testing the procedures to avoid lengthy transmittance calculations but is an essential part of the development of the Abel equation inversion. The prospects appear poor for modification to the more general situation where the strong line approximation is not valid. In order to do this we have to find an X_i which is a function of the measured transmittance and an $x(r)$ which is a function of the concentration to use in equation (4. 23). However transmittance is expressed as an integral over wavenumber of the monochromatic transmittance, which is itself an exponential of integral along the line of sight.

Robel and Hays (1972), working in the UV spectral region, were able to overcome this difficulty by assuming that the monochromatic transmittance was independent of wavelength over small wavelength regions and that other spectral parameters were independent of altitude. Both these approximations are invalid in the infrared region of the spectrum.

The errors in T_{m_i} will cause X_i and correspondingly the coefficients A_i and B_i to have included error terms. Roble and Hays (1972) have given expressions for the standard deviation of the retrieved constituent density errors due to statistical errors in the measurements.

4. 4 Results and Discussion

Inversion for CO_2 concentration in a 10 shell model atmosphere is tried as a first step. The atmosphere between 70 and 20 km. is divided into 10 shells each 5 km. thick. The atmospheric pressure and temperature at the mid-altitude of shell (from standard atmospheric tables) is used as the assumed constant pressure and temperature in each shell. Assuming CO_2 mixing ratio of 320 ppm., "measured" transmittances T_{m_i} are generated at spectral region of 655 cm^{-1} where $S = 3.2\ cm^{-1}(atm \cdot cm)^{-1}$ and $\alpha_o = 0.07\ atm^{-1}cm^{-1}$.

The T_{m_i} are used in the inversion procedures to obtain the CO_2 mixing ratio in the atmosphere. The results are shown in Table 1. The onion peeling method requires an initial guess of mixing ratio at the topmost shell and is taken as 300 ppm. The other methods shown in Table 1 require an initial guess of the concentrations in all shells, and this guess is taken as 300 ppm. All techniques retrieve the 320 ppm. mixing ratio of CO_2 above 30 km. In the Kalman-Bucy filter technique a noise R= 1. E-14 is used to obtain results shown in Table 1.

In the eigenvector method, the last two eigenvalues are zero. As no noise in measurements (T_{m_i}) is assumed, we use the first eight eigenvectors for the calculation. In the smoothing matrix γ = 160. is used to obtain solution shown in Table 4. 1. Further decrease in γ will improve the solution for the top 3 levels.

At tangent heights of 25 km. and below the atmosphere is opaque. (T_m=0) and retrievel of concentration of CO_2 in the last two shells is not possible because of lack of information.

Using the onion peeling technique, there is no retrievel for the bottom two shells because the partial derivative in the expression for C_i is zero. In the matrix methods as discussed earlier, the initial guess of concentration in the last two shells is retained as the measurements contain no information on the concentration.

To study the effect of random noise, the generated T_{m_i} are rounded off to the second decimal place, and the inversion procedures are tried using the same initial guesses of CO_2 mixing ratio. The onion peeling method retrieves the concentration profile fairly accurately between altitudes 50 and 30 km. At the top of the atmosphere there is larger error because here even for comparatively large changes in mixing ratio of CO_2, the transmittance does not change very significantly. No smoothing of retrieved profile is incorporated in the results shown for the onion peeling method, so that the noise dominates.

The results from the eigenvectors method using 5 eigenvectors to calculate the solution are shown in Table 1. The 10 eigenvalues and eigenvectors of matrix B'B are shown in Table 4. 2. We see that eigenvalues λ_9 and λ_{10} are 0, and λ_8 is approximately 10^4 times smaller than λ_1 and the inclusion of the smaller eigenvalues λ_8 and λ_7 in the calculation contributes little to actual solution but will greatly increase the error terms. Truncation after 5 eigenvectors gives a solution which appears the closest to the actual solution we desire of 320 ppm., the maximum deviations being + 19 and -20 ppm. The improvement and subsequent worsening of solution as the number of eigenvectors(and eigenvalues) used is increased is shown in Table 3. The retrievel of CO_2 profile is best between 50 and 30 km. where the information content of data is maximum. An idea of the information content of the measurements can be obtained by studying the eigenvectors and locating the largest terms in each vector.

Results from the smoothing matrix method, using the identity matrix for H and $\gamma = 6800.$ are shown in Table 1. Various other values for γ are tried. The value 6800. corresponds to the 5-th eigenvalue λ_5 of (B'B) and we see the solution is very close to that obtained from the eigenvector method truncated after 5 eigenvector terms.

In performing the eigenvector and smothing matrix methods we tacitly have assumed a linear approximation for the relationship between T_{m_i}, T_{c_i} and C_i. If our initial guess of constituent profile is not close to the actual, such an approximation is not valid. It is desirable to perform an itterative procedure similar to the one carried out in the onion-peeling method. For each new itteration, the initial guess of concentration is the one calculated in the previous itteration. The itterative procedure is continued until a desired convergence criteria is met.

The solutions from the Kalman Bucy filter technique are consistent with results from the other methods (Table 1). A noise of R=1.E-12 is used in Table 1 for inversion using T_{m_i} with random error. The selection of the initial covariance matrix and the value of R for given data and the effect of these quantities on the inversion is being studied.

A similar set of calculations for CO inversion in a 10 shell model atmosphere from 55 to 5 km. with 5 km. thick shells are shown in Table 4. Results of inversion for CO_2 in a 22 shell atmosphere using the Abel equation technique are shown in Table 5. Results from Abel equation inversion for CO_2 using a 10 shell atmosphere with 5 km. thick shells (not included) are poor because of the assumptions made in calculating T_{m_i}.

By using the simple closed form expression for calculation of transmittances T_{c_i}, we were able to calculate the partial derivatives $\partial T_{c_i} / \partial C_K$ quite easily. When using the more detailed methods for calculating T_{c_i}, the partial derivatives have to be calculated by using the finite defference approximation $\frac{\partial T_{c_i}}{\partial C_K}$. This requires calculating the transmittance with a small perturbation of assumed concentration in the shells. This procedure is very time consuming when the exact expressions for transmittance are used.

As seen above there are a variety of methods for inverting and smoothing of data. A particular technique may be ideal in some situations. In the inversion using the Abel equation no initial estimate of the constituent profile is necessary. This method although has some advantages is very difficult to apply in the case where we do not assume a simple closed form expression for transmittance. The technique using the Kalman Busy filter requires the additional calculations of the covariance matrices which is a drawback for quick calculations, although providing a more detailed description of the information content of the measurements. The smoothing matrix and eigenvector methods are very similar. The smoothing matrix method is the faster and more efficient technique while the eigenvector method gives more insight into the information content of the measurements. The onion reeling method is very simple and easy to apply. Incorporating smoothing of input transmittances or smoothing of retrieved constituent profiles, reduces the effect of random errors on the inversion.

The effect of other errors like bias and scale errors etc. will be further studied. Selection of an initial estimate of the constituent profile, which should be close to actual constituent profile, required for some of the inversion techniques is sometimes difficult to make. We have assumed n measurements, and n tangent heights. It would be preferable to have more measurements, from which the random error component can be minimized. The selection of a model atmosphere and especially the thickness of shells is being further studied. Thick shells give coarse results with all the atmospheric fine structure of constituent profile hidden. Dividing the atmosphere into very thin shells is preferred but in some of the methods this could cause instability. Depending on the constituent profile, a model atmosphere consisting of shells of suitably varying thickness can be constructed, giving the fine structure by having thin shells where required, and eliminating problems of instability by having thick shells where necessary. Newell and Gray (1972) using the Kalman-Bucy filter point that in some cases to prevent premature convergence, the tangent height data was sampled in coarse intervals repeatedly. The above mentioned techniques can easily be extended to retrieve two and more constituents simultaneously. Study of inversion of aerosols and selection of the optimum amount of smoothing for given data and separation of noise from measurements will be continued.

TABLE 4.1

Inversion for CO_2 Mixing Ratio

T_{m_i} Calculated at 655 cm^{-1} Using S = 3.2 cm^{-1} $(atm.\ cm)^{-1}$,

α_o = 0.07 and Mixing Ratio of CO_2 of 320 ppm.

			Mixing Ratio ppm					Mixing Ratio ppm			
Shell i	Tangent Ht km	T_{mi}	Onion Peeling	Eigen-Vector (8 terms)	Smoothing Matrix γ=160	Kalman Filter R=1.E-14	T_{mi} with Error	Onion Peeling	Eigen-Vector (5 terms)	Smoothing Matrix γ=6800	Kalman Filter R=1.E-12
1	65	.99204	320	320	311	320	.99	505	300	306	478
2	60	.98389	320	319	316	322	.98	492	301	314	488
3	55	.96887	320	320	319	322	.97	270	307	301	297
4	50	.94144	320	320	320	323	.94	339	339	321	340
5	45	.89160	320	320	320	323	.89	329	328	324	333
6	40	.78849	320	320	320	322	.79	313	313	313	317
7	35	.56759	320	320	320	322	.57	316	316	316	318
8	30	.08438	320	320	320	322	.08	324	323	323	325
9	25	0	-	300	300	300	0	-	300	300	300
10	20	0	-	300	300	300	0	-	300	300	300

TABLE 4.2

Eigen Values and Eigen Vectors of Matrix B'B

CO_2 Inversion

i	1	2	3	4	5	6	7	8	9	10
Eigen values λ_i	$1.8 \times 10^{+6}$	$3.9 \times 10^{+5}$	9.0×10^{4}	2.3×10^{4}	6.8×10^{3}	1.9×10^{3}	5.5×10^{2}	1.6×10^{2}	0	0
Eigen Vectors v_i	0.000	0.000	0.000	0.002	0.007	0.030	0.155	0.988	0.0	0.0
	0.000	0.000	0.002	0.008	0.032	0.152	0.975	-0.157	0.0	0.0
	0.000	0.001	0.007	0.035	0.160	0.974	-0.158	-0.006	0.0	0.0
	0.001	0.006	0.030	0.167	0.971	-0.167	-0.007	-0.001	0.0	0.0
	0.004	0.024	0.141	0.974	-0.174	-0.007	-0.001	-0.000	0.0	0.0
	0.020	0.125	0.981	-0.146	-0.006	-0.001	-0.000	-0.000	0.0	0.0
	0.117	0.985	-0.129	-0.006	-0.001	-0.000	-0.000	-0.000	0.0	0.0
	0.993	-0.118	-0.005	-0.001	-0.000	-0.000	-0.000	-0.000	0.0	0.0
	0.0	0.0	-0.0	0.0	-0.0	0.0	-0.0	-0.0	1.000	0.0
	0.0	0.0	-0.0	0.0	-0.0	0.0	-0.0	-0.0	0.0	1.000

TABLE 4.3

Inversion of CO_2 Using Method of Eigen Vectors

T_{mi} With Random Error

No. Of Eigen vectors included \ Shell	Mixing Ratio ppm.									
	1	2	3	4	5	6	7	8	9	10
1	300	300	300	300	300	301	303	325	300	300
2	300	300	300	300	300	302	318	323	300	300
3	300	300	300	301	303	318	316	323	300	300
4	300	300	301	306	334	314	316	323	300	300
5	300	301	307	339	328	313	316	323	300	300
6	300	301	305	340	328	313	316	323	300	300
7	330	492	274	338	328	313	316	323	300	300
8	479	468	273	338	328	313	316	323	300	300
9	-	-	-	-	-	-	-	-	-	-
10	-	-	-	-	-	-	-	-	-	-

TABLE 4.4

Inversion for CO Mixing Ratio

T_{mi} Calculated at 2173 cm^{-1} using $S = 9.0\ cm^{-1}\ (atm^{-1}\ cm^{-1})$ and $\alpha_o = .065$

Shell	Tangent ht	Mixing ratio ppm assumed for calculating T_{mi}	T_{mi}	T_{mi} with error used in inversion methods	Initial guess of mixing ratio	Onion Peeling	Eigen Vectors Method (9 terms)	Kalman Bucy Filter R = 1.E - 17
1	50	.12	.99799	.998	.13	.119	.129	.118
2	45	.10	.99611	.996	.11	.107	.105	.105
3	40	.08	.99310	.993	.081	.0821	.082	.0815
4	35	.05	.98905	.989	.051	.0502	.0502	.0502
5	30	.02	.98507	.985	.021	.0202	.0201	.0201
6	25	.03	.96582	.97	.03	.0223	.0218	.0217
7	20	.04	.91533	.92	.041	.0360	.0359	.0351
8	15	.05	.78508	.79	.051	.048	.0479	.0474
9	10	.06	.52498	.52	.06	.0617	.0617	.0613
10	5	.08	0	0	.081	–	.081	.081

TABLE 4.5

Inversion Using the Abel Equation

22 Shell Model Atmosphere

Smoothing Parameter   M = 2

Shell	Tangent ht km	T_{mi}	CO_2 mixing ratio ppm
1	69	.997	-
2	68	.996	-
3	67	.995	-
4	66	.994	74
5	65	.993	165
6	64	.992	232
7	63	.991	183
8	62	.989	158
9	61	.987	294
10	60	.986	350
11	59	.984	273
12	58	.981	304
13	57	.979	332
14	56	.976	331
15	55	.973	339
16	54	.969	340
17	53	.965	336
18	52	.960	339
19	51	.955	338
20	50	.949	-
21	49	.942	-
22	48	.934	-

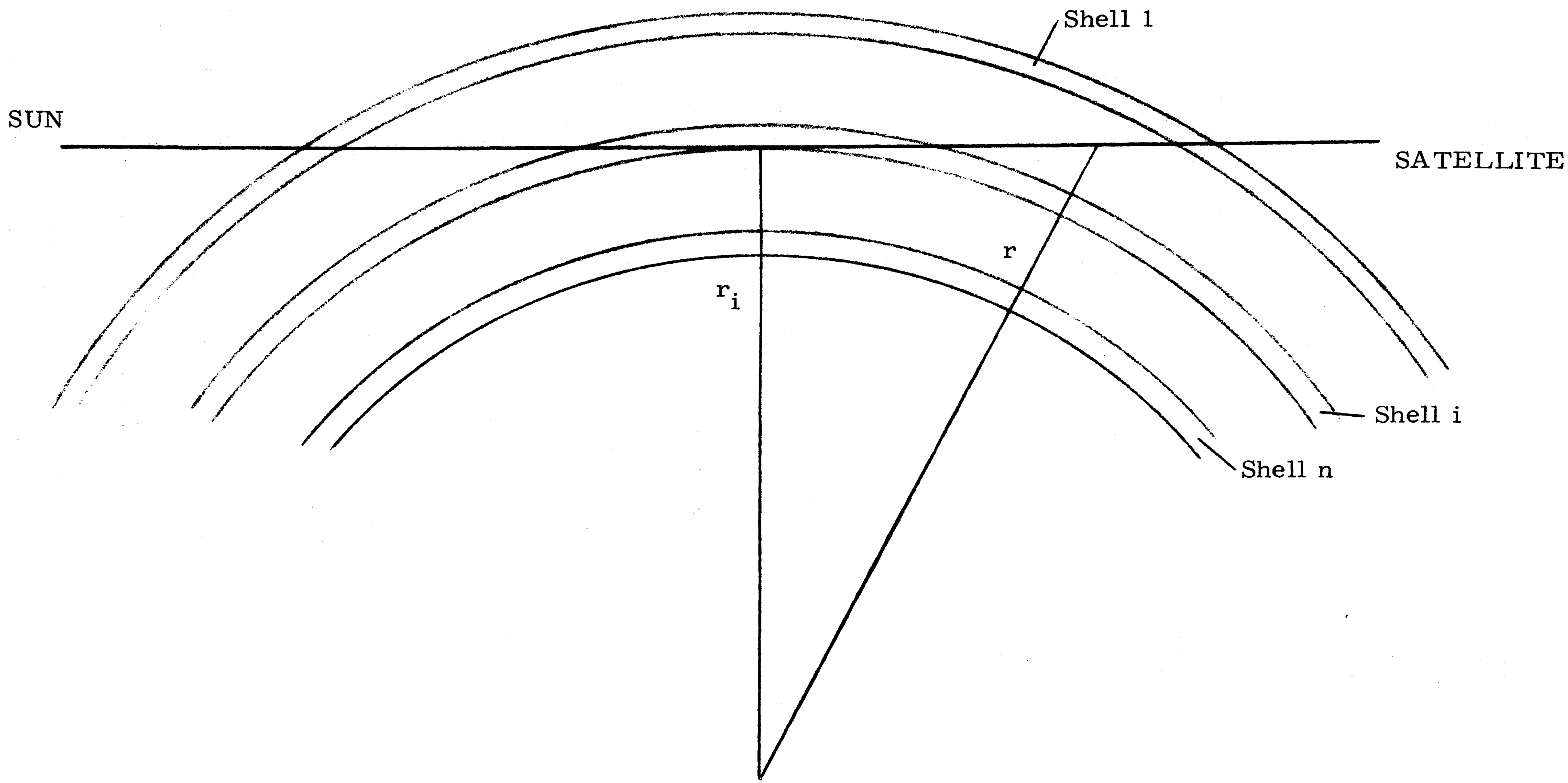

Figure 4.1 Geometry of Solar Occultation Experiment

REFERENCES

Burn, J. W. and W. G. Uplinger (1970), The Determination of Atmospheric Temperature Profiles From Planetary Limb Radiance Profile, NASA CR-1513.

Chahine, M. T. (1968), Determination of the Temperature Profile in an Atmosphere From its Outgoing Radiance, J. Opt. Soc. of AM. 58, 1634.

Conrath, B. J. (1969), On the Estimation of Relative Humidity Profiles from Medium Resolution Spectra Obtained form a Satellite. J. G. R. 74, 3347.

Davis, R. E. (1969), A Limb Radiance Calculation Approach for Model Atmospheres Containing Horizontal Gradients of Temperature and Pressure, NASA TN-D 5495.

Drayson, S. R. (1966), Atmospheric Transmission in the CO_2 Bands Between 12 and 18 μm., App. Optics. 5, 385.

Gille, J. C. (1968), On the Possibility of Estimating Diurnal Temperature Variation at the Stratopause from Horizon Radiance Profiles, J. G. R. 73, 1863.

Goody, R. M. (1964), Atmospheric Radiation, I-Theoretical Basis., Oxford at the Clarendon Press.

Gray, C. R., H. L. Malchow, D. C. Merritt, R. E. Var and C. K. Whitney (1973), Aerosol Physical Properties from Satellite Horizon Inversion, NASA CR-112311.

House, F. B. and G. Ohring (1969), Inference of Stratospheric Temperature and Moisture Profiles from Observations of the Infrared Horizon NASA CR-1419.

Kaplan, L. D. (1959), Inference of Atmospheric Structure from Remote Radiation Measurements, J. Opt. Soc. of Am. 49, 1004.

King, J. I. F. (1964), Inversion by Slabs of Varying Thickness, J. Atm. Sc. 21, 324.

Kunde, V. G. (1967), Theoretical Computations of the Outgoing Infrared Radiance from a Planetary Atmosphere. NASA TN-D-4045.

Mateer, C. L. (1964), A Study of the Information Content of Umkehr Observations, Tech. Rep. No. 2., NSF Grant No. G-19131., Coll. of Eng., University of Michigan

McKee, T. B. and S. K. Cox (1973), Stratospheric Temperature Profiles from Limb Radiance Measurements., J. App. Meteor. 12, 867.

McKee, T.B., R.I. Whitman and J. J. Lambiotte (1969), A Technique to Infer Atmospheric Water Vapor Mixing Ratio from Measured Horizon Radiance Profiles, NASA TN-D-5252.

Newell, R.E. and C.R. Gray (1972), Meteorological and Ecological Monitoring of the Stratosphere and Mesosphere, NASA CR-2094.

Phillips, D. L. (1962), A Technique for the Numerical Solution of Certain Integral Equations of the First Kind., J. Assoc. Comp. Mach 9, 84.

Prabhakara, C., B.J. Conrath, R.A. Hanel and E.J. Williamson (1970), Remote Sensing of Atmospheric Ozone Using the 9.6 μm Band.

Roble, R.G. and P.B. Hays (1972), A Technique for Recovering the Vertical Number Density Profile of Atmospheric Gases from Planetary Occultation Data., Planet. Sp. Sci., 20, 1727.

Roble, R.G. and R.B. Norton (1972), Thermospheric Molecular Oxygen From Solar u-v. Occultation Data., J.G.R. 77, 3524.

Rodgers, C.R. (1970), Remote Soundings of the Atmospheric Temperature Profile in the Presence of Could., Quat. J. Roy. Met. Soc. 96, 102.

Russell, J.M. (1970), The Measurement of Atmospheric Ozone Using Satellite Infrared Observations in the 9.6 μm Band, Rep. No. 036350-1-T, High Alt. Eng. Lab., Univ. of Mich.

Russell, J.M. and S.R. Drayson (1972), The Inference of Atmospheric Ozone Using Satellite Horizon Measurements in the 1042 cm^{-1} Band, J.Atm. Sci. 29, 376.

Russell, J.M. and S.R. Drayson (1973), The Inference of Atmospheric Ozone Using Satellite Nadir Measurements in the 1042 cm^{-1} Band, NASA TR-R-399.

Smith, W.L. (1970), Iterative Solution of the Radiative Transfer Equation for the Temperature and Absorbing Gas Profile of an Atmosphere, App. Optics. 9, 1993.

Smith, W. L. (1972), Satellite Techniques for Observing the Temperature Structure of the Atmosphere, Bull. A.M.S. 53, 1074.

Twomey, S. (1963), On the Numerical Solution of Fredholm Integral Equations of the First Kind by the Inversion of the Linear System Produced by Quadrature, J. Ass. Comp. Mach. 10, 97.

Venkateswaran, S.V., J. G. Moore and A.J. Krueger (1961), Determination of the Vertical Distribution of Ozone by Satellite Photometry, J.G. R. 66, 1751.

REFERENCES (continued)

Wark. D. Q. (1970), SIRS: An Experiment to Measure the Free Air Temperature From a Satellite, App. Optics. 9, 1761.

Wark, D. Q. and H. E. Fleming (1966), Indirect Measurements of Atmospheric Temperature Profiles from Satellite: I Introduction Mon. Wea. Rev. 94, 351.

Yamamoto, G. and M. Tanaka (1967), Estimation of Water Vapor Distribution in the Atmosphere from Satellite Measurements, Application Satellites Edited by M. Lunc., Gordon and Breach Inc., New York.

Chapter 5. Discussion and Calculations.

Although this study is not yet complete it is already evident that useful measurements of stratospheric distribution of some minor constituents can be made from a satellite using the solar occultation technique in the infrared spectral region. Furthermore comparatively simple instrumentation of medium spectral resolution (a few wavenumbers) may be employed for the more abundant of the minor molecular constituents such as water vapor, carbon dioxide, methane, nitrous oxide, ozone and perhaps carbon monoxide and nitric acid. Details of the absorption in different spectral regions have been given in the second chapter and recommendations on the spectral intervals to make measurements have been made for most of the molecules. Carbon dioxide has not been included in the chapter as it would probably be difficult to improve on our present knowledge of its stratospheric concentration. It is possible, however, that measurements in the Q-branch near 668 cm^{-1} or in the 4.3 μm band could yield information on the lower mesospheric distribution. Similarly nitric acid vapor has not been included, in this case because of the difficulty in determining its stratospheric absorption. The most promising spectral regions appear to be the Q-branches near 879 and 897 cm^{-1}, although special care is needed to distinguish between nitric acid absorption and extinction by aerosols.

In most of the stratospheric absorption calculations a band model was employed. In the majority of our future calculations we expect to use the line-by-line integration method for greater accuracy, although errors introduced by the band model do not affect the feasibility aspect of the study. For some of the molecules the more sophisticated technique may not be justified at the present time because of the inadequacy of the spectral line parameters needed as input to the computer programs. This is certainly true for most of the ozone bands and probably for methane also. It is clear that a careful and comprehensive comparison between theoretical and laboratory data is required, not only for room temperature measurements but also for measurements taken at stratospheric temperatures. 220 K is a representative temperature in the lower stratosphere and few absorption measurements have been taken under these conditions. We recommend that laboratory absorption measurements of this nature be undertaken.

Sulphuric acid aerosols in the lower stratosphere have been shown to give large values of extinction between about 800 and 1600 cm^{-1}, the exact characteristics depending on their concentration, size distribution, etc. This is encouraging for those who would like to study the aerosols, but adds another uncertainty to the determination of the concentrations of the molecular constituents. We need to be able to predict the extinction by the aerosols, possible by measureing the extinction in a spectral region close to that chosen for the molecule. The extinction calculations described are for realistic values of parameters but need to be extended to different ranges of size, concentration, composition, height distributions and spectral regions.

Several different inversion techniques have been developed and tested but it is not yet apparent how best to incorporate the smoothing which is necessary to prevent the domination of noise. We expect to use the inversion programs to study the effect of many sources of error and will eventually be able to predict uncertainties in the concentrations of the retrieved profiles. A major problem will be the computation of the transmittances in the inversion program, made difficult by the large amount of computer time needed to calculate them accurately.

For the reasons stated in the first chapter we have largely confined our discussions to the more abundant of the minor constituents. Other molecules such as NO and NO_2 are of great interest but their absorption is smaller and would require more sophisticated instrumentation. We plan to examine some of these but may be limited by the absence of adequate spectral data, both theoretical and experimental.

APPENDIX

Computer Programs for Line-by-Line Transmittance Calculations

The computer programs written for the line-by-line calculation of atmospheric transmittances for the occultation geometry have been adapted from the already existing programs for slant path transmittance which assumed a plane parallel atmosphere. The atmosphere is divided into concentric shells and the regions between shells are assumed to be homogeneous. The program calculates the optical masses for each tangent height path in each region and uses them to compute the monochromatic transmittance along the tangent path. Refractive effects have not been incorporated but this would be easy to do since they would affect slightly the optical masses. Integration over wavenumber intervals of 0.1 cm^{-1} is accomplished by numerical quadrature.

The following is a brief description of the input/output of the programs which are written in Fortran IV. Two programs are used:

1. SETUPV This program processes the line parameter data and outputs quadrature intervals, wing contributions, etc.
2. HSLANV computes the transmittances using the data out putted by SETUPV.

Input /Output of SETUPV

Line 23	Input of line parameters from binary file or tape.	
	BNUS (I)	Line wavenumber (cm^{-1}), rounded to two decimal places
	TS (J, I)	Line intensities at 6 temperatures 300, 275, 250, 225, 200, 175 K corresponding to J = 1, 6.
	AR (I)	Line halfwidth (cm^{-1}) at 1 atm. and 300K.

Line 34. ANUZ — The starting wavenumber (cm^{-1})

NUMBER — The number of 1 cm^{-1} intervals for which transmittance calculations are to be made.

All output statements write data to be used by HSLANV

Input/Output of HSLANV

Line 29. Namelist NAM1.

PCRIT — Pressure (mb) below which Voigt profile is used

WTM — Molecular weight of the molecule

NQI, NQC — Gaussian quadrature parameters, have value of 2 or 4 giving maximum efficiency and lowest accuracy or less efficiency and greater accuracy respectively.

KMAX — The number of tangent heights calculated.

Altitude Z (km), pressure P(mb), temperature T(K) and concentration CONC must be specified at the (K + 1) bounding shells, starting with the highest altitude. CONC is mixing ratio by volume for IS = 1, or number density mol cm^{-3} for all other values of IS.

Line 49.5. Prints the parameters inputted in line 29.

Line 82. Namelist NAM2.

ANUZ and NUMBA — correspond to ANUZ and NUMBER in program SETUPV.

All other input statements use the output from SETUPV.

Line 397. ANUZ — center of 1 cm^{-1} interval for which calculation is made.

TRAN (J, K) — transmittance for tangent altitude

Z(K + 1) and pressure P (K + 1) for 10 intervals averaged over 0.1 cm^{-1}. J = 1 corresponds to interval (ANUZ - 0.5, ANUZ - 0.4), J = 2 to the next highest etc.

```
C  THIS PROGRAM IS CALLED SETUPV FCRTRAN IV
      COMMCN NCSTRG,L,NCINT,NOIN,NEND,IWARN
      EQUIVALENCE (ST(1),TS(1))
      DIMENSION NOSTRG(10),L(100),NOINT(72),NEND(144),IWARN(10)
      DIMENSION ISTRGL(100),         BNUS(2200),INUS(2200),IABOVE(100),
     1IBELOW(1C0),D(2200),SM(18),ISS(2200),ST(13200),AR(2200),TS(6,2200)
     1 ,IVST(2200)
      DATA I1,I2,IONE,I3,KID,ISTC,IC,JJ/8*1/
      DATA JJJ, ITWO/4,0/
  200 FORMAT (F6.2,6E10.4)
 201  FORMAT(F7.2,I5)
 202  FORMAT(F7.2,6E10.4,F6.4,I9)
  281 FORMAT (2I5,F6.1)
 250  FORMAT(F7.2,I2,2I4,11I2,10I1/(6E10.4))
  252 FCRMAT (9(2I2,I4))
  253 FORMAT (24I3)
  203 FORMAT (I2)
      DIST=3.5
      MS=2200
      IDIST=DIST*100.
      DO 301 I=1,MS
      READ(7,END=1301) BNUS(I),(TS(J,I),J=1,6),AR(I)
 301  ISS(I)=(I-1)*6
      CALL ERROR
 1301 MS=I-1
      MSP=MS+1
      INUS(MSP)=10C000000
      DO 303 I=1,MS
      IF (ST(JJJ)-.1) 304,304,305
  305 IVST(JJ) = I
      JJ = JJ+1
  304 JJJ = JJJ+6
  303 INUS(I)=(BNUS(I)+.001)*1CC.
      JJ = JJ-1
  802 READ (5,201,END=1CCC) ANUZ,NUMBER
 1802 CONTINUE
      NUZ=ANUZ+.001
      NUZZ=(NUZ/10)*10
      AVNU=NUZZ
      AVNU=4.5+AVNU
      NUZY=NUZZ*100
      NUZX=NUZY-IDIST
      IS=IONE
      DO 600 I=IS,MS
      IF (NUZX-INUS(I)) 601,601,600
  601 ICNE=I
      GO TO 602
  600 CCNTINUE
      IONE=MSP
      ITWO1=MS
      GO TO 607
  602 NUZV=NUZY+900+IDIST
      IS=MAXO(ITWO,1)
      DO 603 I=IS,MS
      IF (NUZV-INUS(I)) 604,6C3,6C3
  604 ITWO1=I-1
      GO TO 607
  603 CONTINUE
      ITWO1=MS
  607 CONTINUE
```

```
      IOUT=MAXO(ITWO+1,IONE)
      ITWO=ITWO1
      NUZY=NUZY-50
      WRITE (6,281) IONE,ITWO,AVNU
      IF (IOUT-ITWO) 611,611,610
  611 WRITE (6,202) (BNUS(I),(TS(J,I),J=1,6),AR(I),I,I=IOUT,ITWO)
  610 CONTINUE
  801 NUZ=(ANUZ-.499)*100.
      DO 311 K=ISTO,MS
      IF (INUS(K)-NUZ) 311,313,313
  313 IST = K
      GO TO 312
  311 CCNTINUE
      IST=MSP
  312 NUZ = ANUZ+.001
      NUZM=NUZ*100-60
      IF (KID.GT.JJ) GO TO 762
      DO 320 K = KID,JJ
      KK = IVST(K)
      KD = K
      IF (INUS(KK)-NUZM) 32C,32C,322
  320 CCNTINUE
      KD=JJ+1
  322 KID = KD-1
      IF (KID .EQ. 0) KID=1
  762 II=1
      ITOTAL = 0
      IIS = 1
      JTOTAL = 0
      DO 351 J=1,10
      INUZM = NUZM + 10*J
      MIDNU = INUZM+5
  331 IF (JJ-KID) 445,446,446
  445 IWARN(J)=1
      GO TO 336
  446 KAD=IVST(KID)
      IF (MIDNU-INUS(KAD)-10) 332,332,333
  333 KID = KID+1
      GO TO 331
  332 IWARN(J) = 1
      IF (IABS(MIDNU-INUS(KAD))-10) 335,336,336
  335 IWARN(J) = 0
  336 CCNTINUE
      NOSTRG(J) = 0
      IO = I
  400 IF (IST-MSP) 410,351,351
  410 JALFA=INUS(IST)-INUZM
      IF (JALFA-10) 350,350,351
  350 L(IIS) = JALFA
      NOSTRG(J) = NOSTRG(J)+1
      JTOTAL = JTOTAL+1
      ISTRGL(IIS)=IST
      IF (JALFA-10) 352,353,352
  353 IABOVE(IIS)=-1
      IBELOW(IIS) = 1
      IF (INUS(IST)-INUS(IST-1)-1) 354,354,355
  354 IBELOW(IIS) = 0
  355 IIS = IIS+1
      GC TO 351
  352 IF (JALFA) 356,356,357
```

```
      356 IABOVE(IIS)=1
          IBELOW(IIS)=-1
          IF (INUS(IST+1)-INUS(IST)-1) 358,358,359
      358 IABOVE(IIS)=0
      359 GO TO 360
      357 IABOVE(IIS)=1
          IBELOW(IIS)=1
          IF (INUS(IST+1)-INUS(IST)-1) 361,361,362
      361 IABOVE(IIS)=0
      362 IF (INUS(IST)-INUS(IST-1)-1) 363,363,364
      363 IBELOW(IIS)=0
      364 CONTINUE
      360 IIS = IIS+1
          IST = IST+1
          GO TO 400
      351 CONTINUE
          ISTO=IST
          BNU=ANUZ-DIST
          IS=MAX0(1,I1)
          DO 460 I=IS,MS
          IF (BNU-BNUS(I)) 461,460,460
      461 I1 = I-1
          GO TO 462
      460 CONTINUE
          I1=MS
      462 BNU=ANUZ+DIST
          IS=I2
          DO  463 I=IS,MS
          IF (BNU-BNUS(I)) 464,464,463
      464 I2 = I
          GO TO 465
      463 CONTINUE
          I2=MSP
      465 IFIRST = I1+1
          ILAST = I2-1
          KK = 0
          DO 370 M1=1,3
          Y=M1-2
          BNL = ANUZ+Y/2.
          DATA DXX/50./
          ISIS=0
          IF (I1)401,401,402
  402     DO 371 I=1,I1
          DXY=BNUS(I)-BNU
          D(I)=DXY*DXY
          IF(D(I).GT.DXX) ISIS=I
  371     CONTINUE
  401     ISIS=ISIS+1
          IF (MS-I2) 403,1401,1401
  403     ISIT=MS
          GO TO 1403
  1401    DO 372 I=I2,MS
          DXY=BNUS(I)-BNU
          D(I)=DXY*DXY
          ISIT=I
          IF (D(I).GT.DXX) GO TO 1404
  372     CONTINUE
          GO TO 1403
  1404    ISIT=ISIT-1
  1403    DO 370 K=1,6
```

```
          S=0.
          KK=KK+1
          IF (I1-ISIS)1405,4C6,4C6
   406    DO 373 I=ISIS,I1
          ISUB=ISS(I)+K
   373    S=S+ST(ISUB)*AR(I)/D(I)
  1405    IF (ISIT-I2)370,4C5,405
   405    DO 374 I=I2,ISIT
          ISUB = ISS(I)+K
    374 S=S+ST(ISUB)*AR(I)/D(I)
    370 SM(KK) = S
        CALL GRONK
        WRITE (6,250) ANUZ,JTOTAL,IFIRST,ILAST,(NOSTRG(I),I=1,10
       1),NOIN,(NOINT(I),I=1,10),(SM(I),I=1,18)
    380 IF (JTOTAL) 383,383,382
    382 WRITE (6,252) (IBELOW(I),IABOVE(I),ISTRGL(I),I=1,JTOTAL)
    383 IF (NOIN) 385,385,384
    384 NON = NOIN*2
        WRITE (6,253) (NEND(I),I=1,NCN)
    385 CCNTINUE
        NLMBER=NUMBER-1
        IF (NUMBER) 802,802,3C6
    306 ANUZ=ANUZ+1.0
        NUZ=ANUZ+0.1
        IF (NUZ-(NUZ/10)*10) 1802,1802,8C1
   1000 STOP
        END
        SUBROUTINE GRONK                                                GRONK 01
        COMMON NCSTRG,L,NOINT,NOIN,NEND,IWARN
        DIMENSION NOSTRG(10),L(100),NOINT(72),NEND(144),IWARN(10)
        KK = 1
        M1 = 1
        DO 300 I = 1,10
        MINIT = M1
        M = 0
        J = NOSTRG(I)
        IF (J) 301,301,302
    301 NEND(M1) = 0
        NEND(M1+1) = 10
        M1 = M1+2
        M = 1
        GO TO 320
    302 K = 1
        IF (L(KK)-2) 330,303,303
    303 NEND(M1) = 0
        NEND(M1+1) = L(KK)-1
        M1 = M1+2
        M = M+1
    330 IF(K-J) 304,34C,304
    304 IF (L(KK+1)-L(KK)-2) 305,305,306
    306 NEND(M1) = L(KK)+1
        NEND(M1+1) = L(KK+1)-1
        M1 = M1+2
        M = M+1
    305 K = K+1
        KK = KK+1
        IF(K-J)  330,34C,330
    340 IF (L(KK)-8)  307,307,350
    307 NEND(M1) = L(KK)+1
        NENC(M1+1) = 10
```

```
      M = M+1
      M1 = M1+2
  350 KK = KK+1
  320 CONTINUE
      IF (IWARN(I)) 311,311,312
  311 MZERC = M
      JJ=1
  201 IF (JJ-MZERO) 321,321,380
  321 IF (NEND(MINIT+1)-NEND(MINIT)-3) 360,360,323
  323 M=M+2
      IX=NEND(MINIT+1)-NENC(MINIT)
      I1=(IX+1)/3
      I2=(2*IX+1)/3
      MALL = M1 - MINIT -1
      DO 37C II=1,MALL
      MSUB = M1-II
  370 NEND(MSUB+4)=NEND(MSUB)
      NEND(MINIT+1)=NEND(MINIT)+I1
      NEND(MINIT+2)=NEND(MINIT+1)
      NEND(MINIT+3)=NEND(MINIT)+I2
      NENC(MINIT+4)=NEND(MINIT+3)
      M1=M1+4
      MINIT=MINIT+4
  360 MINIT = MINIT+2
      JJ=JJ+1
      GO TO 201
  380 CCNTINUE
  312 NOINT(I) = M
  300 CONTINUE
      M1 = M1-1
      NOIN = M1/2
      RETURN
      END
END OF FILE
```

```
C       PROGRAM HSLANV FORTRAN IV
C       MODIFIED FOR 2 OR 4 POINT QUADRATURE
        COMMON ANU,ANUZ,SEC,SN,TRAN,WWA,II,IST,JMAX,KADD,KSLA,KMAX,M,
       1     KMESS,KSTOP,IE,AVNU,KCRIT,K,P,ZEN,AL2,AL,ALP,X,Y,ZERO,LS,ANZ,
       2   ANY,C,JUMP,AR,GNU,ARR,GNUU,ST
        COMMON /ADD/ CC(630)
        DIMENSION ANU(250),IST(250),ANZ(250),ANY(250),C(35),SEC(10),
       1     SN(150),ST(8750),TRAN(2800),IE(8),P(36),AL2(35),AL(35),
       2     ALP(35),X(35),Y(35),ZERO(35),JUMP(35)
        DIMENSION BNU(250),IBELOW(200),ENDPT(200),ENGTH(36),SM(18),T(36),
       1     TM(35),WAB(4),ISTRGL(100),IA(250),ITN(35),NOINT(10),
       2     NOSTRG(10),IABOVE(100),X1(35),Y1(35),ZERO1(35),B(6),WA(4)
        DIMENSION AR(250),GNUU(20),ARR(250),GNU(20)
        DIMENSION CONC(36),Z(36),XX(35)
        NAMELIST /NAM1/ PCRIT,WTM,KMAX,NQI,NQC,CONC,Z,IS,P,T
        NAMELIST /NAM2/ NUMBA,ANUZ
    902 FORMAT (2I5,F6.1)
    904 FORMAT(F7.2,6E10.4,F6.4)
    905 FORMAT(F7.2,I2,2I4,11I2,10I1/(6E10.4))
    906 FORMAT (9(2I2,I4))
    907 FORMAT(24F3.2)
    800 FORMAT(F10.1,F10.2,4I6/(F8.1,F10.2,2E14.4))
    801 FORMAT (2I6/(10F8.3))
        DATA NQI/2/,NQC/2/,WTM/44./
        DATA ENDPT/.0,.001,.002,.003,.005,.01/
        DATA ACIST/.8/,ANDIST/.099/,PCRIT/100./,PPP/1013.25/,PCO2/.032/
        KCRIT=0
        TTT=298.0
        AAA=1.0
        ISWCH=1
        I1=0
        PIE=3.1415927
        READ (5,NAM1)
        KSLA=1
        NCC=NQC*5
        NCB=NQC*4
        II=1
        DO 100 I=1,5
        CALL GAUSSN(ENDPT(I),ENDPT(I+1),GNU(II),ENGTH(II),NQC)
    100  II=II+NQC
        DO 101 I=1,NCC
        GNUU(I)=GNU(I)*GNU(I)
    101 ENGTH(I)=ENGTH(I)*10.0
        DOP=3.581136E-7/SQRT(WTM)
        ALOG2=ALOG(2.)
        ALOG2=SQRT(ALOG2)
        ROOTPI=SQRT(PIE)
        KMESS=10*(KMAX-1)
        KO=KMAX*KSLA
        KLCT=KO*10
        KADD=KMAX*10
        KPLUS=KMAX+1
        WRITE(6,800)PCRIT,WTM,NQI,NQC,KMAX,IS,(Z(K),T(K),P(K),
       1CONC(K),K=1,KPLUS)
        AAA=AAA/PPP
        ALPHA=AAA*AAA*TTT
        DO 102 I=1,225
        JA=I-1
        IST(I)=KMAX*JA
    102 IA(I)=6*JA
```

```
      KZ=1
      DO 103 K=1,KMAX
      TA=(T(K)+T(K+1))/2.
      PA=(P(K)+P(K+1))/2.
      AL2(K)=ALPHA/TA*PA*PA
      AL(K)=SQRT(AL2(K))
      ALP(K)=AL(K)/PIE
      C(K)=(CONC(K)+CONC(K+1))*.5
      IF (IS.EQ.1) C(K)=C(K)*PA/(TA*1.38054E-19)
      ZZ=(6378.+Z(K+1))*2.
      DO 1033 I=1,K
      HH=Z(I)-Z(K+1)
 1033 XX(K)=SQRT(HH*(ZZ+HH))
      XX(K+1)=0.
      DO 1034 I=1,K
      CC(KZ)=(XX(I)-XX(I+1))*C(I)*8.176E-15
 1034 KZ=KZ+1
      IF (PA-PCRIT) 104,105,105
  104 JUMP(K)=1
      KCRIT=K
      AD=DOP*SQRT(TA)
      X1(K)=ALOG2/AD
      Y1(K)=AL(K)*X1(K)
      ZERO1(K)=X1(K)/ROOTPI
      GO TO 106
  105 JUMP(K)=0
  106 TAA=TA-275.
      DO 107 N=2,5
      IF (TAA) 107,107,108
  108 ITN(K)=N
      GO TO 109
  107 TAA=TAA+25.0
      ITN(K)=5
  109 TN=ITN(K)
      TP=325.-25.*TN
  103 TM(K)=(TA-TP)/25.
  190 READ (5,NAM2)
      WRITE (6,NAM2)
      IS5=4
  110 READ (5,902) IFIRST,ILAST,AVNU
      DO 111 K=1,KCRIT
      X(K)=X1(K)/AVNU
      Y(K)=Y1(K)/AVNU
  111 ZERO(K)=ZERO1(K)/AVNU
      IJ=IFIRST-1
      IMAX=ILAST-IJ
      GO TO (401,402),ISWCH
  401 IJKL=1
      GO TO 403
  402 IJK=ILASTA-IFIRST+1
      IF(IJK) 401,401,404
  404 ISHIFT=IMAXA-IJK
      IF (ISHIFT) 410,410,411
  411 DO 405 I=1,IJK
      J=I+ISHIFT
      AR(I)=AR(J)
      ARR(I)=ARR(J)
  405 BNU(I)=BNU(J)
      ISHIFT=ISHIFT*KMAX
      IJKJ=IJK*KMAX
```

```
      DO 406 I=1,IJKJ
      J=I+ISHIFT
  406 ST(I)=ST(J)
  410 IJKL=IJK+1
  403 IF (IMAX-IJKL) 412,413,413
  413 ISUB=IST(IJKL)
      DO 450 I=IJKL,IMAX
      READ (5,904) BNU(I),(B(J),J=1,6),AR(I)
      ARR(I)=AR(I)*AR(I)
      DO 451 K=1,6
      B(K)=B(K)*AR(I)
  451 B(K)=ALOG(B(K))
      DO 450 K=1,KMAX
      ISUB=ISUB+1
      JA=ITN(K)
      S1=B(JA-1)
      S2=B(JA)
      S3=B(JA+1)
  450 ST(ISUB)=(EXP(S2+((S1+S3-S2-S2)*TM(K)+S1-S3)*TM(K)/2.))*ALP(K)
  412 ILASTA=ILAST
      IMAXA=IMAX
      ISWCH=2
  120 READ (5,905) ANUZ,JTOTAL,I1,I2,(NOSTRG(I),I=1,10),NOIN,(NOINT(I),
     1      I=1,10),(SM(I),I=1,18)
      IF (JTOTAL) 600,600,601
  601 READ (5,906) (IBELOW(I),IABCVE(I),ISTRGL(I),I=1,JTOTAL)
  600 NON=NOIN*2
      IF (NOIN) 602,602,603
  603 READ (5,907) (ENDPT(I),I=1,NON)
  602 CONTINUE
      I1=I1-IJ
      I2=I2-IJ
      IE(1)=I1
      IE(6)=I2
      DO 130 K=1,KMAX
      DO 130 N=1,3
      JA=IA(N)+ITN(K)
      SUM1=SM(JA-1)
      SUM2=SM( JA)
      SUM3=SM(JA+1)
      ISUB=IST(N)+K
  130 SN(ISUB)=(SUM2+((SUM3+SUM1-2.*SUM2)*TM(K)+SUM1-SUM3)*TM(K)/2.0)
     1      *ALP(K)
      M1=1
      M2=1
      IF (I1-I2) 170,170,171
  170 CONTINUE
      DO 121 I=I1,I2
      A=BNU(I)-ANUZ
      IF (A) 122,122,123
  122 N=(A-.005)*100.
      GO TO 125
  123 N=(A+.005)*100.
  125 A=N
  121 ANU(I)=A/100.
  171 CONTINUE
      DO 124 N=1,KLOT
  124 TRAN(N)=0.0
      DO 303 M=1,10
      ANUO=M-6
```

```
      ANUO=ANUO/10.
      ANUA=ANUC+.05
      IEA=LOOP(I1,I2,ANUA-ADIST,ANU)
      IE(1)=IEA-1
      IE(6)=LOOP(IEA,I2,ANUA+ADIST,ANU)
      CALL LOOKBY(ANUA,I1,I2,3,ANUA)
      IE(1)=IE(1)+1
      IE(6)=IE(6)-1
      NOIE=NOINT(M)
      IF (NOIE) 180,180,181
  181 CONTINUE
      DO 306 MM=1,NOIE
      KSTOP=KMAX+1
      CALL GAUSSN(ENDPT(M1),ENDPT(M1+1),WAB,WA,NQI)
      DO 200 III=1,NQI
      II=III
      BAD =WAB(II)+ANUO
      WWA=WA(II)*10.
      IEA=LOOP(IE(1),IE(6),BAD-.2,ANU)
      IE(2)=IEA-1
      IE(5)=LOOP(IEA,IE(6),BAD+.2,ANU)
  200 CALL LOOKBY(BAD,IE(1),IE(6),1,10.*WAB(II)-.5)
  306 M1=M1+2
  180 CONTINUE
      NOIE=NOSTRG(M)
      IF(NOIE)182,182,183
  183 CONTINUE
      DO 309 MM=1,NOIE
      LS=ISTRGL(M2)-IJ
      FREQ=ANU(LS)
      IE(3)=LOOP(IE(1),IE(6),FREQ-.199,ANU)
      IE(2)=IE(3)-1
      IE(7)=LOOP(IE(3),IE(6),FREQ-ANDIST,ANU)-1
      IE(8)=LOOP(LS+1,IE(6),FREQ+ANDIST,ANU)
      IE(5)=LOOP(IE(8),IE(6),FREQ+.199,ANU)
      IE(4)=IE(5)-1
      IXI=(FREQ-ANUA)*100.1
      BAD=IXI
      CALL LOOKBY(FREQ,IE(1),IE(6),0,BAD/10.)
      IE(7)=IE(7)+1
      IE(8)=IE(8)-1
      IE(3)=LS-1
      IE(4)=LS+1
      IF (IBELOW(M2)) 141,142,143
 142  ISUBB=NCB
      GO TO 144
 143  ISUBB=NCC
  144 DO 145 III=1,ISUBB
      II=III
      BAD=FREQ-GNU(II)
      WWA=ENGTH(II)
  145 CALL LOOKBY(BAD,IE(7),IE(8),2,-GNU(II)*50.)
  141 IF (IABOVE(M2)) 146,147,148
 147  ISUBB=NCB
      GO TO 149
 148  ISUBB=NCC
  149 DO 150 III=1,ISUBB
      II=III
      BAD=FREQ+GNU(II)
      WWA=ENGTH(II)
```

```
  150 CALL LOOKBY (BAD,IE(7),IE(8),2,GNU(II)*50.)
  146 CONTINUE
  309 M2=M2+1
  182 CONTINUE
  303 CONTINUE
      CALL PRIPUN(IS5)
      NUMBA=NUMBA-1
      IF (NUMBA) 151,151,152
  151 GO TO 190
  152 NUZ=ANUZ+1.1
      IF(NUZ-(NUZ/10)*10)110,110,120
      END
      SUBROUTINE GAUSS(AA,BB,C,D)
      DIMENSION C(4),D(4)
      B=BB
      A=AA
      X1=.8611363116
      X2=.3399810436
      Y1=.3478548451
      Y2=.6521451549
      X=(1.-X1)*.5
      Y=(1.+X1)*.5
      C(1)=B*X+A*Y
      C(4)=B*Y+A*X
      X=(1.-X2)*.5
      Y=(1.+X2)*.5
      C(2)=B*X+A*Y
      C(3)=B*Y+A*X
      A=(B-A)*.5
      D(1)=Y1*A
      D(4)=D(1)
      D(2)=Y2*A
      D(3)=D(2)
      RETURN
      END
      FUNCTION LOOP(IA,IB,ZA,ZB)
      DIMENSION ZB(250)
      IF (IA-IB) 100,100,101
 101  LOOP=IA
      RETURN
 100  CONTINUE
      DO 202 I=IA,IB
      IF (ZB(I)-ZA) 202,202,103
 103  LOOP=I
      RETURN
 202  CONTINUE
      LOOP=IB+1
      RETURN
      END
      FUNCTION VOIGT (XIN,YIN)
      REAL*4 HH(2)/.8049141,.8131283E-01/,XX(2)/.5246476,1.650680/,A(42)
     1 /0.0,.2,0.,-.184,0.0,.15584,0.0,-.121664,0.0,.8770816E-1,0.0,-.5
     2 851412E-1,0.0,.3621573E-1,0.0,-.2084976E-1,0.0,.1119601E-1,0.0,-
     3 .5623190E-2,0.0,.2648763E-2,0.0,-.1173267E-2,0.0,.4899520E-3,0.0
     4 ,-.1933631E-3,0.0,.7228775E-4,0.0,-.2565551E-4,0.0,.8662074E-5,0.
     5 0,-.2787638E-5,0.0,.8566874E-6,0.0,-.2518434E-6,0.0,.7093602E-7/
      DIMENSION RA(32),CA(32),RB(32),CB(32),B(44),AK(5),AM(5),DY(4)        VOIGT003
      X=XIN
      Y = YIN                                                               VOIGT010
      X2 = X*X                                                              VOIGT011
```

```
      Y2 = Y*Y                                                        VOIGT012
      IF (X-7.0) 200,201,201                                          VOIGT013
  200 IF (Y-1.) 202,202,203                                           VOIGT014
  203 RA(1) = 0.                                                      VOIGT015
      CA(1) = 0.                                                      VOIGT016
      RB(1) = 1.                                                      VOIGT017
      CB(1) = 0.                                                      VOIGT018
      RA(2) = X                                                       VOIGT019
      CA(2) = Y                                                       VOIGT020
      RB(2) = .5-X2+Y2                                                VOIGT021
      CB(2) = -2.*X*Y                                                 VOIGT022
      CB1 = CB(2)                                                     VOIGT023
      UV1=0.                                                          VOIGT025
      DO 250 J=2,31                                                   VOIGT026
      JMINUS = J-1                                                    VOIGT027
      JPLUS = J+1                                                     VOIGT028
      FLOATJ = JMINUS                                                 VOIGT029
      RB1 = 2.*FLOATJ+RB(2)                                           VOIGT030
      RA1 = -FLOATJ*(2.*FLCATJ-1.)/2.                                 VOIGT031
      RA(J+1)=RB1*RA(J)-CB1*CA(J)+RA1*RA(J-1)
      CA(J+1)=RB1*CA(J)+CB1*RA(J)+RA1*CA(JMINUS)
      RB(J+1)=RB1*RB(J)-CB1*CB(J)+RA1*RB(J-1)
      CB(J+1)=RB1*CB(J)+CB1*RB(J)+RA1*CB(J-1)
      UV=(CA(JPLUS)*RB(JPLUS)-RA(JPLUS)*CB(JPLUS))/(RB(JPLUS)*RB(JPLUS)+VOIGT036
     1CB(JPLUS)*CB(JPLUS))                                            VOIGT037
      IF(ABS(UV-UV1)-1.E-6) 251,25(,250
  250 UV1=UV                                                          VOIGT039
  251 VOIGT=UV/1.772454                                               VOIGT040
      RETURN                                                          VOIGT041
  202 IF (X-2.) 301,301,302                                           VOIGT042
  301 AINT = 1.                                                       VOIGT043
      MAX = 12.+5.*X2                                                 VOIGT044
      KMAX = MAX-1                                                    VOIGT045
      KO=0
      DO 303 K=KO,KMAX
      AJ = MAX-K                                                      VOIGT047
  303 AINT = AINT*(-2.*X2)/(2.*AJ+1.)+1.                              VOIGT048
      U = -2.*X*AINT                                                  VOIGT049
      GO TO 304                                                       VOIGT050
  302 IF (X-4.5) 305,306,306                                          VOIGT051
  305 B(43)=0.                                                        VOIGT052
      B(44) = 0.                                                      VOIGT053
      J = 42                                                          VOIGT054
      DO 307 K = 1,42                                                 VOIGT055
      B(J) = .4*X*B(J+1)-B(J+2)+A(J)                                  VOIGT056
  307 J = J-1                                                         VOIGT057
      U = B(3)-B(1)                                                   VOIGT058
      GO TO 304                                                       VOIGT059
  306 AINT = 1.0                                                      VOIGT060
      MAX = 2.+40./X                                                  VOIGT061
      AMAX = MAX                                                      VOIGT062
      DO 308 K=1,MAX                                                  VOIGT063
      AINT = AINT*(2.*AMAX-1.)/(2.*X2)+1.                             VOIGT064
  308 AMAX = AMAX -1.                                                 VOIGT065
      U = -AINT/X                                                     VOIGT066
  304 V = 1.772454*EXP(-X2)                                           VOIGT067
      H = .02                                                         VOIGT068
      JM = Y/H                                                        VOIGT069
      IF (JM) 310,311,310                                             VOIGT070
  311 H=Y                                                             VOIGT071
```

```
  310 Z = 0.                                                            VOIGT072
      L = 0                                                             VOIGT073
      DY(1) = 0.                                                        VOIGT074
  312 DY(2) = H/2.                                                      VOIGT075
      DY(3) = DY(2)                                                     VOIGT076
      DY(4) = H                                                         VOIGT077
  318 AK(1) = C.                                                        VOIGT078
      AM(1) = 0.                                                        VOIGT079
      DO 313 J=1,4                                                      VOIGT080
      YY = Z+DY(J)                                                      VOIGT081
      UU = U+.5*AK(J)                                                   VOIGT082
      VV = V+.5*AM(J)                                                   VOIGT083
      AK(J+1) = 2.*(YY*UU+X*VV)*H                                       VOIGT084
      AM(J+1) = -2.*(1.+X*UU-YY*VV)*H                                   VOIGT085
      IF (J-3) 313,314,313                                              VOIGT086
  314 AK(4)=2.*AK(4)                                                    VOIGT087
      AM(4) = AM(4)+AM(4)                                               VOIGT088
  313 CONTINUE                                                          VOIGT089
      Z=Z+H                                                             VOIGT090
      L = L+1                                                           VOIGT091
      U = U+.1666667*(AK(2)+2.*AK(3)+AK(4)+AK(5))                       VOIGT092
      V = V+.1666667*(AM(2)+AM(3)+AM(3)+AM(4)+AM(5))                    VOIGT093
      IF(JM) 315,320,315                                                VOIGT094
  315 IF (L-JM) 318,317,320                                             VOIGT095
  317 AJM = JM                                                          VOIGT096
      H=Y-AJM*H                                                         VOIGT097
      GO TO 312                                                         VOIGT098
  320 VOIGT= V/1.772454                                                 VOIGT099
      RETURN                                                            VOIGT100
  201 F1 = 0.                                                           VOIGT101
      DO 330 J=1,2                                                      VOIGT102
  330 F1=F1+HH(J)/(Y2+(X-XX(J))*(X-XX(J)))+HH(J)/(Y2+(X+XX(J))*(X+XX(J))VOIGT103
     1)                                                                 VOIGT104
      VOIGT=Y*F1/3.1415927                                              VOIGT105
      RETURN                                                            VOIGT106
      END                                                               VOIGT107
C     PRIPUN HAS BEEN MODIFIED FOR USE WITH SLANTV
      SUBROUTINE PRIPUN(IS5)
      COMMON ANU,ANUZ,SEC,SN,TRAN,WWA,II,IST,JMAX,KADD,KSLA,KMAX,M,
     1    KMESS,KSTOP,IE,AVNU,KCRIT,K,P,ZEN,AL2,AL,ALP,X,Y,ZERO,LS,ANZ,
     2  ANY,C,JUMP,AR,GNU,ARR,GNUU,ST
      DIMENSION ANU(250),IST(250),ANZ(250),ANY(250),C(35),SEC(10),
     1    SN(150),ST(8750),TRAN(10,280),IE(8),P(36),AL2(35),AL(35),
     2    ALP(35),X(35),Y(35),ZERO(35),JUMP(35)
      DIMENSION BNU(250),IBELOW(200),ENDPT(200),ENGTH(36),SM(18),T(36),
     1    TM(35),WAB(4),ISTRGL(100),IA(250),ITN(35),NOINT(10),
     2    NOSTRG(10),IABOVE(100),X1(35),Y1(35),ZERO1(35),B(6),WA(4)
      DIMENSION AR(250),GNUU(20),ARR(250),GNU(20)
900   FORMAT (16H1  INTERVAL IS  ,F6.1//(1H ,10F9.6,F10.2,I5))
      IS5=1
      KMID=KMAX*KSLA
      WRITE (6,900) ANUZ,((TRAN(J,K),J=1,10),P(K+1),K,K=1,KMID)
       WRITE(8) ANUZ,((TRAN(J,K),K=1,KMID),J=1,10)
      RETURN
      END
C     LOOKBY HAS BEEN MODIFIED FOR USE WITH SLANTV
      SUBROUTINE LOOKBY(FREQUE,III1,III2,II4,Z)
      COMMON ANU,ANUZ,SEC,SN,TRAN,WWA,II,IST,JMAX,KADD,KSLA,KMAX,M,
     1    KMESS,KSTOP,IE,AVNU,KCRIT,K,P,ZEN,AL2,AL,ALP,X,Y,ZERO,LS,ANZ,
     2  ANY,C,JUMP,AR,GNU,ARR,GNUU,ST
```

```
      COMMON /ACD/CC(630)
      DIMENSION ANU(250),IST(250),ANZ(250),ANY(250),C(35),SEC(10),
     1    SN(150),ST(8750),TRAN(2800),IE(8),P(36),AL2(35),AL(35),
     2    ALP(35),X(35),Y(35),ZERO(35),JUMP(35)
      DIMENSION AR(250),GNUU(20),ARR(250),GNU(20)
      DIMENSION COEF(35)
      DIMENSION SZ(105),SA(105)
      FREQ=FREQUE
      II1=III1
      II2=III2
      I4=II4+1
      ZZ=Z
      ZZZ=ZZ*2.
      KP=2
      GO TO (100,101,102,103),I4
  100 DELTA=.01
      GO TO 104
  103 DELTA=.05
  104 IC=-1
      GO TO 403
  101 IY=IE(2)+1
      IZ=IE(5)-1
  102 JSLANT=M+KMESS
      F=0.
  403 IF (II1-II2) 180,180,181
  180 DO 200 I=II1,II2
      ANZ(I)=ABS(ANU(I)-FREQ)
  200 ANY(I)=ANZ(I)*ANZ(I)
  181 CONTINUE
      KPP=2
      DO 202 KK=1,KMAX
      K=KK
      GO TO (110,111,111,113),I4
  111 CONTINUE
  501 GO TO (121,121,122),I4
  113 SN1=SN(K)
      JA=K+KMAX
      SN2=SN(JA)
      JA=JA+KMAX
      SN3=SN(JA)
      GO TO 105
  122 SN1=SZ(KP-1)
      SN2=SZ(KP)
      SN3=SZ(KP+1)
      GO TO 105
  121 CONTINUE
  110 SN1=SA(KPP-1)
      SN2=SA(KPP)
      SN3=SA(KPP+1)
      KPP=KPP+3
  105 SRE=((SN3+SN1-SN2-SN2)*ZZZ+SN3-SN1)*ZZ+SN2
      GO TO (130,131,132,133),I4
  131 IF (JUMP(K))134,134,135
  134 SRE=SRE+RNTZ(II1,II2)
      GO TO 136
  135 SRE=SRE+RNTZ(II1,IE(2))+RNTZ(IE(5),II2)+XED(IY,IZ)
      GO TO 136
  132 IF (JUMP(K))137,137,138
  137 SRE=SRE+RNTZ(II1,IE(3))+RNTZ(IE(4),II2)
      AKNU=AR(LS)*AL(K)
```

```
      IB=IST(LS)+K
      SRE=SRE+ST(IB)/(GNLU(II)+AL2(K)*ARR(LS))
      GO TO 136
138   SRE=SRE+XED(II1,IE(3))+XED(IE(4),II2)
      IB=IST(LS)+K
      SRE=SRE+ST(IB)/ALP(K)/AR(LS)*VOIGT(GNU(II)*X(K),Y(K)*AR(LS))*
     1    ZERO(K)
136   COEF(K)=SRE





      GO TO 202
130   IF (JUMP(K)) 150,150,151
150   SZZ=RNTZ(II1,IE(7))+RNTZ(IE(8),II2)
      GO TO 152
151   SZZ=RNTZ(II1,IE(2))+RNTZ(IE(5),II2)+XED(IE(3),IE(7))+XED(IE(8),IE(
     14))
152   SZ(KP)=SZZ+SRE
      GO TO 202
133   SA(KP)=SRE+RNTZ(II1,IE(1))+RNTZ(IE(6),II2)
202   KP=KP+3
      GO TO (160,1661,1661,160),I4
1661  JSLANT=M
      KX=1
      DO 503 J=1,KMAX
      F=0.
      DO 502 K=1,J
      F=F-CC(KX)*COEF(K)
502   KX=KX+1
      TRAN(JSLANT)=TRAN(JSLANT)+WWA*EXP(F)
503   JSLANT=JSLANT+10
      GO TO 161
160   IC=IC+1
      ID=IC+1
      GO TO (170,171,172),ID
170   KP=1
      FREQ=FREQ-DELTA
      IF (I4-1) 173,174,173
174   ZZ=ZZ-.1
      GO TO 175
173   ZZ=FREQ
175   ZZZ=ZZ*2.
      GO TO 403
171   KP=3
      FREQ=FREQUE+DELTA
      IF (I4-1) 176,177,176
177   ZZ=Z+.1
      GO TO 178
176   ZZ=FREQ
178   ZZZ=ZZ*2.
      GO TO 403
172   CONTINUE
161   RETURN
      END
C      XED HAS BEEN MODIFIED FOR USE WITH SLANTV
      FUNCTION XED(IA,IB)
      COMMON ANU,ANUZ,SEC,SN,TRAN,WWA,II,IST,JMAX,KADD,KSLA,KMAX,M,
     1     KMESS,KSTOP,IE,AVNU,KCRIT,K,P,ZEN,AL2,AL,ALP,X,Y,ZERO,LS,ANZ,
```

```
      2   ANY,C,JUMP,AR,GNU,ARR,GNUU,ST
       DIMENSION ANU(250),IST(250),ANZ(250),ANY(250),C(35),SEC(10),
      1     SN(150),ST(8750),TRAN(2800),IE(8),P(36),AL2(35),AL(35),
      2     ALP(35),X(35),Y(35),ZERO(35),JUMP(35)
       DIMENSION AR(250),GNUU(20),ARR(250),GNU(20)
       IF (IA-IB) 100,100,101
100    KUP=IST(IA)+K
       SUM=0.0
       XA=X(K)
       YA=Y(K)
       DO 102 I=IA,IB
       SUM=SUM+ST(KUP)*VOIGT(ANZ(I)*XA,YA*AR(I))/AR(I)/ALP(K)
102    KUP=KUP+KMAX
       XED=SUM*ZERO(K)
       RETURN
101    XED=0.0
       RETURN
       END
C      RNTZ HAS BEEN MODIFIED FOR USE WITH SLANTV
       FUNCTION RNTZ(IA,IB)
       COMMON ANU,ANUZ,SEC,SN,TRAN,WWA,II,IST,JMAX,KADD,KSLA,KMAX,M,
      1     KMESS,KSTOP,IE,AVNU,KCRIT,K,P,ZEN,AL2,AL,ALP,X,Y,ZERO,LS,ANZ,
      2   ANY,C,JUMP,AR,GNU,ARR,GNUU,ST
       DIMENSION ANU(250),IST(250),ANZ(250),ANY(250),C(35),SEC(10),
      1     SN(150),ST(8750),TRAN(2800),IE(8),P(36),AL2(35),AL(35),
      2     ALP(35),X(35),Y(35),ZERO(35),JUMP(35)
       DIMENSION AR(250),GNUU(20),ARR(250),GNU(20)
       IF (IA-IB) 100,100,101
100    KUP=IST(IA)+K
       SUM=0.0
       A=AL2(K)
       DO 102 I=IA,IB
       SUM=SUM+ST(KUP)/(ANY(I)+A*ARR(I))
102    KUP=KUP+KMAX
       RNTZ=SUM
       RETURN
101    RNTZ=0.0
       RETURN
       END
       SUBROUTINE GAUSSN(AA,BB,C,D,N)
       DIMENSION C(4),D(4)
       DATA A/.2886751/
       IF (N.EQ.4) GO TO 100
       IF (N.EQ.2) GO TO 200
       WRITE(6,950) N
       STOP
950    FORMAT('0 WRONG QUADRATURE: N=',I4)
200    CC=(AA+BB)*.5
       DC=BB-AA
       DD=DC*A
       C(1)=CC-DD
       C(2)=CC+DD
       D(1)=DC*.5
       D(2)=D(1)
       RETURN
100    CALL GAUSS(AA,BB,C,D)
       RETURN
       END
END OF FILE
```